

ISTANBUL TECHNICAL UNIVERSITY ★ GRADUATE SCHOOL OF SCIENCE
ENGINEERING AND TECHNOLOGY

**DETERMINATION OF A METHODOLOGY TO DEVELOP
DURABILITY APPROVAL TEST OF COMMERCIAL VEHICLE AXLES**

Ph.D. THESIS

Metin TOPRAK

Department of Mechanical Engineering

Mechanical Engineering Doctorate Programme

JUNE 2014

ISTANBUL TECHNICAL UNIVERSITY ★ GRADUATE SCHOOL OF SCIENCE
ENGINEERING AND TECHNOLOGY

**DETERMINATION OF A METHODOLOGY TO DEVELOP
DURABILITY APPROVAL TEST OF COMMERCIAL VEHICLE AXLES**

Ph.D. THESIS

**Metin TOPRAK
(503082029)**

Department of Mechanical Engineering

Mechanical Engineering Doctorate Programme

Thesis Advisor: Prof. Dr. Murat EREKE

JUNE 2014

İSTANBUL TEKNİK ÜNİVERSİTESİ ★ FEN BİLİMLERİ ENSTİTÜSÜ

**TİCARİ TAŞITLARDAKİ AKSLARIN DAYANIM ONAY TESTİNİ
OLUŞTURMAK İÇİN BİR YÖNTEM GELİŞTİRİLMESİ**

DOKTORA TEZİ

**Metin TOPRAK
(503082029)**

Makina Mühendisliği Anabilim Dalı

Makina Mühendisliği Doktora Programı

Tez Danışmanı: Prof. Dr. Murat EREKE

HAZİRAN 2014

Metin TOPRAK, a **Ph.D.** student of ITU **Graduate School of science engineering and technology** student ID **503082029**, successfully defended the **thesis** entitled “**DETERMINATION OF A METHODOLOGY TO DEVELOP DURABILITY APPROVAL OF COMMERCIAL VEHICLE AXLES.**”, which he prepared after fulfilling the requirements specified in the associated legislations, before the jury whose signatures are below.

Thesis Advisor : **Prof. Dr. Murat EREKE**

İstanbul Technical University

Jury Members : **Prof. Dr. Ahmet GÜNEY**

İstanbul Technical University

Prof. Dr. İrfan YAVAŞLIOL

Yıldız Technical University

Prof. Dr. H. Ertuğrul Arslan

İstanbul Technical University

Doç. Dr. Muammer Özkan

Yıldız Technical University

Date of Submission : 24 March 2014

Date of Defense : 03 June 2014

To my family,

FOREWORD

I would like to express my gratitude to all those who gave me the opportunity to complete this thesis. I am deeply indebted to my supervisor Prof. Dr. Murat Ereke for his guidance, contribution and suggestion during all phases of my study. I would also like to thank all my friends and colleagues for their help and support.

Furthermore, I have to thank especially Prof. Dr. Ahmet Güney, Prof. Dr. İrfan Yavaşlıođ, Dipl.-Ing. Manfred Streicher and Dr.-Ing. Martin Küppers for supporting me with brilliant ideas.

Finally, I should say many thanks to my family for all their patience and encouragement at every phase of my studies.

June 2014

Metin TOPRAK
(R&D Engineer)

TABLE OF CONTENTS

	<u>Page</u>
FOREWORD	ix
TABLE OF CONTENTS	xi
ABBREVIATIONS	xv
LIST OF TABLES	xix
LIST OF FIGURES	xxi
SUMMARY	xxiii
ÖZET	xxvii
1. INTRODUCTION	1
2. ASSIGNMENT OF TASKS	3
2.1 Aim of the Study	3
2.2 Advantage of the Study within the Scope of Axle Development	3
2.3 Description of Further Development Needs.....	4
2.4 Actual Test Method for Durability Approval of Commercial Vehicle Axles....	4
2.4.1 Advantages and disadvantages.....	4
2.4.1.1 Advantages	4
2.4.1.2 Disadvantages	5
2.4.2 Test-rig setup.....	6
2.4.3 Derivation of design and test spectrum.....	6
2.4.4 Release criteria	6
2.5 Methodical and Systematical Approach.....	7
3. STATE OF THE SCIENTIFIC AND TECHNICAL KNOWLEDGE	9
3.1 Objectives of SLH's and General Possibilities of Application	11
3.2 General Areas of Standardized Load-Time Histories (SLH's) Application	12
3.3 Existing Standardized Load Time-Histories	13
3.4 General (Simplified) Approach for the Generation of SLH's.....	13
4. ROAD LOAD DATA ACQUISITION (RLDA)	17
4.1 Phase 1: Definition of Customer Usage Profile and RLDA at CU	17
4.1.1 Route classification, different road classes	20
4.1.1.1 National connections.....	20
4.1.1.2 Regional connections	21
4.1.1.3 Local connections.....	22
4.1.1.4 Main city traffic.....	22
4.1.1.5 Local city traffic	23
4.1.2 Reference-customer usage profile in Turkey	24
4.2 Phase 2: Vehicle Instrumentation.....	26
4.2.1 Application of sensors.....	26
4.2.1.1 Load-cells in the air springs:	27
4.2.1.2 Shock absorbers:	30
4.2.1.3 Suspension arms (links):	31
4.2.1.4 Wheel force transducers (WFT).....	32

4.2.1.5 Strain-gages at the body	37
4.3 Summary of the Vehicle Instrumentation Plan	39
4.3.1 Suspension arms	39
4.3.2 Wheel forces.....	40
4.3.3 Shock absorbers.....	41
4.3.4 Air spring forces.....	42
4.3.5 Anti-roll bar.....	43
4.4 Vehicle Data and Vehicle Loading Conditions at the Measurements	44
4.5 Phase 3: RLDA at the Proving Ground Location (PG)	45
5. LOAD DATA ANALYSIS ON THE CUSTOMER USAGE	49
5.1 Step 1: Identification of All Operational Conditions and Loads (B_i).....	51
5.2 Step 2: Determination of the Partial Spectrum [$H(B_i)$]	52
5.2.1 Pre-processing of load signals.....	52
5.2.2 Derivation of the partial spectrum.....	54
5.3 Definition of Operation Life (H_i) and Weighting of Partial Spectrum (A_i)	55
5.4 Step 4: Extrapolation of Partial Spectrum to the Operation Life $H_i(B_i, t_i)$	57
5.5 Step 5: Superposition to Design Spectrum $H(B, t_N)$	58
5.6 Step 6: Scaling Factors of Wheel Forces (f_i).....	59
5.7 Summary of the first 6 Steps on the customer usage (CU)	61
6. LOAD DATA ANALYSIS AT THE PROVING GROUND	63
6.1 Step 1: Measurement at Various Vehicle Loading Conditions	64
6.2 Summary of the first 6 Steps at the proving ground (PG).....	65
6.3 Scaling Factors of Suspension Arms (f_i)	70
7. COMPARISON OF SCALING FACTORS (f_i) OF WHEEL FORCES	73
8. DERIVATION OF EXTREME LOADS	75
9. DETERMINATION OF THE PHASE RELATIONSHIP.....	85
9.1 Amplitude, Frequency, and Phase of a Sinusoidal Signal.....	87
9.2 Determination of a Phase Angle of a Periodic Non-Sinusoidal Signal	89
9.2.1 Zero-crossing methods	89
9.3 Determination of a Phase Angle of a Non-Sinusoidal Signal	95
9.3.1 Frequency response analysis (FRA).....	95
9.3.1.1 Fourier-series and fourier transforms.....	96
Fourier-Series	96
The Fourier transform	97
Frequency from the transfer function.....	98
Filter – signal processing.....	101
Terminology of the filter functions	102
9.3.2 Coherence – Signal Processing (C_{xy})	103
9.3.2.1 Definition and formulation of the coherence	104
9.3.3 Application of the Frequency Response Analysis (FRA)	106
9.3.3.1 The Coherence functions of the wheel forces	106
9.3.3.2 The Phase responses of the wheel forces	108
9.3.3.3 Reproduction of the longitudinal and lateral wheel forces	110
9.3.4 Correlation Analysis with Cross Plots – Lissajous Curve	112
9.3.4.1 Cross Plots of the normalized wheel forces (for case of $a = b$).....	113
10. CALCULATION OF THE SHAPE PARAMETERS (v)	121
11. CONCLUSIONS.....	129
REFERENCES	139
CURRICULUM VITAE	141

ABBREVIATIONS

*	: Convolution
$\bar{\nu}$: Wave Number
 G 	: Magnitude of the Spectral Density
a (t_i)	: a Pair of Counts at Which the Signal Polarity Changes
a (t_j)	: First Transition of Signal
a (t_w)	: a Pair of Counts at Which the Signal Polarity Changes
A	: Length of the Former Slot
A	: Peak Amplitude
a_i	: Extrapolation Factors
A_i	: Weighting of Partial Spectrum
a_N	: Total Extrapolation Factor
AR	: Amplitude Response or Gain
B₁	: Length of the Slot Thread
B_i	: Loads at Relevant Operational Conditions
BRT	: Bad Road Testing
C (s)	: Transfer Function
CAN	: Controller Area Network
CDF	: Cumulative Distribution Function
c_k	: k th Filter Constants
CU	: Customer Usage
C_{xy}	: Coherence
d	: Wheel Radius
DD	: Driving Direction
d_k	: k th Filter Constants
f	: Frequency
FEM	: Finite Element Methods
FFT	: Fast Fourier Transform
f_i	: Scaling Factors of Wheel Forces
FIR	: Finite Impulse Response
F_{L,X}	: Longitudinal Wheel Force Front Left
F_{L,Y}	: Lateral Wheel Force Front Left
F_{L,Z}	: Vertical Wheel Force Front Left
F_{R,X}	: Longitudinal Wheel Force Front Right
F_{R,Y}	: Lateral Wheel Force Front Right
F_{R,Z}	: Vertical Wheel Force Front Right
FRA	: Frequency Response Function
F_x	: Longitudinal Wheel Force
F_y	: Lateral Wheel Force
F_z	: Vertical Wheel Force
F_{z,stat.}	: Wheel load
G (iω)	: Fourier Transform of the Impulse Response
GVWR	: Gross Vehicle Weight Rating

G_{xx}	: Auto spectral Density of x
G_{xy}	: Cross-Spectral Density between x and y
G_{yy}	: Auto spectral Density of y
H (B, t_N)	: Superposition to the Design Spectrum
H (B_i)	: Partial Spectrum
h (t)	: Impulse Response
H	: Half the Maximum Vertical Height of the Ellipse
H₀	: Block Size (Number of Rainflow Cycles)
H_i (B_i, t_i)	: Extrapolation of the Partial
H_i	: Cumulative Frequency of Load Cycles for Load Level S _{a,i}
H_i	: Total Operation Life
ID	: Identification
IFFT	: Inverse Fast Fourier Transformation
IIR	: Infinite Impulse Response
k	: Angular Wave Number
LBF	: Laboratorien für Betriebsfestigkeit
LTI	: Linear Time-Invariant Theory
M	: Number of the Filter Constants Used
MGraph	: Data Analysis Software - Stiegele Datensysteme GmbH
M_x	: Wheel Moment in Longitudinal Direction
M_y	: Wheel Moment in Lateral Direction
M_z	: Wheel Moment in Vertical Direction
N	: Number of the Filter Constants Used
NORMSINV	: Inverse of the Cumulative Normal Distribution
P	: Probability
PG	: Proving Ground
r	: Distance between Load-Cells and Wheel Center
Re {.	: Real Part
R_{L,X}	: Longitudinal Wheel Force Rear Left
R_{L,Y}	: Lateral Wheel Force Rear Left
R_{L,Z}	: Vertical Wheel Force Rear Left
RLDA	: Road Load Data Acquisition
RMS	: Root Mean Square
R_{R,X}	: Longitudinal Wheel Force Rear Right
R_{R,Y}	: Lateral Wheel Force Rear Right
R_{R,Z}	: Vertical Wheel Force Rear Right
s	: Time
SLH's	: Standardized Load-Time Histories
SPRILOS	: SPRIng LOad Sequence
T	: Period
t	: time
t_i	: Cumulative Frequency of the Extrapolated Spectrum
t_N	: Cumulative Frequency of the Partial Spectrum
WFT	: Wheel Force Transducers
X	: Displacement
X_{data}	: Ranges of Each Interval
Y (f)	: Fourier Transform of y(t) and H(f)
Y	: Intercept on the Y-Axis
Y_{Label}	: Inverse of the Standard Normal Cumulative Distribution
Y_{rank}	: Z-Scores

$z(t)$: Complex Phasor
α	: Angle between Load-Cells at The Wheel
$\Delta\phi$: Difference of the Phase Angle
v	: Shape Parameter of the Spectrums
ϕ	: Phase Angle
φ	: Phase Response
ϕ	: Relative Phase Difference
ϕ_0	: Phase at Time $t = 0$
ϕ_a	: Phase of the Signal (a)
ϕ_b	: Phase of the Signal (b)
Ω	: Angular frequency

LIST OF TABLES

	<u>Page</u>
Table 4.1 : Route classification - different types of roads.	20
Table 4.2 : Distribution of the road types.....	25
Table 4.3 : Distribution of the road types.....	26
Table 4.4 : Overview of the measurement channels.	27
Table 4.5 : Measured WFT forces from different driving maneuvers.	37
Table 4.6 : Vehicle data.....	44
Table 4.7 : Vehicle loading conditions.	44
Table 4.8 : Various testing programs at proving ground - durability program I.....	45
Table 4.9 : Various testing programs at proving ground - durability program II.	46
Table 4.10 : Reference test program at the proving ground.....	47
Table 5.1 : The Characteristic roads.....	52
Table 5.2 : Definition of the total operation life on the customer usage.....	56
Table 5.3 : The Extrapolation factors based on customer usage.	56
Table 5.4 : Scaling factors of wheel forces on the customer usage [f _i].....	61
Table 6.1 : Definition of the total operation life and the extrapolation factors.....	64
Table 6.2 : Scaling factors of suspension arms at the proving ground [f _i].	71
Table 8.1 : Z-Scores or Yrank.....	76
Table 8.2 : Calculated Ylabel values corresponding to the probability values.	78
Table 9.1 : Arithmetic mean of the calculated phase angle with error percentage. ...	93
Table 9.2 : Arithmetic mean of the calculated phase angle with error percentage. ..	95
Table 10.1 : Spectrum shape parameters ν for typified amplitude spectra.....	122
Table 10.2 : Overview of the spectrum shape parameters [ν] and break of slope. .	128
Table 11.1 : Characterization of load spectrum of a two-axle coach.....	137

LIST OF FIGURES

	<u>Page</u>
Figure 2.1 : Flowchart of axle testing.	4
Figure 2.2 : Actual testing method.	6
Figure 2.3 : Methodical and systematical approach.	7
Figure 3.1 : Forces acting on a wheel.	10
Figure 3.2 : Example of load factors and spectra definition for a heavy truck axle.	11
Figure 3.3 : Definition of a design spectrum.	11
Figure 3.4 : General approach for the SLH's (example: passenger vehicle).....	14
Figure 3.5 : Compilation of relevant procedures for load analysis.....	15
Figure 4.1 : Influence parameters on the durability of trucks.....	18
Figure 4.2 : National connections.	21
Figure 4.3 : Regional connections.....	21
Figure 4.4 : Local connections.....	22
Figure 4.5 : Main city traffic.....	23
Figure 4.6 : Local city traffic.	23
Figure 4.7 : RLDA on Turkish reference-customer usage.....	24
Figure 4.8 : Distribution of the road types.....	25
Figure 4.9 : Istanbul city route.	26
Figure 4.10 : Calibration sheet of the load-cell in the air spring.	28
Figure 4.11 : Mounting configuration of the load-cell in the air springs.....	29
Figure 4.12 : The instrumented air spring at the rear axle.	29
Figure 4.13 : Calibration sheet of the shock absorber at the rear axle.....	30
Figure 4.14 : Calibration sheet of the transverse control arm.....	31
Figure 4.15 : Configurations of the measuring chain & technical data.	33
Figure 4.16 : Instrumented WFTs at the test vehicle.	34
Figure 4.17 : The Principal of WFT (forces and calculated moments).....	34
Figure 4.18 : Coordinates of the forces and moments acting on wheel.....	36
Figure 4.19 : Measured WFT forces from different driving maneuvers.....	36
Figure 4.20 : Overview of the strain gages at the body.	38
Figure 4.21 : Instrumentation plan of the suspension arms.	39
Figure 4.22 : Instrumentation plan of the wheel force transducers.....	40
Figure 4.23 : Instrumentation plan of the shock absorbers.	41
Figure 4.24 : Instrumentation plan of the air spring forces.....	42
Figure 4.25 : Instrumentation plan of the anti-roll bar.....	43
Figure 4.26 : Test track.	48
Figure 5.1 : Methodical and systematical approach.....	51
Figure 5.2 : Wheel longitudinal force front left – highway (732 km).	52
Figure 5.3 : Principal of range pair counting and wave pairs.	54
Figure 5.4 : Partial Spectrum of the wheel longitudinal force front left – highway.	55
Figure 5.5 : Extrapolation of the partial spectrum – highway (100000 km).....	57
Figure 5.6 : Design spectrum of the wheel longitudinal force front left (10 ⁶ km). ..	58

Figure 5.7 : Normalized design spectrums of the wheel forces to the max force.	60
Figure 5.8 : Scaled design spectrums of the wheel forces based on vertical force. ..	60
Figure 5.9 : Summary of the six steps of the load data analysis on the CU.....	62
Figure 6.1 : Measured WFT forces from the reference test program.....	65
Figure 6.2 : Summary of the first six steps of the load data analysis at the PG.....	67
Figure 6.3 : Normalized design spectrum of suspension arms at the PG.....	68
Figure 6.4 : Normalized design spectrum of air spring forces at the PG.....	68
Figure 6.5 : Normalized design spectrum of shock absorbers at the PG.	69
Figure 6.6 : Scaled design spectrums of the suspension arms.	70
Figure 7.1 : Comparison of the scaling factors between the CU and the PG.....	74
Figure 8.1 : Comparison of the various grading methods in a normal distribution. .	77
Figure 8.2 : Cumulative normal probability of the wheel longitudinal force.	79
Figure 8.3 : Extreme load for the suspension arms, air spring and anti-roll bar.	84
Figure 9.1 : Types of the signals.	86
Figure 9.2 : Time and frequency domain of the signals.....	86
Figure 9.3 : The Phase of a periodic sinusoidal signal (the time scale is arbitrary)..	87
Figure 9.4 : Two Signals with a relative phase difference of φ between them.....	88
Figure 9.5 : A Complex rotating phasor, $A\exp(j\omega t + \varphi_0)$	89
Figure 9.6 : Zero-crossing in a waveform representing amplitude vs. time.	89
Figure 9.7 : A Pair of counts $a(t_w)$ and $a(t_i)$ at which the signal polarity changes. ...	90
Figure 9.8 : Time signal of the suspension arms 13 & 14 at the proving ground.	91
Figure 9.9 : Excel sheet for the application of the method, step-1.....	92
Figure 9.10 : Excel sheet for the application of the method, step-2.....	92
Figure 9.11 : Time signal of the wheel forces rear right Z&Y at the RG.	94
Figure 9.12 : Explanation of the gain and phase.....	100
Figure 9.13 : Explanation of the frequency response analysis.....	101
Figure 9.14 : Time domain filters.	103
Figure 9.15 : Filtering in the frequency domain.	103
Figure 9.16 : The Coherence functions of the wheel forces.	107
Figure 9.17 : The Phase responses of the wheel forces.....	108
Figure 9.18 : Reproduction of longitudinal and lateral wheel force.	110
Figure 9.19 : Wheel longitudinal forces-front right (measured & calculated).....	111
Figure 9.20 : Wheel lateral forces-front right (measured & calculated).	111
Figure 9.21 : Wheel lateral forces-rear right (measured & calculated).....	112
Figure 9.22 : A Pure Phase Shift affects the eccentricity of the lissajous oval.	114
Figure 9.23 : Lissajous figures for two signals.	115
Figure 9.24 : Cross Plots of the normalized wheel forces at the PG and CU.	119
Figure 9.25 : Correlated wheel forces at the some intervals (schematically).	120
Figure 10.1 : Typified load amplitude spectra.	121
Figure 10.2 : Spectrum shape parameters and break of slope of CU and PG.	124
Figure 10.3 : Comparison of shape parameters on the CU and PG.	125
Figure 10.4 : Comparison of break of the spectrum slopes at the proving ground.	126
Figure 10.5 : Difficulty to calculate shape parameter of the CU for $R_{L,x}$	127
Figure 11.1 : Flow Chart of the methodical and systematical approach.	133

DETERMINATION OF A METHODOLOGY TO DEVELOP DURABILITY APPROVAL TEST OF COMMERCIAL VEHICLE AXLES

SUMMARY

The demands for cost and weight reduction in connection with an increase in payload are top priorities in lightweight construction of commercial vehicles, especially safety components must not be failed under operational conditions. Axles and axle guiding components (suspension parts) are subjected to various external loads dependent of the field of the application (long-distance or short-distance vehicles, off-road trucks, and busses), the stiffness of the vehicle structure, the nominal payload and the road conditions. Based on this knowledge, a load spectrum to perform the experimental durability tests of commercial vehicle axles has to be derived taking into account the service loading conditions.

In order to derive of a load spectrum for the structural durability approval of commercial vehicle axles, it is necessary to perform vehicle measurements as much as possible on the characteristic routes with the wheel force transducers (WFT). Thus, the loads acting on the axles can be measured and lately analyzed in terms of structural durability. For this purpose, a long-term vehicle measurement (Road Load Data Acquisition) is done on the characteristic routes (customer-usage, CU) in Turkey with a two-axle coach (an independent front axle and rigid rear axle) for the first measurement campaign. Afterwards, another measurement is also performed at the proving ground location (PG) of commercial vehicle manufacturer.

In this study, it has been observed that there are some main factors to be calculated in order to derive a load spectrum for structural durability approval of commercial vehicle axles. With respect to durability point of view, some main factors such as scaling factors, phase relationship between wheel forces, extreme loads and shape parameters of the spectrums has been investigated by means of this methodology. This developed methodology, which is necessary to derive a standardized load spectrum to generate a test procedure for structural durability approval of commercial vehicle axles, differentiate from other studies in the way of systematical analysis procedure. All the mentioned technique and methods in this study are also available in literature; however, these techniques and methods are used to create a systematical data analysis procedure for the commercial vehicle axles. This is the main difference of this study from others.

Based on the measurements on the customer usage and at the proving ground, it is aimed to determine these parameters, which helps us lately to develop a test procedure for the structural durability approval of commercial vehicle axles.

The main problem to derive a load spectrum for commercial vehicle axles is economic cost because the required long-time road load-data acquisitions with wheel force transducers are expensive. Apart from this, the analysis of the measured data is also significant time-consuming. On the other hand, the advantages of a load

spectrum are significant simplification of transfer the realistic load assumption from forerunner design to the new design and a time-optimized determination of test programs; as a result, the weak points will be rapidly identified.

As long as we do not have any idea of the loading acting to the axle, or if previous measurements are not available, then we have to perform some measurements, where we can define the loads acting to axle. This is a very important step of this study because of their costs and preparation. Certainly, it is also a point to discuss, which roads should be measured with which vehicle. The characteristic routes or so-called reference-customer usage profile is formed that contains all relevant loads of partially very different customer operations. During the customer-usage profile measurement, the vehicle was always full loaded. The choices of the roads have been done according to the traffic volume distributions with reference to the Turkey General Directorate of Highways and the information of the truck & bus services of commercial vehicle manufacturer.

The aim of this phase is to record all the relevant load information on the vehicle through Turkish roads following the route defined. The results of this activity were the time histories of the signals coming from the sensors located in the vehicle during the RLDA (Road Load Data Acquisition) performed over Turkish customer usage. In addition, another measurement is performed at the proving ground, where we can calibrate/rearrange our test track according to the measurement of the customer usage. Another main concern of this measurement is the make a comparison between the customer and test track, thus we can say how far our test track remain from the customer usage results. The output of this comparison is a relation or a function between test track and customer usage. Thus, it is possible to derive load spectrums without any expensive and time-consuming customer usage measurements.

Product validation tests are essential at later design stages of product development. In the automotive industry, durability testing in a laboratory is an accelerated test that is specifically designed to replicate fatigue damage and failure modes from proving grounds (PG) testing. Detailed damage analysis is needed to correlate the accelerated test to PG testing. Therefore, accurate representation of PG loading is essential for laboratory-durability test development. PG loading is measured by driving an instrumented vehicle over the PG. The vehicle is equipped with the same transducers for component loading histories and same sensors for other important vehicle parameters as mentioned. The proving ground (test track) measurement campaign is performed with three different vehicle loading conditions (empty, half-loaded and loaded).

In the next step, which is the load data analysis on the customer usage and the proving ground, is a significant step to determine and describe the service loads that in most cases display a random nature. In such cases, they can be illustrated through so-called design spectrum. In this point, we have determined the cumulative frequency of the spectrum. After obtained design spectrum, the scaling factors are calculated. The idea behind of this, it is a factor, which helps us to scale the wheel forces in one direction to another direction. As explained above, those factors give us enormous benefit to calculate or estimate the other wheel forces such as lateral and longitudinal when only vertical wheel forces are available.

Apart from these, high loads in the driving are considered as extreme loads. The probability of these loads rises with the increasing mileage, which means that these are single events with low occurrences relevant to customers. These extreme loads

are closely related to the dimensioning consideration of the components. Therefore, the derivation of reliable extreme load assumptions is necessary. These extreme values are derived based on Gumbel's approximation from the short-term measurement on the customer usage with fully loaded case with 3664 km mileages in Turkey, which can be expected after 1 million km.

In the second phase of the load data analysis, is the determination of the phase angle, if it exists, between the wheel forces acting to directly to the commercial vehicle axles. In literature, there are some ways to determine the phase angles of stationary random signals in a rough estimate. It is intended to evaluate and determine the phase angles of non-sinusoidal signals of the wheel forces, which are measured on the customer usage and at the proving ground. This information enables us to evaluate and define whether the high loads occur simultaneously or chronologically in the each channel (each direction) of the wheel forces by the experimental durability tests of the axles.

In order to achieve this, three methods are used for the phase angle of a periodic non-sinusoidal signal and non-periodic non-sinusoidal signal. These methods are zero-crossing method, frequency response analysis (FRA) and correlation analysis with cross plots respectively. In conclusion, when we consider all the methods explained above in order to find the phase relation of the different wheel forces at the customer usage and at the proving ground, we can say that there is no representative and dominant phase relation between the measured wheel forces. On the other hand, there are some good correlation results between some investigated wheel forces; however, it is not valid for all the measurement intervals.

In fact, all the wheel forces occur arbitrary due to the nature of road excitation at the customer usage. The result of this analysis is the systematical analysis procedure to evaluate and determine the phase angle of wheel forces.

Finally, one of the most important parameter of a load or test spectrum is the shape parameter. In order to characterize the shape of the spectrum of individual load-time histories by a single number, the “spectrum shape parameter” is also calculated. Shape parameters have traditionally been used in various formats, for example in fatigue standards, in order to characterize the combined effect of block size and cumulative frequency of load amplitudes – partly adopting Miner’s rule. Those shape parameters are calculated for both measurement campaigns.

Based on the outcome of the studies conducted, the four main parameters for the definition of a load or test spectrum have been found/calculated for the experimental durability tests of the axle of a two-axle coach. At the last phase of this study, all the results/obtained parameters are summarized and documented. These calculated parameters define the load spectrum for the experimental durability tests of the axle of a two-axle coach. If the same methodical and systematical approach is considered and executed for the next long-term commercial vehicle measurements (for example, a truck measurement), then it is also possible to derive the standardized load sequence for the experimental durability tests of the commercial vehicle axles. Therefore, with the help of all these tests and improvements, this methodology can be beneficial reference/method for the generation and use of standardized load spectrum and load–time histories of the commercial vehicle axles that will be experimentally tested in the future. Another beneficial output of this study is the derivation the load spectrums without any expensive and time-consuming customer usage measurements because of the obtaining the parameters mentioned above.

TİCARİ TAŞITLARDAKİ AKSLARIN DAYANIM ONAY TESTİNİ OLUŞTURMAK İÇİN BİR YÖNTEM GELİŞTİRİLMESİ

ÖZET

Bir taşıt tasarımının gerçekleştirilmesi birçok etkene bağlı olmaktadır. Kullanıcı ile imalatçı arasındaki bilgi transferinin sağlandığı servis noktaları, ürünün farklı kullanıcılar için veri bankaları olduğundan, tasarımın geliştirilmesi açısından oldukça önemli bir nokta teşkil etmektedir. Ortaya çıkarılacak ürünün çalışma dayanımının tespit edilmesi gerekmektedir. Bir taşıtın veya parçanın çalışma dayanımının saptanabilmesi için gerekli olan dört ana parametre vardır. Bunlar çevre koşullarının da dâhil olduğu yükleme durumu, ürünün geometrisi, malzemesi ve imalat özellikleridir. Uygun bir tasarımın gerçekleştirilebilmesi için de, çalışma sırasında karşılaşılan dış yüklerin, ürünün kritik bölümlerine etkiyen bölgesel gerilmelerin, malzemenin yorulma davranışıyla ilgili özelliklerinin bilinmesi gereklidir. Bu şekilde, taşıt veya taşıta ait bir parça için gerekli olan “güvenirlilik” ve “emniyet” faktörleri saptanmış olacaktır. Dolayısıyla aşırı yükleme gibi özel durumlarda ürünün minimum ömrünün saptanması bu açıdan önem kazanmaktadır. Ürün ömrünün belirlenmesi veya biçilen ömür içerisinde bütün fonksiyonlarını yerine getirmesi üründen istenen temel özelliktir. Bu sebeple günümüz ürün geliştirme kavramında, taşıt, aks ve bileşenlerinin yorulma ve ömür kavramları ön plana çıkmış bulunmaktadır.

Taşıtların yorulmadan kaynaklanan ömürlerinin saptanması amacına yönelik çeşitli yöntemler geliştirilmiştir. Bu yöntemlerin en basiti, taşıtı belirlenen yol güzergâhlarında (müşteri odaklı testler) öngörülen kilometre kadar yol kat edilmesi ile gerçekleştirilen testlerdir. Taşıtın karayollarında test edilmesi, basit olmasına rağmen oldukça zaman alıcı, pahalı ve tekrarlanabilirliği hemen hemen imkânsız bir süreçtir. Diğer bir test yöntemi, belirli yol kalitelerinden meydana gelen özel pistlerde taşıtın test edilmesidir. Bu şekilde zaman süreci belli ölçülerde azaltılmış olmakta, ancak bu yöntemde de gizlilik sorunu aşılammamaktadır. Mevcut son yöntem gerçek yol verisi kullanmak suretiyle taşıtın laboratuvar ortamında test edilmesidir. Günümüz otomotiv sanayinde gerçek yol verileri kullanılarak hızlandırılmış yorulma ömrü testleri ürün geliştirme aşamasında yaygın olarak uygulanmaya başlamıştır. Ancak gerçek yol verisinin elde edilmesi ve buna ait teknik özelliklerin belirlenmesi hayli karmaşık ve ölçüm hatalarını da içeren bir faaliyettir.

Taşıt bir bütün olarak düşünülürken ve istenilen ömür doğrultusunda hareket edilerek hesaplamalar yapılmaktadır. Örneğin bir binek otosu için 300,000 km bir yorulma ömrü otomotiv üreticileri için global hale gelmiş bir değerdir. Bu değer, ticari vasıtalarda 1.000.000 km veya daha yüksek değerlere çıkabilmektedir. Bir taşıtın ömrünü belirleyebilmek için, o taşıttan beklenen özellikler önemli bir yer tutmaktadır. Bu taşıt bir arazi aracıysa, dağlık arazilerde ve düz yollarda gidecek şekilde tasarımın oluşturulması gerekecektir. Dolayısıyla ömür hesaplamasında taşıta gelen yüklerin bu şartlar düşünülerek hesap edilmesi gerekecektir. Önceden de söz

edildiği üzere; bir taşıtın geliştirme sürecindeki önemli bir kısmını oluşturan dayanım test süreci, söz konusu taşıtın kullanım şartları ve aynı zamanda o bölgede veya ülkedeki yol şartlarına göre, genel olarak 3 farklı şekilde gerçekleştirilmektedir:

1. Müşteri odaklı testler (Müşteri çevrimindeki taşıt testleri)
2. Kötü yol test pistindeki testler (Hızlandırılmış test parkuru)
3. Laboratuvar testleri (Hidrolik sarsıcılarda hızlandırılmış ömür testi)

Müşteri odaklı testler genelde bir ticari taşıt üreticisi için 1 milyon kilometredir. Bu değer ticari taşıt üreticinin söz konusu taşıt için belirlediği ömürdür. Hedef, taşıtın güvenlik açısından önemli olan süspansiyon ve aks elemanlarının, bu süre içerisinde kırılmaması veya hasarlanmamasıdır. Genelde, bu elemanlarda çalışma şartları altında gerçekleşen kırılmalar yorulma hasarlarından kaynaklı yorulma kırılmalarıdır. Kötü yol test pistindeki testlerde ise esas hedef, test süresini kısaltmaktır. Yukarıda söz edildiği gibi müşteri odaklı testlerdeki 1 milyon hedef kilometresine ulaşılabilmesi için gerekli süre, genelde bir veya iki yıl olabildiğinden, kötü yol test pistlerinde bu süreyi altı aya kadar düşürebilmek mümkündür. Elde edilen en önemli kazanç ise, test süresinin kısaltılmasıdır. Laboratuvar testlerinde ise amaç, en kısa zamanda en doğru şekilde kıyaslanabilir ve tekrarlanabilir veriler veya sonuçlar elde edebilmektir. Örnek olarak burada sözü geçen dayanım test süresi 3-5 hafta arasında değişebilmektedir.

Özetle, ömür testlerinde; kullanım ömrü boyunca taşıt akslarının işletme şartları altındaki dayanıklılığın belirlenmesi ve yorulma açısından incelemesine ihtiyaç duyulmaktadır. Bu nedenle, taşıt aks ve süspansiyon parçalarının tasarımında yorulma ve ömür kavramları günümüz ürün geliştirme kavramında ön plana çıkmış bulunmaktadır. Zira taşıtlar yolda seyir halinde iken aks ve diğer elemanları dinamik yüklere maruz kalmakta, bunun sonucunda da bazen yorulmaya bağlı hasarlar, öngörülen kullanım ömründen daha önce ortaya çıkabilmektedir. Bu amaçla, taşıt aks ve diğer süspansiyon elemanlarının günümüze uygun tasarımında yol verilerinin kullanıldığı incelemelere, testlere ihtiyaç vardır. Bir taşıt aksının yorulmadan kaynaklanan ömrünün hesaplanabilmesi amacıyla ilk önce taşıtın normal işletme koşullarını tanımlayarak tasarım spektrumu'nun oluşturulması gereklidir. Söz konusu makina parçasına etki eden kuvvet, moment, ivme veya deplasman genliklerinin belirli bir zaman süresine göre istatistiksel dağılımı "Yükleme Kolektifi" olarak adlandırılır. Yorulma ömrü boyunca yükleme kolektifi az veya çok sayıda tekrarlanır. Belli bir zaman dilimi için elde edilmiş yükleme grafiğinden yararlanarak "yükleme birikim eğrisi" elde edilir. Bu eğri, ele alınan işletme zamanı içinde belirli bir seviyedeki yüklemenin, kendisinden yüksek olanlarla birlikte ne kadar sürdüğünü gösterir. Tasarım spektrumu ise, taşıt üreticisinin işletme koşullarını tanımladığı parçaya belli bir zaman dilimi için elde edilmiş bir yükleme birikim eğrisidir. Diğer önemli bir tanım ise test spektrumu'dur. Test spektrumu, yukarıda belirtilen tasarım spektrumunun laboratuvar testlerine aktarılmasıdır. Bu işlemde, küçük yüklerin ihmal edilmesi ile birlikte orta büyüklükteki yüklerin çevrim sayısının artırılmasıdır.

Taşıtların ömürleri boyunca, farklı şartlarda kullanılanlar da olmakla birlikte, istatistikî olarak ortalama % 60 iyi, % 40 kötü yol şartlarına maruz kaldığı kabul edilebilir. Bu yaklaşım taşıt imalatı açısından genel bir yaklaşım olup, imalatçının veya tasarımcının o araçtan istediği özelliklere göre bu oranları değiştirmesi veya sınıflandırmayı çoğaltması ile mümkündür. Bu belirtilen tasarım spektrumu verilerine göre müşteri odaklı testler gerçekleştirilmiştir. Müşteri çevrimindeki taşıt testlerinde toplamda 3664 km'lik kuvvet, moment, ivme ve yer-değiştirme genlikleri

ölçülmüştür. Ölçümleri gerçekleştirebilmek için ölçüm donanımlarının kalibrasyonu ve taşıta yerleştirilmesi gerekmektedir. Bu ölçüm donanımları arasında birçok algılayıcılar bulunmaktadır. Kuvvet algılayıcıları (yük hücreleri), birim şekil değişimlerini ölçmek için gerekli algılayıcılar (Strain-Gage), mesafe algılayıcıları, ivme-ölçerler gibi algılayıcılar olarak sıralanabilir. Strain-Gage gibi algılayıcıların özel bir sinyal koştulamaya gereksinimi vardır. Ölçülecek bölgeye göre değişiklik gösteren düzlemsel gerilme-şekil değiştirme bağlantılarını elde edebilmek için, sinyal koştulamada değişik köprü-kablo bağlantılarına ihtiyaç vardır (örneğin; çeyrek, yarım veya tam köprü kablo bağlantıları). Süspansiyon elemanlarında, özellikle süspansiyon kollarında, Strain-Gage (SG) (birim uzama-şekil değiştirme elemanı) uygulamasından sonra kalibrasyon işlemi gerçekleştirilerek parça üzerine gelen kuvvetler ölçülmüştür. Tekerlekten yük ölçerler yardımıyla aksel, yanal ve dikey kuvvetler (F_x , F_y , F_z) ve bunlara karşılık gelen momentler (M_x , M_y , M_z) elde edilmiştir. Malzemede oluşan iç gerilmeleri bulmak için malzeme yüzeylerindeki “strain” (birim uzama-şekil değiştirme) değerleri ölçülmüştür.

Tasarım spektrumu verilerine göre müşteri odaklı testler gerçekleştirilmiştir. Müşteri çevrimindeki taşıt testlerinde toplamda 3664 km’lik kuvvet, moment, ivme ve yer-değiştirme genlikleri ölçülmüştür. Her taşıt üreticisi tarafından belirlenen referans müşteri, taşıtın veya parçanın ömrü boyunca maruz kaldığı en yüksek dinamik yüklerin gerçekleştiği yol şartı ve kullanım koşuludur. Bu çalışmadaki referans müşteri, söz konusu ticari taşıtın seyir halinde en yüksek gerilme genliklerinin gerçekleştiği Türkiye müşterisidir. Taşıt üreticileri tarafından referans müşterinin belirlenmesindeki 3 önemli parametre aşağıdaki gibi sıralanmıştır.

1. Taşıtın yüklenmesi (yolcu ve yükleme durumu)
2. Yol kalitesi
3. Seyir ve sürüş biçimi

Türkiye Kara Yolları Genel Müdürlüğü’nden alınan taşıt yoğunluk haritalarındaki bilgiler ve satış sonrası hizmetlerin verileri neticesinde Türkiye ölçümü iki akslı bir şehirlerarası otobüsü ile belirli yol güzergâhlarında gerçekleştirilmiştir. Taşıt izin verilen maksimum aks yüklerinde yüklenmiştir. İki akslı bir şehirlerarası otobüsünün ön aksi bağımsız, arka aksi ise katı (rijit) bir akstır.

Tüm yol tipi, ilgili işletme şartları ve yükleme genliklerinin belirlenmesi için zaman bazındaki verilerin tek parametrelili sayma yöntemlerinden Range-Pair ile kısmi yükleme birikim eğrisi (H_{Bi}) oluşturmuştur. Range-pair bir sayma yöntemi olup, bu yöntem ile salınım bölgelerinin frekansını tespit edilir. Bir salınım bölgesi eşdeğer boyutlu pozitif ve negatif dönüşlere sahiptir. Eşdeğer salınımlar toplanıp, sonuç kümülatif frekans değişimi olarak temsil edilir. Elde edilen kısmi yükleme birikim eğrilerinden tasarım spektrumunu oluşturabilmek için doğrusal ekstrapolasyon (matematikte dış değer biçmek) ve süperpozisyon matematiksel işlemlerinin gerçekleştirilmesi gerekmektedir. Doğrusal ekstrapolasyon, bilinen bir yükleme birikim eğrisinin bir teğet doğrusunu oluşturup bu doğruyu bu sınırdan daha ileriye uzatmak suretiyle elde edilir. Doğrusal ekstrapolasyonun iyi sonuçlar vermesi şartları bilinen yükleme birikim eğrisinin yaklaşık olarak doğrusal değişimleri ve ekstrapolasyonun bilinen verilerden çok daha uzak olmamasıdır. Süperpozisyon ilkesi, iki veya daha fazla doğrusal ekstrapolasyonu gerçekleştirilmiş yükleme birikim eğrilerinin aritmetik toplamı olarak ifade edilir. Ölçülen yol verilerine bu matematiksel işlemler uygulanarak parçaya ait tasarım spektrumu oluşturulur.

Yol-verisinin incelenmesinde diğerk bir nokta da düzeltme faktörlerinin hesaplanmasıdır. Düzeltme faktörleri, farklı tekerlek kuvvetlerine ait tasarım spektrumlarının arasındaki matematiksel oran olarak tanımlanabilir. Bu sayede, dikey tekerlek kuvvetlerine ait yükleme birikim eğrisine göre değişken “bağlı tekerlek kuvvetleri yükleme birikim eğrisi” elde edilir. Tüm yükleme birikim eğrileri dikey tekerlek kuvvetine ait eğriye göre ayrıştırılmıştır (Normalizasyon). Buna göre, tekerlek göbeği üzerinden aksa gelen zorlamaların dağılımı bilinmektedir. Zorlanmalara ait bu dağılım, sonrasında laboratuvar ortamında hidrolik sarsıcılar yardımıyla parça üzerinde de elde edilmeye çalışılacaktır. Bu veriler ile birlikte, test spektrumunu oluşturmak için faz açısı (Φ) da hesaplanmalıdır. Söz konusu faz farkı neticesinde, parça üzerinde farklı genlikte zorlanmalar meydana gelebilmektedir. Ancak, tekerleğe gelen yükler neticesindeki aks ve aks elemanları üzerindeki dinamik, tekrarlı veya sürekli olmayan (rastlantısal) zorlamalarda faz farkını elde etmek için literatürde bir çözüm yoktur. Bunun yerine bazı yaklaşımlar geliştirilmiştir.

Tekerlek kuvvetleri arasındaki faz açısının incelenmesi dayanım testleri açısından önemlidir. Yorulma teorisinde, bir makina parçasına etkiyen maksimum gerilme genliğinin artması parça ömrünü azalmaktadır. Ölçülen tekerlek kuvvetleri laboratuvar ortamındaki hidrolik sarsıcılarda aks üzerine uygulanacağından, kuvvetlerin aks veya tekerlek göbeği üzerine eş ya da farklı zaman sürelerinde etkimesi farklı test sonuçlarına sebebiyet verecektir. Bu nedenle faz ilişkisinin de incelenmesi gerekmektedir. Söz konusu faz ilişkisinin incelenmesi için geliştirilen bir yöntem de korelasyon analizi yöntemidir.

Korelasyon analizi; dinamik, tekrarlı veya sürekli olmayan (rastlantısal) zorlamalarda tekerlek üzerinden ölçülen kuvvetler arasındaki ilişkiyi tanımlar. Korelasyon, iki rastlantısal değişken arasındaki doğrusal ilişkinin yönünü ve gücünü belirtir. Genel olarak veri analizi kullanımında korelasyon, bağımsızlık durumundan ne kadar uzaklaşıldığını gösterir. Buna göre, tüm yol tiplerinde elde edilen tekerlek yüklerine ait korelasyon analizleri gerçekleştirilmiştir. Tekerlek kuvvetleri arasındaki ilişki tam olarak tanımlanamaması ile birlikte, faz açılarının rastlantısal olarak oluştuğu yani belirgin bir faz açısının olmadığı tespit edilmiştir.

Müşteri çevrimindeki ölçüm yaklaşık 3000 km’lik bir ölçümdür. Bu ölçümde tekerleğe etkiyen maksimum kuvvet genlikleri taşıtın ön görülen 1.000.000 km içinde etkiyen maksimum genliklerden büyük olasılıkla düşük olacaktır. Taşıtın daha uzun kullanımında karşılaşılabilecek kötü yol karakterlerinde oluşan bu kuvvet genliklerini Gumbel uç değer teorisi yöntemi ile istatistiki olarak modelleyip hesaplamak mümkündür. Gumbel uç değer teorisi, tekrarlanan örneklemelerdeki en küçük veya en büyük değerlerden oluşan rastgele değişkenlerin olasılık dağılımlarını göz önüne alan bir teoridir. Gumbel uç değer teorisi yöntemi yardımıyla maksimum tekerlek kuvvetleri hesaplanmıştır.

Diğerk önemli bir parametre ise, yükleme kolektiflerini nitelendirmek için gerekli olan kolektifin şekil parametresidir (v). Hesaplanan bu parametreler ise, yükleme genliklerinin matematiksel olarak tanımlanmasıdır.

Yol-verilerinin incelenmesi neticesinde elde edilen yükleme birikim eğrileri ve bunlara ait parametreler son bölümde özetlenmeye çalışılmıştır. Laboratuvarda taşıt testlerinin gerçekleştirilebilmesi için elde edilen bu parametrelerin, hidrolik test standındaki sisteme girilmesi gerekmektedir. Bunun neticesinde; yol ölçümünde elde edilen aks üzerindeki zorlanmalar, hidrolik sarsıcılar tarafından test standında tekrar

oluşturulabilmektedir. Elde edilen sonuçlar ışığında, tekerlek kuvvetlerinden yola çıkarak oluşturulan test spektrumuna ait yüklenme birikim eğrisinin parametreleri yardımıyla laboratuvar da taşıt testleri gerçekleştirilir.

Neticede, günümüzde taşıtların geliştirme faaliyetlerinde yüksek dayanımlı parçaların yanı sıra, hafiflik ve konfor gibi diğer parametrelerin de gittikçe önem kazanması ile birlikte, taşıt üreticileri de bu talepleri karşılayacak yeni yöntemlerin geliştirilmesine çalışmaktadır. Ürün geliştirme sürecindeki yöntemleri sürekli bu değişen talepleri karşılayacak şekilde geliştirilmesi de bazı çalışmaların yapılmasına olanak sağlamaktadır. Bu çalışmada da ticari taşıtlarda kullanılan aksların işletme şartları altındaki yüklemelerin sistematik bir biçimde incelenip, yorulma dayanımını belirleyen parametreler açısından değerlendirilerek dayanım test yönteminin belirlenmesi ve iyileştirilmesi amaçlanmıştır.

Taşıt aks ve süspansiyon parçalarının, günümüzde tekrarlı dinamik yüklemeye göre tasarımına uygun yol verilerinin kullanıldığı incelemelere ve araştırmalara ihtiyaç vardır. Ömür ile ilgili dayanımının belirlenmesi amacıyla yapılacak araştırmalarda kullanılacak yüklenme değerlerinin belirlenmesi için gerçek yol ve kullanım şartlarında parçaya etki eden yüklemelerin bilinmesi gereklidir. Söz konusu olan bu yüklemeler, yüklemelerin tekrar sayısı ve salınımların genlik çiftlerinin belirlenmesi ile birlikte, yüklenme birikim eğrileri elde edilir ve laboratuvar ortamında da bu yüklemeler hidrolik sarsıcılar yardımıyla parça üzerinde tekrar oluşturularak ömür testleri gerçekleştirilir. Müşteri odaklı ve kötü yol test pistindeki ölçümlerde akslar üzerinden elde edilen veriler, sistematik olarak yorulma dayanımı açısından incelenmiştir. Bu çalışmada oluşturulan veri inceleme yöntemi sonucunda, yüklenme birikim eğrilerine ait parametreler hesaplanmıştır. Hesaplanan parametreler; maksimum yüklenme genlikleri (F_{max}), yüklenme genliklerinin tekrar sayıları (H), tekerlek kuvvetlerinin faz açısı (ϕ), kolektife ait şekil parametresi (v) ve düzeltme faktörleri (f_i) olarak özetlenebilir.

Hesaplanan düzeltme faktörleri incelenecek olursa, ön ve arka akstaki eksenel ve dikey tekerlek kuvvetleri arasında 2,5 oranında bir değer olduğu görülmektedir. Aks gövdesine etkiyen dikey tekerlek kuvvetlerinin %40'ı eksenel kuvvet olarak aks gövdesine de etki etmektedir. Bununla birlikte yine aynı şekilde, yanal ve dikey tekerlek kuvvetleri arasında 3,3 oranında bir değer hesaplanmıştır. Bu da, dikey tekerlek kuvvetlerinin %30'unun yanal tekerlek kuvveti olarak aks gövdesi üzerinde zorlanmalara neden olduğu şeklinde yorumlanabilir. Gumbel uç değer teorisi yöntemine göre, müşteri çevrimi ölçümü neticesinde her bir tekerlekten elde edilen maksimum yüklenme genlikleri, test pisti referans değerlerinden çok farklılık göstermemektedir. Faz farkının incelenmesine yönelik çalışmalar neticesinde ise, tekerlek kuvvetleri arasında herhangi bir baskın faz açısı bulunmamaktadır. Aks gövdesi üzerindeki zorlanmaların, tekerlekten gelen uyarı sinyalleri arasındaki ilişkiden bağımsız olduğu belirlenmiştir.

Sonuç olarak, aksların çalışma koşulları altında elde edilen yol verilerinin (müşteri çevrimi ölçümleri) incelenip bir dayanım test yöntemi oluşturulmaya çalışılmıştır. Bu çalışmada hesaplanan parametrelerin, hidrolik test standındaki sisteme girilmesi ile birlikte aksların laboratuvar ortamında hızlandırılmış ömür testlerinin gerçekleştirilmesi amaçlanmıştır. Aynı zamanda, müşteri çevrimi ile test pisti arasındaki ilişki de oluşturulmuş ve hali hazırdaki test yöntemi içerisindeki uzun müşteri çevrimi ölçümlerinin sayısı azaltılarak, giderlerin azaltılmasına yönelik sonuçlar da elde edilmiştir.

1. INTRODUCTION

It is well established that the structural durability performance of materials and structures may be very sensitive to the specifics of the loading encountered. Beside constant amplitude testing, therefore, tests with realistic load sequences are often required in order to assess any susceptibility to the specifics of variable amplitude loading and to demonstrate the in-service life for given materials and structures.

For these purposes standardized load-time histories (SLH's) have been developed for 30 years since it has been recognized that the use of SLH's a series of advantages – both for studies of a more generic nature and practical applications [1].

In this study, the external and internal loads of axles on commercial vehicles (especially trucks and buses) will be measured on the customer and reference routes and afterwards their phase relationships will be examined in order to create realistic test procedure for the related axles.

2. ASSIGNMENT OF TASKS

2.1 Aim of the Study

The aim of the study is to derive an experimental structural durability approval of commercial vehicle axles with respect to the standardized load sequence with easy adaptability to the different vehicles and axle loads considering the realistic phase relationships of external loads in the service load-data acquisition.

The study will be focused on (according to the methodical and systematic approach);

- the heavy and light range,
- drive, non-driven axles,
- fast and accurate derivation of the customer-oriented loads on test-rig,
- transferability to the future axle concepts and tests,
- load data acquisition with wheel force transducers and applied strain gages on chassis components,

2.2 Advantage of the Study within the Scope of Axle Development

- significant simplification of transfer the realistic load assumption from forerunner design to the new design,
- time-optimized determination of test programs, as a result the weak points will be rapidly identified.

At the following figure, the flow chart of the axle testing can be seen.

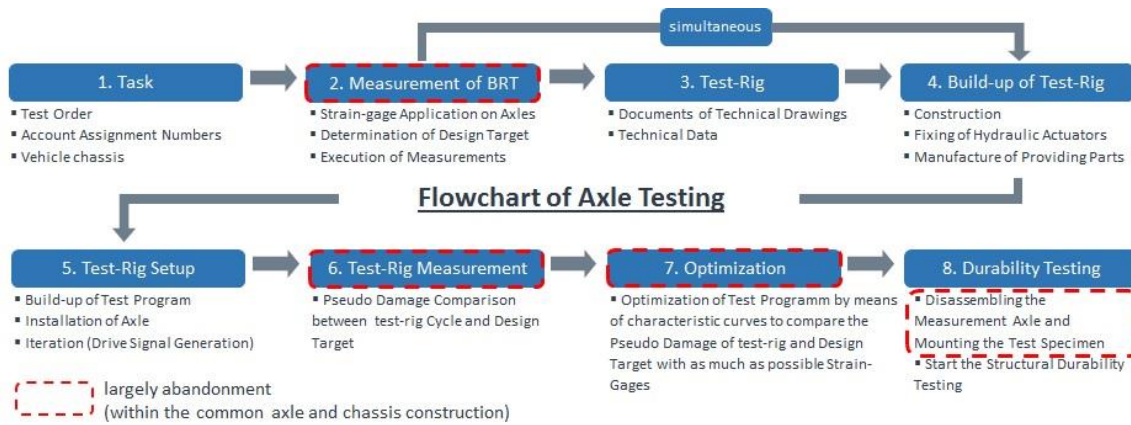


Figure 2.1 : Flowchart of axle testing.

2.3 Description of Further Development Needs

- Enabling realistic service load simulation on the basis of measured wheel force/moment (wheel force transducer) with dominant phase relationships,
- Reproduction of exact local stress from measured wheel forces,
- Building a methodical and systematic approach,
- Simulation of external loads (load time histories) on the test-rig, in which adjusts realistic kinematical relationship through the usage of original structural,
- Attachment parts as in the vehicle,
- Actualization of test program and procedure according to vehicle types and usage regions,
- Optimization of the calibrations between test-rig and vehicle.

2.4 Actual Test Method for Durability Approval of Commercial Vehicle Axles

2.4.1 Advantages and disadvantages

2.4.1.1 Advantages

1. Block program testing
 - exact repeatability,
 - easy and precise adjustment of test-rig (Iteration),

- applicable to compare the component variants,
2. Low-frequency testing with synthetic block programs
 - longtime experience about the adjustment of the test-rig,
 - the test program and all necessary parameters can be easily generated with the help of a tool,
 3. Longtime Field Proven Approach
 - However: over dimensioned components

2.4.1.2 Disadvantages

1. Measurement a test cycle on the test-rig and calibration with the peak values of strain-gages on the bad road measurements
 - high development costs
2. Due to the missing phase information (phase effect), it could be not determined if the high loads occur simultaneously or chronologically in the each channel
 - derivation of the test program is only limited possible,
 - reduction of the load data only is limited possible,
 - overall insufficient description of loading situation,
3. Difficulty of the lifetime prediction based on block program testing
 - Adjustment of the realistic phase relationships for the quasi-determined loads is only limited possible
4. Through the fixed load-level sequence is reproduced the sequence effect by experience
 - unreliable reproduction of the load sequence effect
5. Synthetic loads are calculated from the functional blocks
 - highly dependent on axle kinematic und physics of driving

2.4.2 Test-rig setup

Build-up of the axle arch on the test-rig in consideration of similar stiffness relationship to the vehicle installation

- Ensuring possible realistic deformation behavior of the axle arch

2.4.3 Derivation of design and test spectrum

The basis is a revised Standard program (SPRILOS "SPRIng LOad Sequence"), which is built up of physically defined loading conditions (Straight driving on the bad roads, Cornering, Braking and Start). At the following figure, actual testing method can be seen.

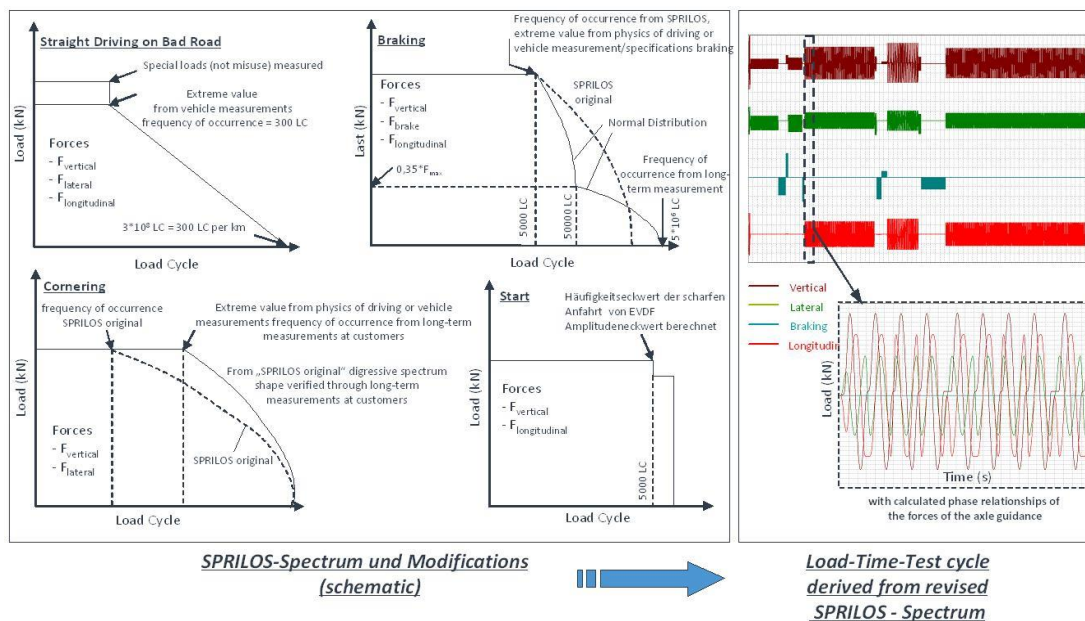


Figure 2.2 : Actual testing method.

Optimization through the variation of phase relationships and the amplitudes of the dynamic forces (load factors from LBF – “Laboratorien für Betriebsfestigkeit” load database) in order to adjustment local stresses on the axle beam at the critical points of axle arch.

2.4.4 Release criteria

1. Number of Test specimens:
 - minimum 3 (known manufacturer)
 - minimum 5 (for new or unknown manufacturer)

2. Failure Criteria:

- technical cracks
- oil-leakage

Assumption of 90% probability of survival with a 90% confidence level of 100% design spectrum.

2.5 Methodical and Systematical Approach

At the following figure, the methodical and systematical approach can be seen.

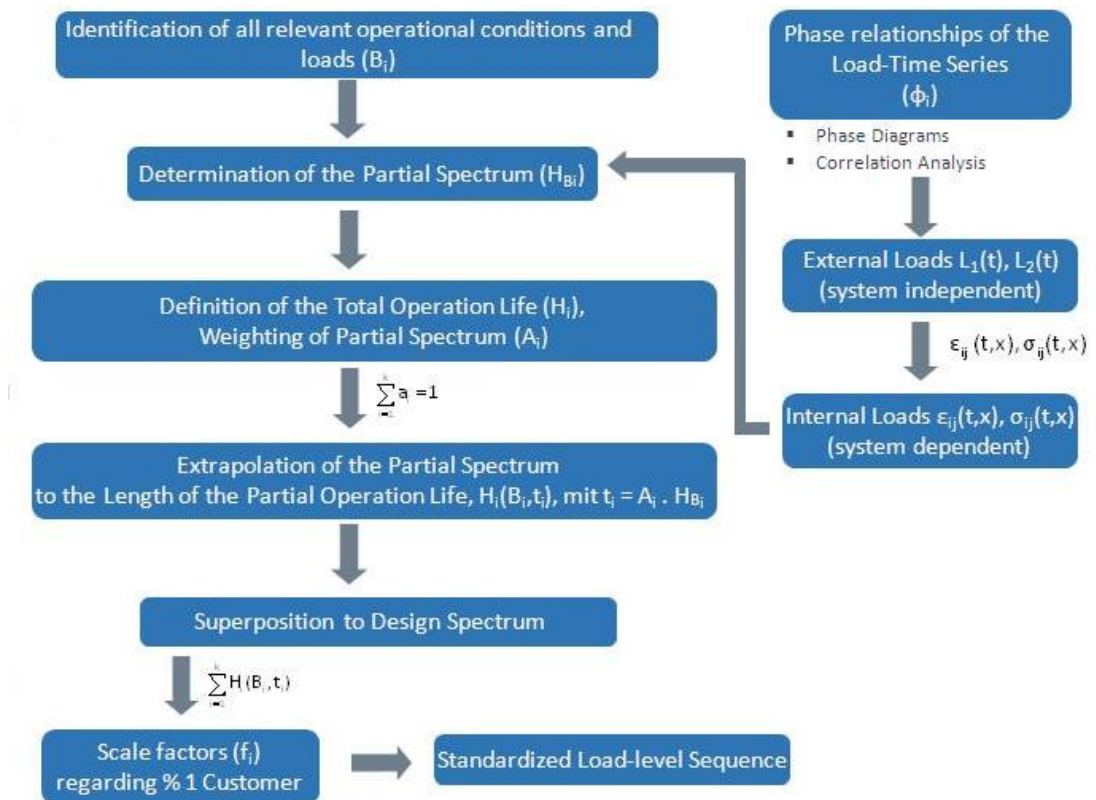


Figure 2.3 : Methodical and systematical approach.

This methodology will be used in the next sections.

3. STATE OF THE SCIENTIFIC AND TECHNICAL KNOWLEDGE

The durability approval of commercial vehicle axles is performed on proving grounds with well-defined road characteristics as well as in laboratory test facilities simulating these loading conditions. These proof-out tests are supposed to reproduce within a reasonable time the customer usage conditions, which are expected during the life of a vehicle taking into account the large scatter of service. The programs and requirements are based on extensive measurements as well as long-term experience. However, the development of vehicles for specific mission profiles as well as the introduction of components from new lightweight material and innovative manufacturing technologies with different durability properties requires procedures for the evaluation of the programs themselves [2]. The design criterion for a commercial vehicle axle is the attainment of the expected service life with the necessary reliability and safety. The service life is influenced mainly by the following interactive parameters: design (geometry), loading, material and manufacturing. The multi-axial loads acting under operational conditions create these stresses. Highly stressed areas depend on the design of the component with respect to the loading: notches, holes, cross section discontinuities as well as the dynamic answer of the system to the variable loads. If the loading conditions in service are known, the stresses occurring in the critical areas can be determined by theoretical calculations or with an experimental stress analysis. For the durability evaluation and approval by tests, the loading conditions and the created stresses are analyzed with respect to amplitudes, mean values, frequency of occurrence and correlation, to determine the design spectrum for the loading. The service conditions of the truck are appointed from field experience and long-term measurements with comparable vehicles and components. In relation to the physical origin of the loads acting on the axle, the physical loading conditions are distinguished: Straight Driving, Cornering and Braking. The load conditions at the wheel create the stress conditions on the axle depending on the transfer functions. Forces acting on a wheel are plotted in the following figure.

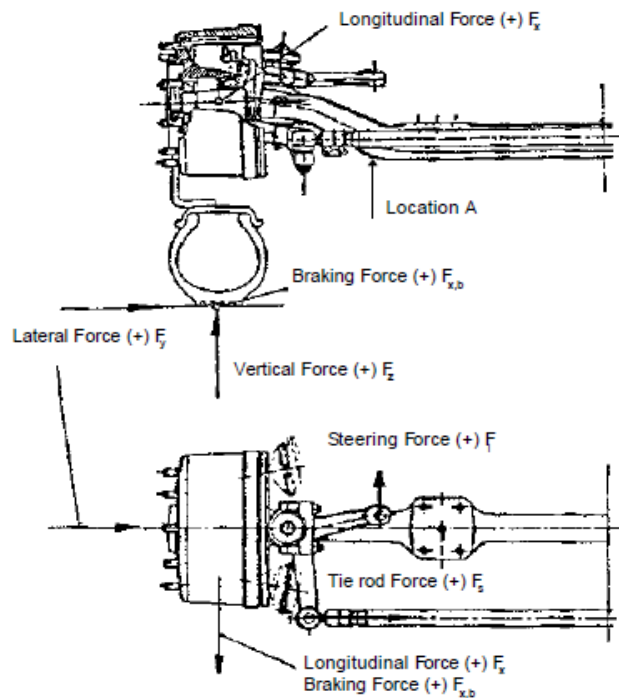


Figure 3.1 : Forces acting on a wheel.

For the following basic investigations, the wheel forces are treated as local stresses. This simulates an investigation of components that are stressed directly by the wheel forces in the individual directions with a linear relation. The load conditions are defined in terms of cumulative frequency distributions with the main parameters:

- The dynamic load factors which correlate the extreme load/stress conditions to the rated wheel load $F_{z,stat}$.
- The cycle number of the distribution H , which shows the total number of small, medium and high cycles of the load/stress time history.
- The shape of the distribution that indicates the relative frequency of the load/stress amplitudes. In practical investigations, the amplitude distribution can be often approximated with standardized distributions. The normal distribution which corresponds to a stationary Gaussian process is usually applied to load/ stress time histories caused by uniform service conditions (e.g. cornering with constant speed on a road with homogeneous surface roughness) and by load/ stress time histories caused by individual events (e.g. braking). The linear distribution well approximates the distribution of a

load/stress time history due to non-uniform service conditions (e.g. driving with variable speed on roads with different roughness) and can be explained by the superposition of several successive stationary Gaussian processes of different stress intensities and duration. These parameters are summarized as an example in the following figures [3].

Load case	Dyn. load factors				Spectrum parameters		
	n_x	$n_{x,b}$	n_y	n_z	H	H_e	Shape
Straight driving	-0.56		± 0.3	0	$0.96 \cdot H_t$	$10^{-6} \cdot H$	Linear
	1.13			2.5			
Corner.			-0.6	0.35	$0.04 \cdot H_t$	$4 \cdot 10^{-6} \cdot H$	Norm.
			0.9	1.7	20		
Braking		0		0.9	10^6	$5 \cdot 10^{-3}$	Norm.
		1.3		1.8			

Design life= 10^8 km
Mean number of cycles/km= 400 Cycles/km
 $H_t = 1000000 \cdot 400 = 4 \cdot 10^8$ Cycles

Figure 3.2 : Example of load factors and spectra definition for a heavy truck axle.

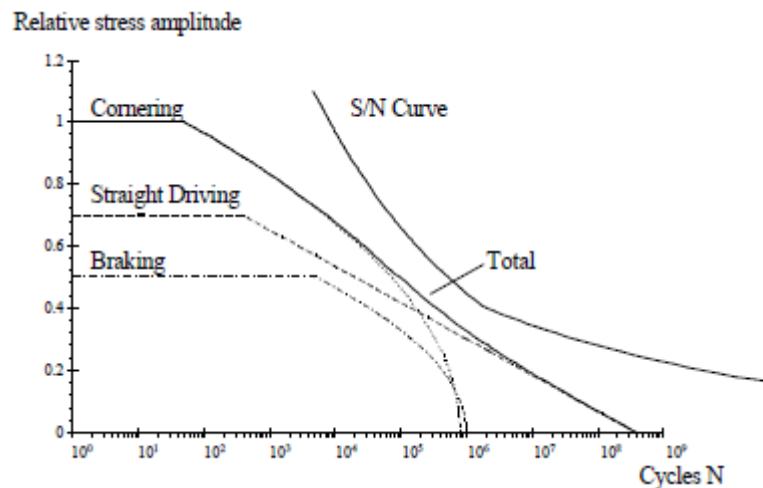


Figure 3.3 : Definition of a design spectrum.

In the next section, the objective of SLH's and their general possibilities of the application will be explained.

3.1 Objectives of SLH's and General Possibilities of Application

After the introduction of servo-hydraulic test machines with closed control circuit at the end of the 1960s, it was possible to replace the constant amplitude and blocked program tests—applied exclusively before this time—by tests with near-service load sequences. However, besides the well-known advantages of these tests this led to an increase of test parameters and, consequently, to a loss of comparability. Yet, the

comparison with already available results is very advantageous especially in case of fatigue tests. For this reason, the first specific loading standards were created quite shortly after the introduction of the servo-hydraulic machines. The use of loading standards is recommended for the following purposes:

- Evaluation of the fatigue strength of specimens or actual components made from different materials or by different manufacturing techniques;
- Optimization of design details;
- Determination of allowable stresses for the preliminary fatigue design of components;
- Investigation of methods to increase fatigue life;
- Verification of models for the prediction of fatigue life and crack propagation;
- Investigations on the scatter of fatigue test lives;
- Basis for comparisons with current in-service measurements;
- Fatigue tests with prototypes as long as no design specific load assumptions are available;
- New application-updating/amendment of directives of authorities.

Essential advantages of the application of service-like loading standards are:

- Availability at every stage of development;
- Reduction of the number of test parameters, comparability of results;
- Reliable (relative) fatigue estimates for current design and loading based on fatigue life curves determined under comparable loading conditions;
- Possible use as a main element of loading specifications for suppliers.

3.2 General Areas of Standardized Load-Time Histories (SLH's) Application

Standardized load-time histories (SLH's) are usually applied in the pre-design stage or for studies of a more generic nature. These may include an evaluation of how different materials, detail geometries, surface treatments or manufacturing routes affect the fatigue behavior of specimens and components. SLH's are also frequently

used in projects to develop or evaluate numerical life prediction models with several participating laboratories on fatigue-related experimental or analytical issues. Results generated by use of SLH's are readily compared at least with regard to the important aspect of the loading environment of a given test series. Thus, a database is created which allows the evaluation of individual test results or of scatter bands and may help to reduce the amount of fatigue testing.

Also for the generation of new load sequences background information and/or generation, principles of SLH's may be very helpful.

3.3 Existing Standardized Load Time-Histories

The SLH's are briefly characterized and some numbers are compiled that enable a first assessment of typical features of the respective load sequence. Further details are given in some overview papers [4–7] and in the respective original papers and reports.

3.4 General (Simplified) Approach for the Generation of SLH's

It is generally agreed that the structural load variations should be characterized in the time domain since in most cases the range (or amplitude) of a load, stress or strain cycle plus its respective max or mean value can be considered as fatigue-relevant. Furthermore, the sequence or mixture of load cycles of different ranges and means must not be neglected.

Many structural loading environments can be described as sequences of different modes that may be a particular flight, driving a car on certain road types. These modes of operation contain load cycles of different, but typical magnitudes and frequencies. Often distinct patterns of grouped load cycles can be distinguished, called a loading event or element, such as braking or cornering of a car, different flight phases or maneuvers of an aircraft. The occurrence of modes and loading events has to be defined in terms of frequency, severity and mixture/sequence, which in summary establish the so-called operating profile, see the following figure.

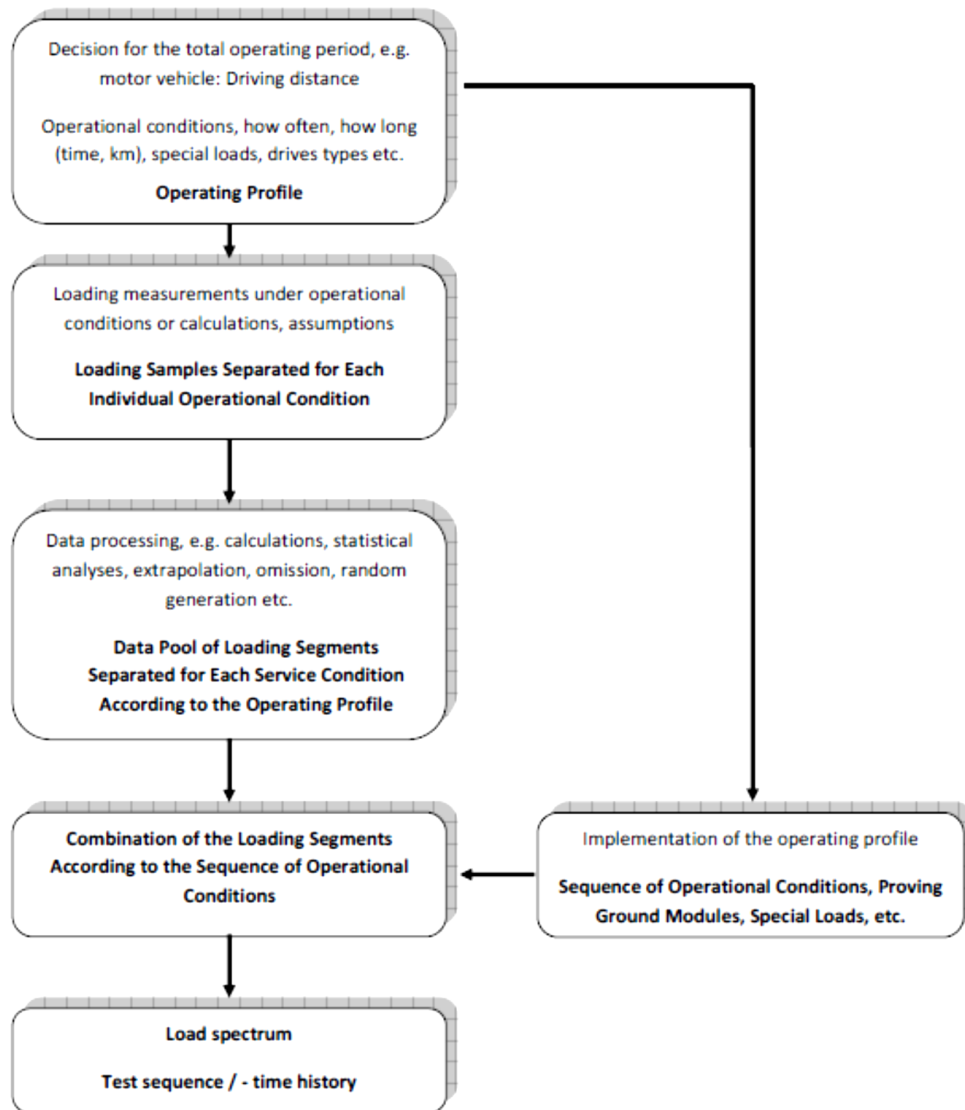


Figure 3.4 : General approach for the SLH's (example: passenger vehicle).

Statistically adequate samples of operational loads have to be available for every load case. These samples are usually acquired by in-service measurements, but they may also be supported by calculations or simple assumptions. Data processing aims at the preparation of the measured samples to be used as a basis for the generation of test load sequences compiled according to the operating profile. Following figure summarizes the procedures that may be applied for analysis purposes.

Procedures to analyse operational loads		Test conditions	
		Stiff component	Dynamic response
Loading conditions	Uniaxial loading	Rainflow counting (level crossings—l.c., range pairs—r.p.)	Additional Fourier analysis (e.g. power spectral density)
	Rotating loading	Rainflow counting (l.c., r.p.) Dwell time and/or revolution-at-level counting	Additional Fourier analysis (e.g. power spectral density)
	Loading under environmental impact	Rainflow counting (l.c., r.p.) Consideration of dwell time (environmental impact)	Additional Fourier analysis (e.g. power spectral density)
	Multiaxial loading	Rainflow counting (l.c., r.p.) Correlation analyses, e.g. joint density (multiaxial dwell time) counting	Additional Fourier analysis (e.g. auto-, cross spectra, coherence functions, transfer matrices)

Figure 3.5 : Compilation of relevant procedures for load analysis.

4. ROAD LOAD DATA ACQUISITION (RLDA)

In order to derive of a standardized load spectrum for structural durability approval of commercial vehicle axles, it is necessary to perform vehicle measurements as much as possible on the characteristic routes with the wheel force transducers (WFT). Thus, the loads acting on the axles will be measured and lately analyzed in terms of structural durability. For this purpose, a long-term vehicle measurement (Road Load Data Acquisition) is done on the characteristic routes in Turkey with a two-axle coach (an independent front axle and rigid rear axle) for the first measurement campaign. Afterwards, another measurement will be performed at the proving ground location (PG) of commercial vehicle manufacturer. The main phases of this chapter will be the following:

- Phase 1: Definition of the Customer Usage Profile and Road Load Data Acquisition (RLDA) in Turkish roads (Customer Usage - CU)
- Phase 2: Vehicle Instrumentation (Wheel Force Transducers, Accelerometers, Strain-Gages, Load cells, Displacement Sensors)
- Phase 3: Road Load Data Acquisition (RLDA) at the Proving Ground (PG) Location

The scope of the work included in each phase is described in the following points.

4.1 Phase 1: Definition of Customer Usage Profile and RLDA at CU

Based on these measurements, a so-called reference-customer usage profile is formed that contains all relevant loads of partially very different customer operations. This reference-customer usage profile is used then in a mapping process to get test procedures that are customer correlated, applications specific and accelerated at the same time. The aim of this phase is to record all the relevant load information on the vehicle through Turkish roads following the route defined. The results of this activity will be the time histories of the signals coming from the sensors located in the vehicle during the RLDA performed over Turkish customer usage. In addition, a

video recording system is installed on the vehicle focusing the roads. When investigating customer load conditions it can be observed that there are a lot of different parameters that influence the resulting loads of a certain customer application. In principle, it can be distinguished between parameters that are related to specific service conditions, like task of transportation and driver influence, others that are directly linked to a specific vehicle configuration and those that cannot be influenced, like environment [8].

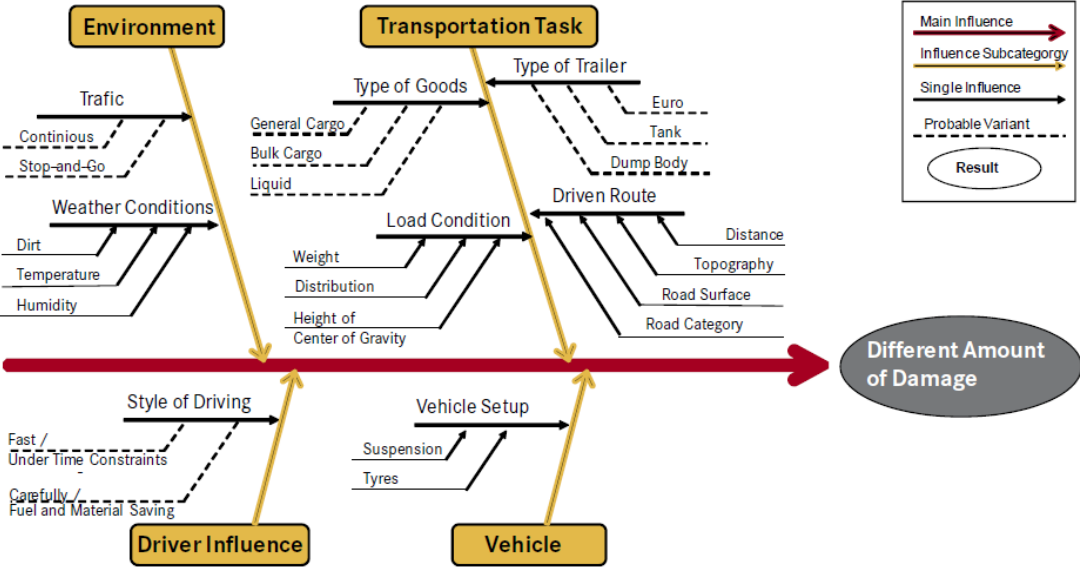


Figure 4.1 : Influence parameters on the durability of trucks.

The objective of this phase (Customer Usage Profile) is to define the following information:

- Type of roads included in the usage profile: urban roads, highway, bad maintenance road, etc.
- Percentage of use on each type of road (i.e. 30% urban road, 40% highway, etc.)
- Vehicle loading conditions included in the usage profile.
- Percentage of use on each vehicle loading condition.

During the customer-usage profile measurement, the vehicle was always full loaded. The choices of the roads have been done according to the traffic volume distributions with reference to the Turkey General Directorate of Highways and the information of the truck services. The types of roads were classified as following and considered to

classify the routes on the customer usage in Turkey. Based on these classifications, the measurement protocols were filled during the measurement. The information about the roads are also listed in these protocols with respect to the road type, road profile and road condition. This route classification enables us to understand the plausibility of the measurement data. Apart from the reference-customer usage profile measurement, some standard measurements with special maneuvers (braking, circular driving etc.) were also completed with fully loaded vehicle in order to check the data logically.

At the following table, the route classification can be seen.

Table 4.1 : Route classification - different types of roads.

Region	Road Type	Function of the Road
County Side	Highway	National Connection - Class 1
	Big Federal Road	
	Small Federal Road	Regional Connection - Class 2
	National / State Road	
	Country Road	Local Connection - Class 3
City	Ring Road	Main City Traffic - Class 4
	Through Road	
	Main Road	Local City Traffic - Class 5
	Minor Road	
	Residential Road	
	Industrial Road	
	Access Road	
Construction-Off Road		Construction Site - Class 6
		Off-road - Class 7
Proving Ground		Proving Ground - Class 0
-1		paved
-0		unpaved

In the next section, we explain the route classification in detail.

4.1.1 Route classification, different road classes

4.1.1.1 National connections

The loads and forces acting on the vehicle are very low on these roads because of the little excitation in vertical, longitudinal and lateral direction of the vehicle. These roads have mainly two or more lanes. The surfaces of these roads are considerably better than all other routes. There are not potholes or patched roads. Examples for these roads can be considered as mainly highways and big federal roads. As seen of the following figure, national connections are highways and big federal roads.

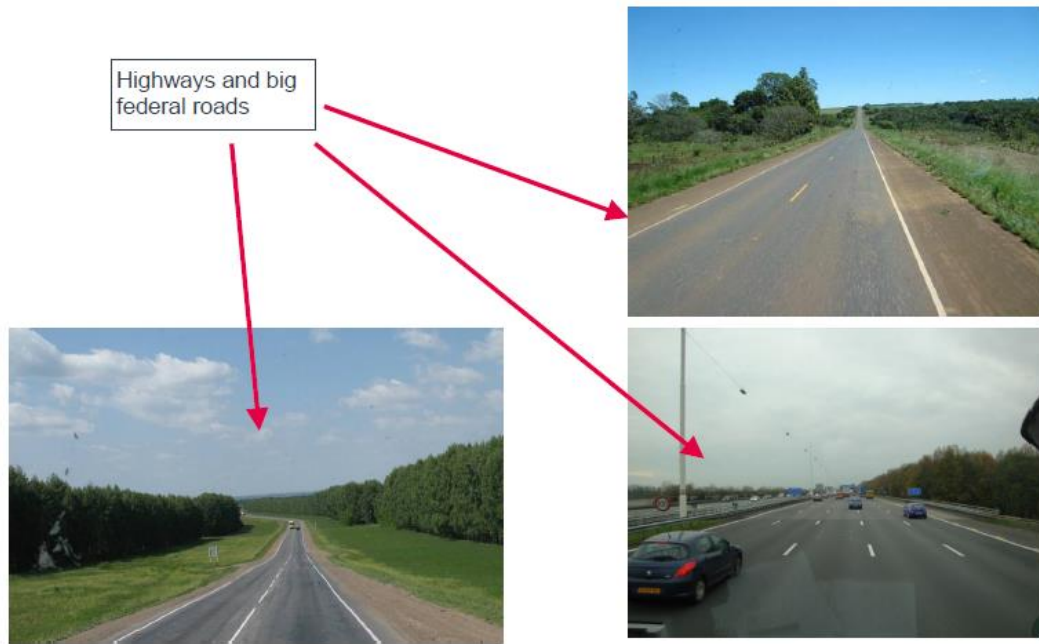


Figure 4.2 : National connections.

Now we explain the regional connections.

4.1.1.2 Regional connections

These roads are mainly one or two way roads. Examples for these roads can be considered small federal roads and state roads. The average speed of the vehicle is less than national connections. As seen of the following figure, regional connections are small federal and state roads.



Figure 4.3 : Regional connections.

Now we explain the local connections.

4.1.1.3 Local connections

These roads are mainly one-way roads such as country roads. As seen of the following figure, local connections are country roads.

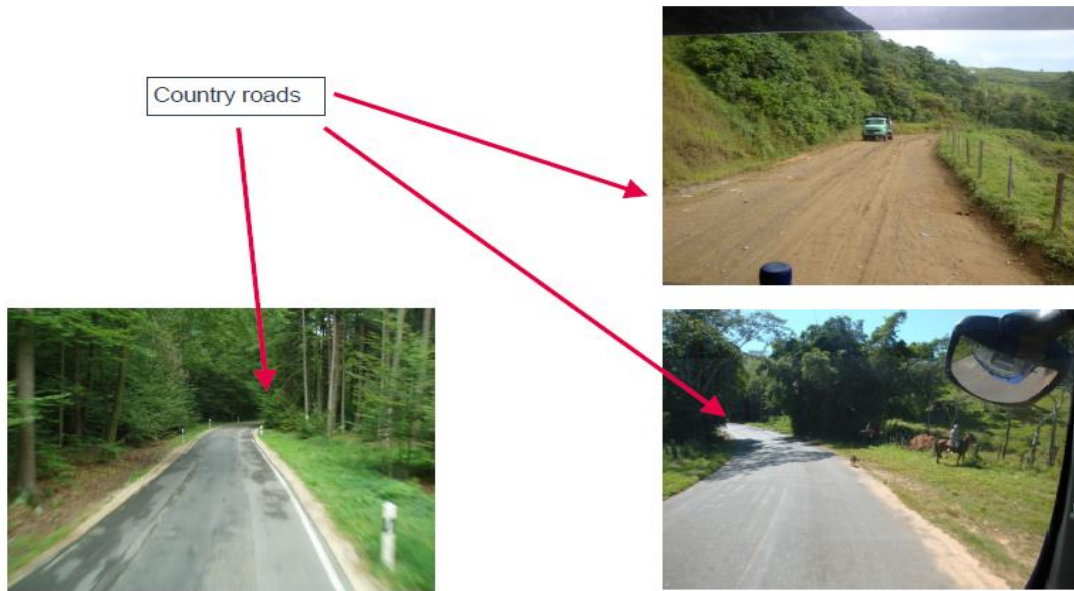


Figure 4.4 : Local connections.

Now we explain the main city traffic.

4.1.1.4 Main city traffic

These roads as seen at the following figure are mainly country roads (for example stop-and-go roads). The average speed is here are lowest than the other route types because of the city traffic.

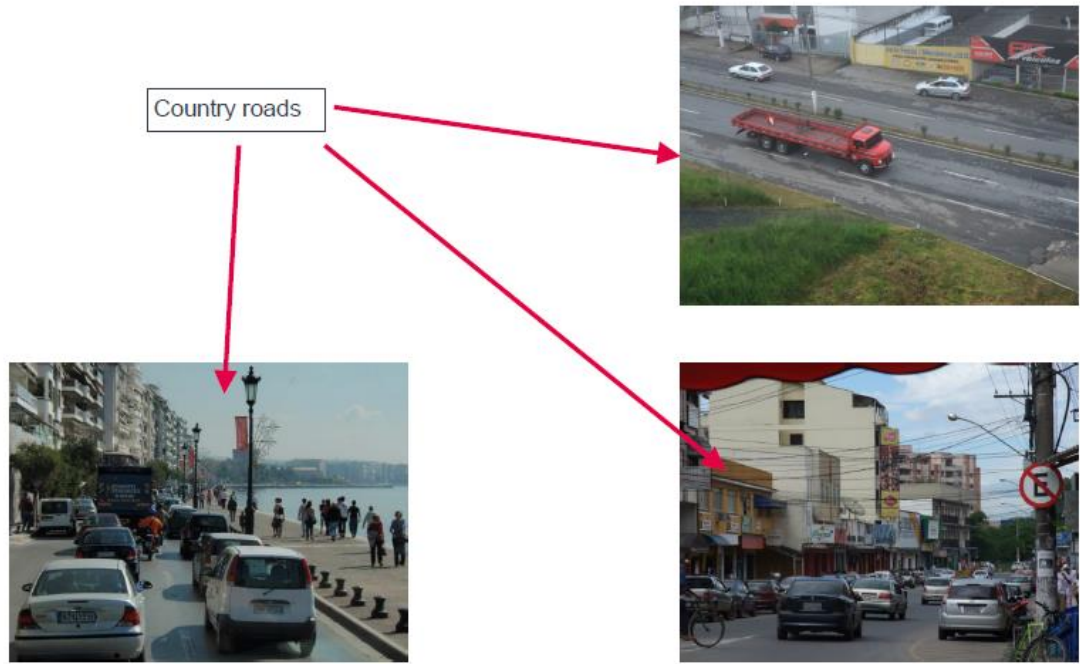


Figure 4.5 : Main city traffic.

Now we explain the local city traffic.

4.1.1.5 Local city traffic

These roads as seen at the following figure are mainly minor, residential, industrial and access roads.



Figure 4.6 : Local city traffic.

In the next section, we explain the reference-customer usage profile in Turkey.

4.1.2 Reference-customer usage profile in Turkey

The reference routes in Turkey are determined according to the characteristic routes, which are mainly driven by customers. These routes must also be representative for the whole service life of the vehicle. Thus, not only good routes with high vehicle speeds are considered, also the bad and city routes are considered to measure. At the following figure can be seen the measured routes in Turkey.

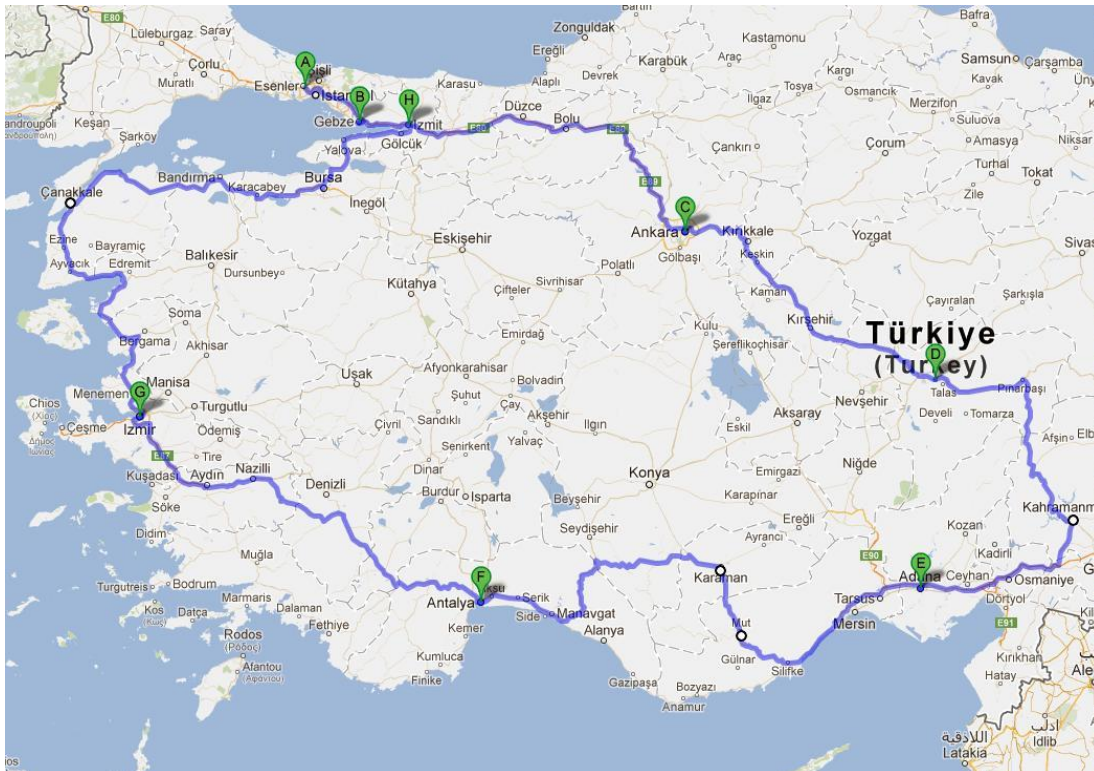


Figure 4.7 : RLDA on Turkish reference-customer usage.

Totally, 3664 km on Turkish market are measured. The distributions of the road types can be seen at the following figure. Four percent of the measured routes belong to city routes (e.g. Istanbul city route, from A to B → from Esenler to Gebze). The city roads in Istanbul are mainly the roads with main city traffic. Therefore, these are very suitable for stop-and-go measurements. Twenty-seven percent of these routes are highways. For example, the famous highway of Turkey (from B to H → from Istanbul to Ankara) is the most frequently used routes in Turkey for coaches & urban busses. This road is completely highway with low road curve and inclination. The most part of the measured routes belong to urban (intercity) roads. These are regular bus routes for coaches & urban busses (a part of the path Istanbul-Ankara to other eastern cities). The urban roads have with two lanes in each direction. From E to F is

chosen to measure the bad routes as much as possible. Apart from the tourist transportation (currently second hand coaches are used instead of urban busses), the focus are given to the routes that are from Silifke over Mut, Karaman to Manavgat, and have higher curve and inclination. The routes from F (Antalya) over G (Izmir) to the A (Istanbul) are known road which are characteristic for the tourist transportation with badly maintained. The measurement plan in Turkey can be seen at the following table.

Table 4.2 : Distribution of the road types.

Classification	Road Type	Length [km]	Ratio [%]
1-P	Highway	732	20%
2-P Federal	Federal road	2165	59%
2-P National	National road	406	11%
3-P	Local Connection Road	258	7%
4-P	Main Traffic City	76	2%
5-P	Local Traffic City	27	1%
Total		3664	100%

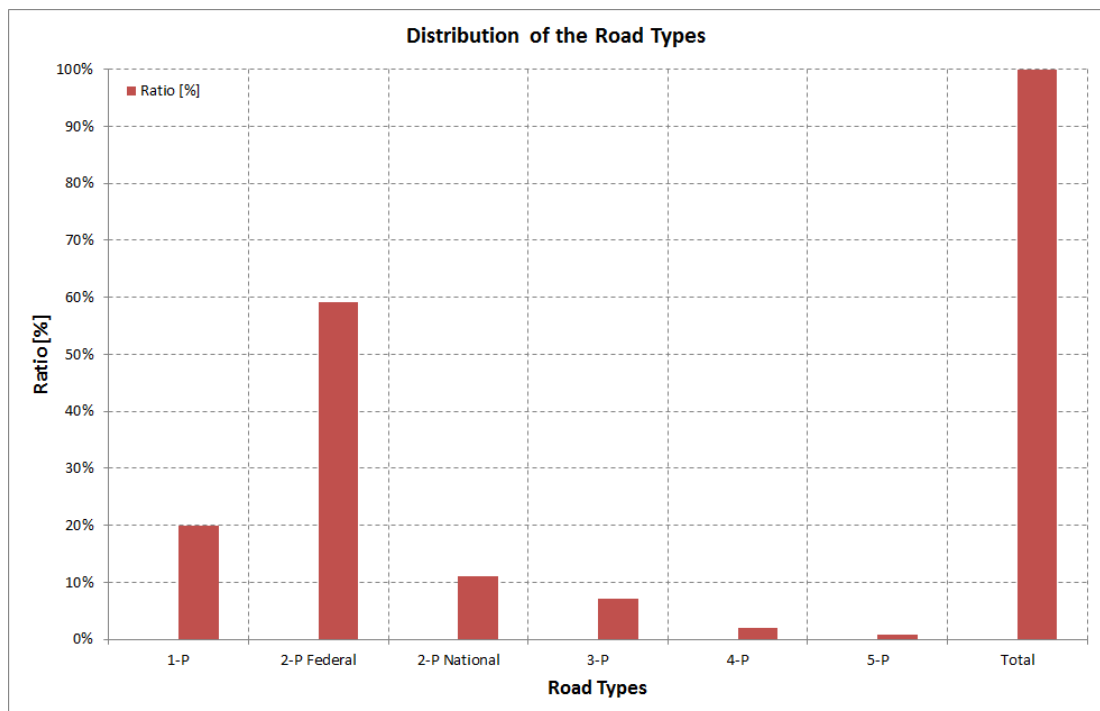


Figure 4.8 : Distribution of the road types.

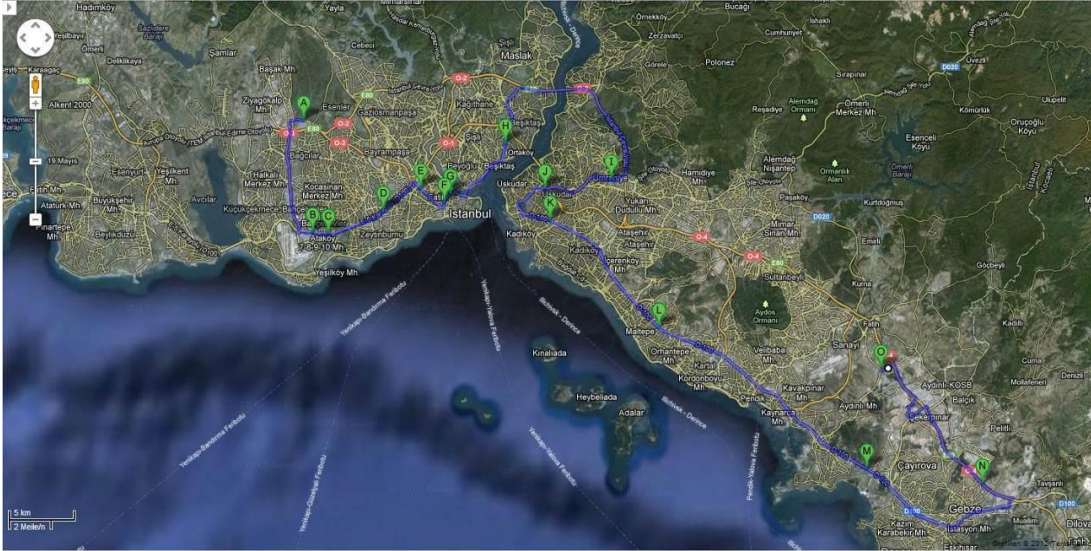


Figure 4.9 : Istanbul city route.

Now we see the distribution of the road types as a table.

Table 4.3 : Distribution of the road types.

Day	Date	Route
Wed	07.11.2012	Customer clearance
Thu	08.11.2012	Vehicle Preparation & Setup Measurement Device
Fri	09.11.2012	Vehicle Preparation & Setup Measurement Device
Sat	10.11.2012	Istanbul City Route
Sun	11.11.2012	Istanbul - Ankara
Mon	12.11.2012	Ankara - Kayseri
Tue	13.11.2012	Kayseri - Adana
Wed	14.11.2012	Adana - Mut - Konya
Thu	15.11.2012	Konya - Alaya - Antalya - Denizli
Fri	16.11.2012	Denizli - Izmir
Sat	17.11.2012	Izmir - Canakkale - Bursa
Sun	18.11.2012	Bursa -Istanbul

In the next section, we explain the vehicle instrumentation.

4.2 Phase 2: Vehicle Instrumentation

4.2.1 Application of sensors

The sensors that are applied to vehicle are necessary to measure the some physical magnitudes in order to have an idea, which forces and moments come from road to the vehicle. Especially the load-cells are inevitable which are in the air springs and also wheel force transducers (WFT) which measure the three forces in translational

direction (F_x , F_y and F_z) and three moments in the rotational direction (M_x , M_y and M_z) respectively. These can be called as external forces. The reaction of the vehicle can also be measured with the help of the calibrated suspension arms. Displacements sensors and accelerometers are only auxiliary materials, which helps us to understand the vehicle behavior at the certain events (braking, curves etc.). All these sensors can only be measured with the help of the measurement device. At the following table can be seen an overview of the measurement channels.

Table 4.4 : Overview of the measurement channels.

Position	Element	Channel Type	Quantity	Unit
Front Axle	Links	SG Full Bridge	12	kN
	Shock Absorbers	SG Full Bridge	2	kN
	Air spring (forces)	LC Full Bridge	2	kN
	Wheel displacement	Analog	2	mm
	Anti-roll bar	SG Full Bridge	1	kN
	Axle accelerations	Analog	6	g
	WFT	Analog	12	kN, kNm
REAR AXLE	Links	SG Full Bridge	4	kN
	Shock Absorbers	SG Full Bridge	4	kN
	Air spring (forces)	LC Full Bridge	4	kN
	Wheel displacement	Analog	2	mm
	Axle accelerations	Analog	6	g
	WFT	Analog	12	kN, kNm
Chassis	Accelerations	Analog	12	g
Body	Strain Gages	SG Full Bridge	15	$\mu\text{m/m}$
Others	Ground speed	Analog	1	km/h

Now we explain the load-cells in the air springs.

4.2.1.1 Load-cells in the air springs:

The load-cells, which are in the air spring carriers, are suitable for high levels of cyclic loading. These load cells have good output symmetry between compression and tension operation. Shear web structure with high vertical and lateral mechanical stiffness. The idea behind the calibration is to measure output voltage for each

applied force values. The force can be applied with a hydraulic actuator and be measured with the help of the load-cells of the actuator. As a result, the following figure can be obtained.

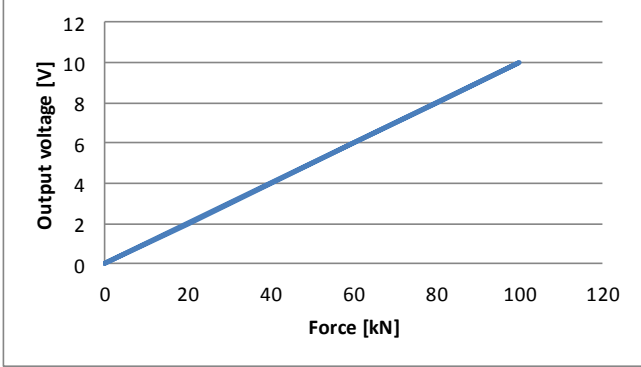
Verification Protocol		T101-M-0006-1-p	
Description of the Test Equipment : Load-Cell (Air Springs)		Test Steps	Measurement Amplifier Output Voltage
Equipment Nr. : 44177		kN	V
Test Equipment Nr. : MTE/02/0006/44177		(Compression)	
Installation Position : -		0	0,00
Projekt		20	2,00
User : Toprak Metin		40	3,98
Department : EVDF		60	6,00
Projekt-ID : P001826		80	8,00
Test Order : 12/B-H-008		100	10,00
K Nr. : K481137		0	0,00
Test Equipmen			
Manufacturer : Althen		reliable Tolerance : 1%	
Type : F254-Z3101		Conclusion : Ok.	
Serial Nr. : 44177		0,5mV/V = 31,48kN	
Measurement Range : 0-200 kN		Signal -	green
Brigde Type : Full Bridge		Input +	red/black
Zero Point : 0,227		Input -	blue/white
Measurement Amplifier		Shield	orange
Equipment Nr. : 24887		Adjustment	
Measurement Range : 1		1,00V = 10 kN	
Zero Point : 0		Taste = 3,148 V	
		Taste = 31,48 kN	
		Inspection Measurement Amplifier	
		Calibrated Eq. Vishay Measurement Amplifier	
		Eq. Nr.182626	KWS 3073
		mV/V	V
		-2,00	-10,00
		-1,50	-7,50
		-1,00	-5,00
		-0,50	-2,50
		0,00	0,00
		0,50	2,50
		1,00	5,00
		1,50	7,50
		2,00	10,00
		Taste = 2,50V	
			
Inspected Test Equipment			
Description - Test Equipment : Load Measurement Chain			
Equipment Nr. : 50kN			
Description - Test Equipment : Multimeter			
Equipment Nr. : 75001191			
Date : 12.10.2012			
Time : 13:15			
Place of Inspection : Workshop			
Authorised Person : Schaller			

Figure 4.10 : Calibration sheet of the load-cell in the air spring.

The mounting procedure of these load-cells is very important in order to measure right values from the load-cells that are in the air springs. Firstly, it has to be checked carefully the length of the winding at the bolts and the screw hole. Washers are also

added. The length of the slot thread (B_1) in the green part is individual and not always the same length. To adjust the length of the former slot (A), the washer should be adapted. Therefore, the slot thread has to be measured first to adapt the thickness of the washer to also ensure that the thickness of the washer is not too wide and too less turns of the thread are supporting. That means, $B_1 < A \rightarrow B_1 + B_2 = A$ as seen at the following figure.

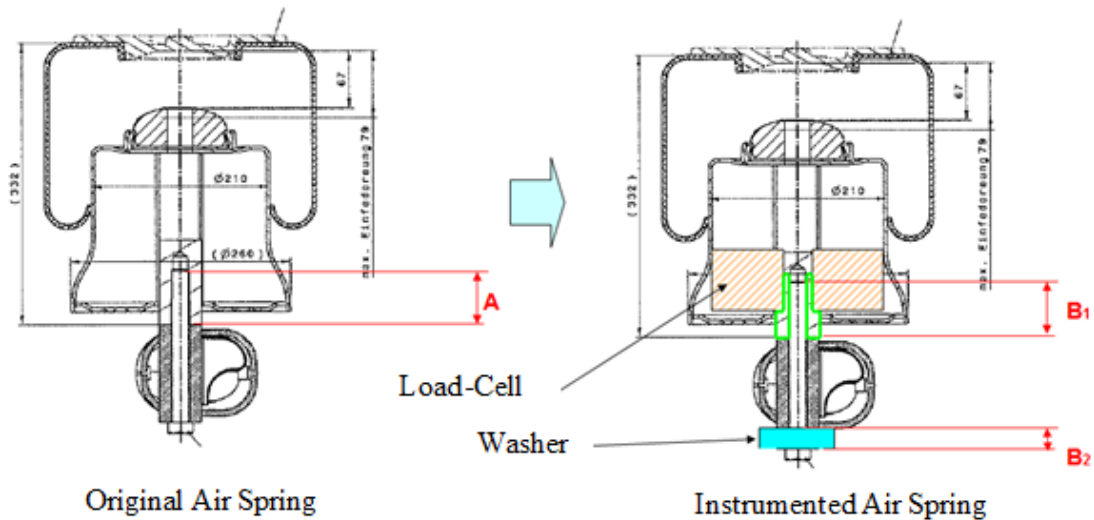


Figure 4.11 : Mounting configuration of the load-cell in the air springs.

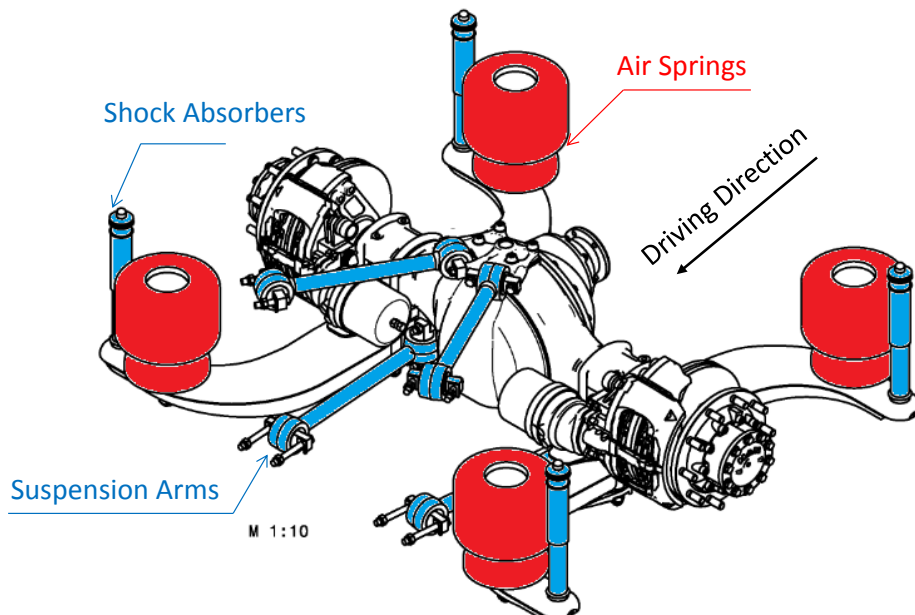


Figure 4.12 : The instrumented air spring at the rear axle.

Now we explain the shock absorbers.

4.2.1.2 Shock absorbers:

The shock absorbers are also calibrated with the hydraulic actuator. Strain-Gages are applied to the absorbers and connected with the full bridge. Afterwards, the same principal of the calibration of load cells are followed. The calibration lines are also obtained. Following figure shows us the calibration sheet of the one shock absorber at the rear axle.

Verification Protocol		T101-M-0001-1-p	
Description of the Test Equipment : Sensor - Shock Absorbers		Test Steps	Measurement Amplifier Output Voltage
Equipment Nr. : 1199		kN (Tension)	V
Test Equipment Nr. : MTE/02/0001/1199		0	0,000
Installation Position : Rear Axle		4	0,998
		8	1,998
Projekt		12	2,999
User : Toprak Metin		16	3,998
Department : EVDF		20	5,000
Projekt-ID : P001826		0	-0,002
Test Order : 12/B-H-008			
K Nr. : K481137			
Test Equipmen		reliable Tolerance: 1%	
Manufacturer :		Conclusion : Ok.	
Serial Nr. : 81.437026045		0,5mV/V = 14,156kN	
Original Vehicle Parts : Yes		Signal + white	
Measurement Range : ±50kN		Input - black	
Brigde Type : Full Bridge		Input + blue	
Strain Gage - Type : 3/350XY31		Signal - red	
K - Factor : a: 1,98 b:1,99		Shield green	
Responsible : Gruber		Adjustment	
Zero Point : -6,24V (-24,96kN)		1,00V = 4kN	
Measurement Amplifier		Taste = 3,539V	
Equipment Nr. : 24887		Taste = 14,156kN	
Measurement Range : 1		Inspection Measurement	
Zero Point : +1		Amplifier	
UB : 5V		Calibrated Eq. Vishay Measurement Amplifier	
		Eq. Nr.182626	KWS 3073
		mV/V	V
		-2,00	-10,00
		-1,50	-7,50
		-1,00	-5,00
		-0,50	-2,50
		0,00	0,00
		0,50	2,50
		1,00	5,00
		1,50	7,50
		2,00	10,00
		Taste = 2,50V	
Inspected Test Equipment			
Description - Test Equipmen : Load Measurement Chain			
Equipment Nr. : 50kN			
Description - Test Equipmen : Multimeter			
Equipment Nr. : 15690384			
Date : 22.10.2012			
Time : 15:00			
Place of Inspection : Workshop			
Authorised Person : Fischhaber			

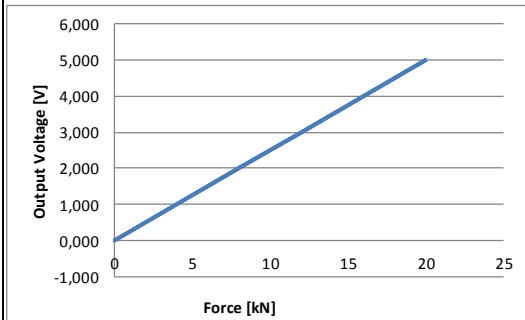


Figure 4.13 : Calibration sheet of the shock absorber at the rear axle.

Now we explain the suspension arms.

4.2.1.3 Suspension arms (links):

The shock absorbers are also calibrated with the hydraulic actuator. Strain-Gages are applied to the absorbers and connected with the full bridge. Afterwards, the same principal of the calibration of load cells are followed. The calibration lines are also obtained. Following figure shows us the calibration sheet of the transverse control arm at the rear axle.

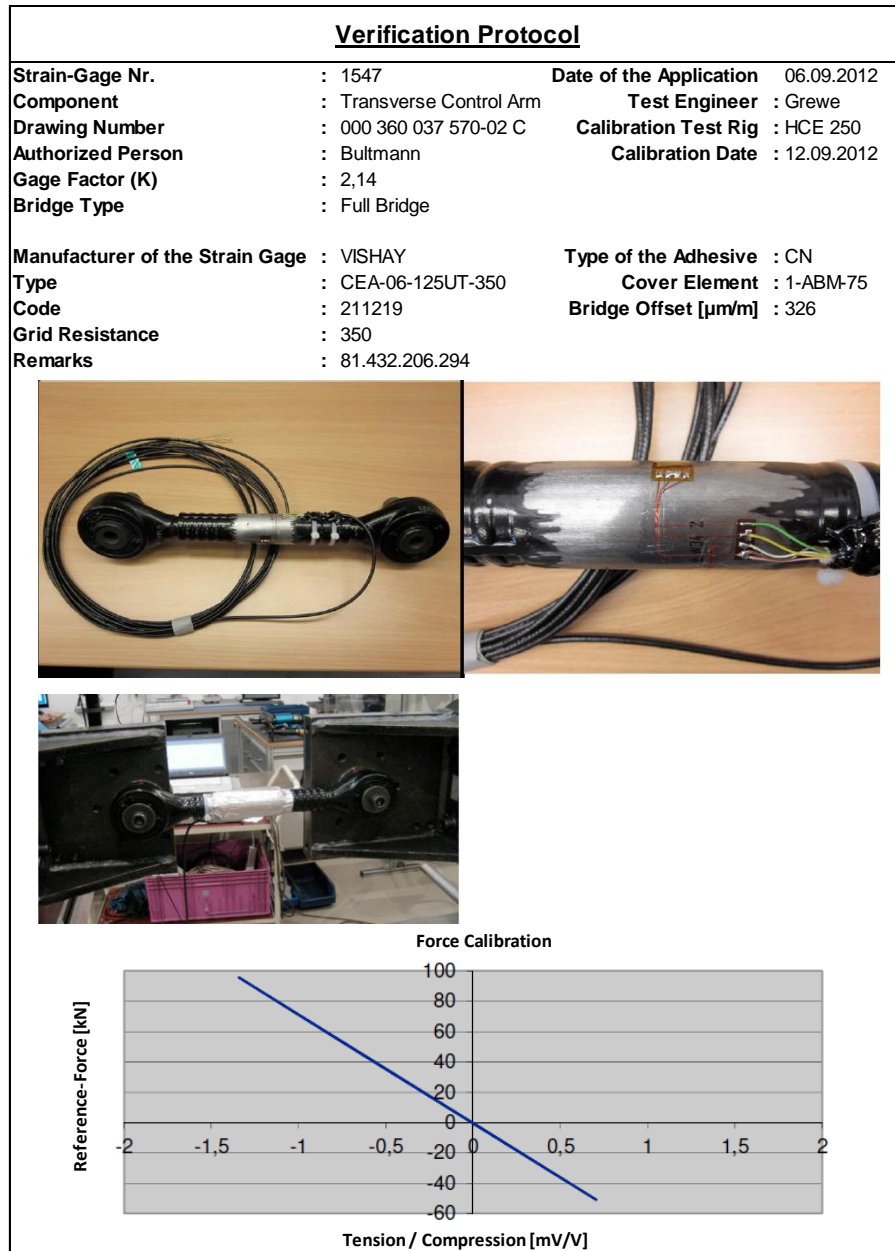


Figure 4.14 : Calibration sheet of the transverse control arm.

Now we explain the wheel force transducers.

4.2.1.4 Wheel force transducers (WFT)

The wheel force transducers are the significant sensors to measure the loads and moments acting to a rotating wheel on the service life of the vehicle. For this purpose, the WFTs of KISTLER are used during the RLDA. The RoaDyn S6HT System 2000 of KISTLER is a multi-axial precision measuring device for use in the development and testing of complete chassis and chassis components of heavy commercial vehicles such as trucks and busses.

Suitable mechanical components like inner part, outer part and wheel-offset adapter are used to mount the six replaceable 3-component load cells between wheel hub and rim ring. Each load cell is individually calibrated to allow replacement by the user without the entire measuring wheel system having to be re-calibrated. The ID (Identification) chip integrated into each load cell stores all important component parameters and prevents a misidentification of the load cell data. When the measuring system is powered up, the data of the components currently in use is imported into the connected System 2000 on-board electronics. The signals are amplified before leaving the load cells and passed on via short connecting cables to the hub electronics for filtering, digitization and encoding. The stream of data is transmitted without contact by means of the rotor (ring antenna) to the fixed stator. A cable then supplies it to the System 2000 on-board electronics, where the physical quantities F_x , F_y , F_z , M_x , M_y and M_z are calculated from the raw signals and transformed from the rotating coordinate system of the wheel into the non-rotating vehicle coordinate system. The measurement data is output in both analog and digital form. The digital output is available in CAN (Controller Area Network), Ethernet or other proprietary data acquisition-system formats [9].

Application;

- Road profile categorization: recording of typical load profiles for selected stretches of road for chassis design
- Individual maneuvers generally involving high loads for verifying design loads and design data
- Input data for multi-body simulation and other virtual loading methods

- Dynamic chassis tuning and development of active braking, traction and chassis control systems.
- Recording of control data for chassis test stands. Use for iteration on multi-axial vehicle test stands
- Determination of characteristic tire data for tire and chassis development
- Use of special load cases in damage analysis of vehicle components
- Special applications on trailers, semi-trailers, construction machinery and special vehicles

The overview of the configuration of the measuring chain with WFTs can be seen at the following table. The required parts can be summarized as follows:

- Wheel Sensor,
- Wheel Electronics,
- Data Transmission,
- Mounting, Connecting Cable,
- On-Board Electronics and a Remote Control Device.

Configurations of Measuring Chain with RoaDyn® S6HT sp System 2000








Wheel Sensor	Wheel Electronics	Data Transmission	Mounting	Connecting Cable
Type 9269A1	Type 5241A...	Type 5248A0 External transmission unit	Type 9893A... for single wheel	Type 30430A... Connection between stator and on-board electronics
			 Type Z31006Q... for dual wheel 	
Control Unit Type 9891A... System 2000 on-board electronics 		Technical Data RoaDyn S6HT¹⁾, without tire Single wheel on 9,00x22.5 kg 72 on 11,75x22.5 kg 74 compared with standard wheel (steel) kg 52 Dual wheel on 2x9,00x22.5 kg 96 compared with standard wheels (steel) kg 106 Shock resistance x, y, z g 50 Maximum speed km/h 200 Degree of protection standard (against dust and moisture) IP65 optional IP67 Operating temperature range °C -20 ... 110		Standard measuring range²⁾ F _x kN ±180 F _y kN ±100 F _z kN ±180 M _x kN-m ±25 M _y kN-m ±50 M _z kN-m ±25 Extended measuring range²⁾ F _x kN ±220 F _y kN ±100 F _z kN ±220 M _x kN-m ±40 M _y kN-m ±60 M _z kN-m ±40 Rotation angle accuracy ° ±0,1 Wheel rigidity as standard wheel Natural frequency range Hz >400 Measuring errors Linearity % FS <±1 Hysteresis % FS <±1 Crosstalk % <±1
		¹⁾ Consisting of complete measuring wheel with its electronics and external transmission unit ²⁾ It is assumed that the maximum forces and torques do not act simultaneously. The torques are specified relative to the center of the wheel		

Figure 4.15 : Configurations of the measuring chain & technical data.

At the following figure, it can be seen the test vehicle with instrumented wheel force transducers.



Figure 4.16 : Instrumented WFTs at the test vehicle.

The three main forces (F_x , F_y and F_z) are measured and their moments (M_x , M_y and M_z) are calculated. It can be seen at the bottom, the main coordinates of the wheel and how to calculate the moments. F_y and M_y are always independent of the wheel angle position. The measured forces are not affected the original wheel coordinate system, they affect the center of tire contact (load application). Also, it can be seen the measured forces and moments from WFTs to check logically the results from different driving maneuvers as an example on the test track at the following figure [10].

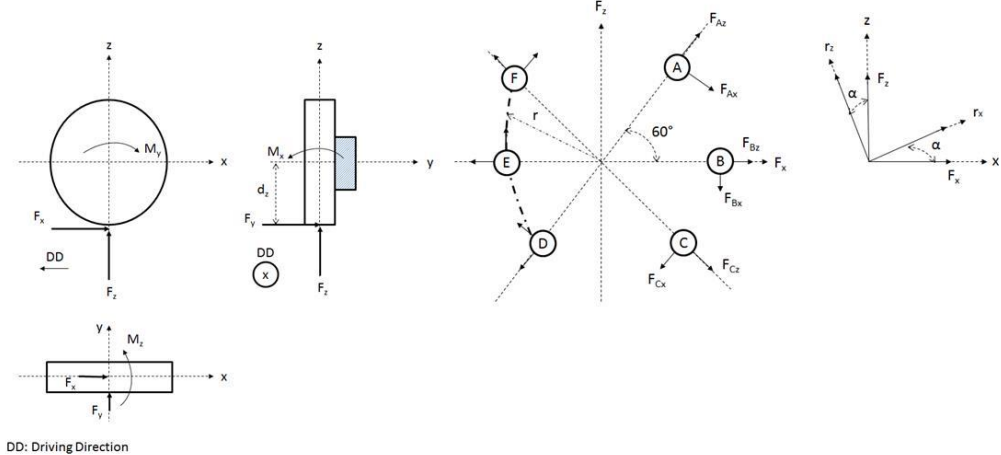


Figure 4.17 : The Principal of WFT (forces and calculated moments).

The equations are explained individually. Firstly, the longitudinal force at the load-cell (4.1);

$$F_{rx} = F_x \cdot \cos \alpha + F_z \cdot \sin \alpha \quad (4.1)$$

Now vertical force at the load-cell (4.2);

$$F_{rz} = F_z \cdot \cos \alpha - F_x \cdot \sin \alpha \quad (4.2)$$

Now lateral force at the load-cell (4.3);

$$F_{ry} = F_y \quad (4.3)$$

Summation of the lateral force (4.4);

$$F_y = \sum_{\alpha=1}^{k=6} F_y \quad (4.4)$$

The moment in longitudinal direction at the load-cell (4.5);

$$M_{rx} = M_x \cdot \cos \alpha + M_z \cdot \sin \alpha \quad (4.5)$$

The moment in vertical direction at the load-cell (4.6);

$$M_{rz} = M_z \cdot \cos \alpha - M_x \cdot \sin \alpha \quad (4.6)$$

The moment in lateral direction at the load-cell (4.7);

$$M_{ry} = M_y \quad (4.7)$$

The moment in longitudinal direction as a function of F_y and F_z (4.8);

$$M_x = f(F_y, F_z) \quad (4.8)$$

The moment in lateral direction as a function of F_x (4.9);

$$M_y = \sum_{\alpha=1}^{k=6} F_x \cdot d \tag{4.9}$$

At the following figure can be seen the coordinates of the forces and moments acting on wheel.

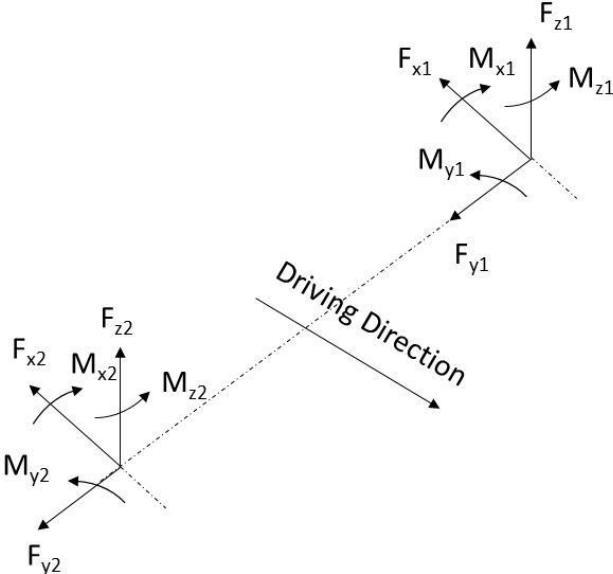


Figure 4.18 : Coordinates of the forces and moments acting on wheel.

At the following figure can be seen the measured WFT forces from different driving maneuvers as a time signal.

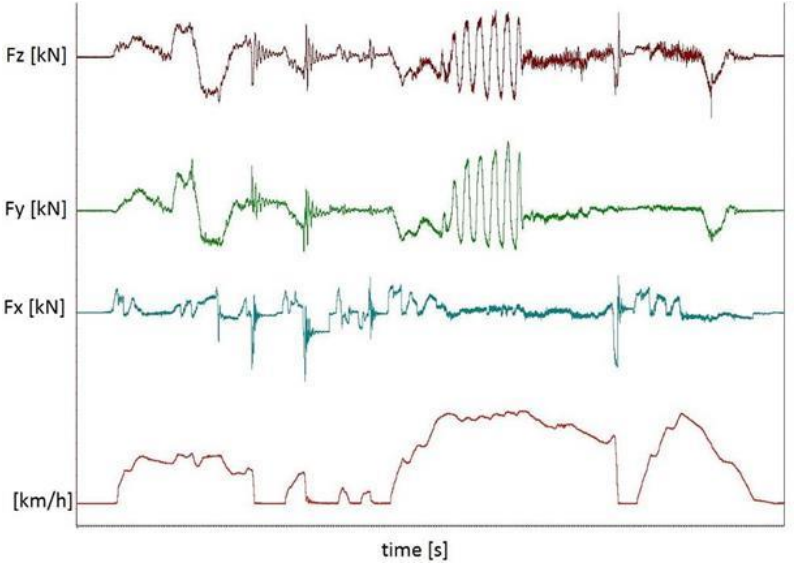


Figure 4.19 : Measured WFT forces from different driving maneuvers.

At the following table can be seen the measured WFT forces from different driving maneuvers.

Table 4.5 : Measured WFT forces from different driving maneuvers.

Program	Vehicle Speed [km/h]	Radius of the Turn [m]
Zero Balance	-	-
Eight Driving	20	-
Circular Driving left + Braking	10	-
Circular Driving right + Braking	10	-
Braking in reverse	5	-
Circular Driving left	35	30
Circular Driving right	35	30
Circular Driving left	0-max	12
Circular Driving right	0-max	12
Drive Line Change	40	-
Full Brake	30	-
Harsh Driveaway with 3. Gear	-	-
Zero Balance	-	-

As we can find out from the measured time histories, the F_x values are reasonably higher in the braking event than others. As a result, the moment in y directions (M_y) can be obtained during these driving maneuvers (braking). Certainly, it can be seen that the F_y values can be measured while the right or left curve events. The bad road has mainly affected the vehicle in z direction because of the potholes. That is why these forces (F_z) are higher than others are.

4.2.1.5 Strain-gages at the body

Strain gages are applied at the critical locations of the body, especially at connection points of the profiles. These locations are chosen by means of experience and Finite Element Methods/Results (FEM). The overview of the points of applied strain gages can be seen at the following figure. The durability characteristics of the vehicles will be investigated by strain measurements. The bus is driven on the Turkish customer routes, which are previously defined. Throughout the measurements, data from 15 strain gages are collected.

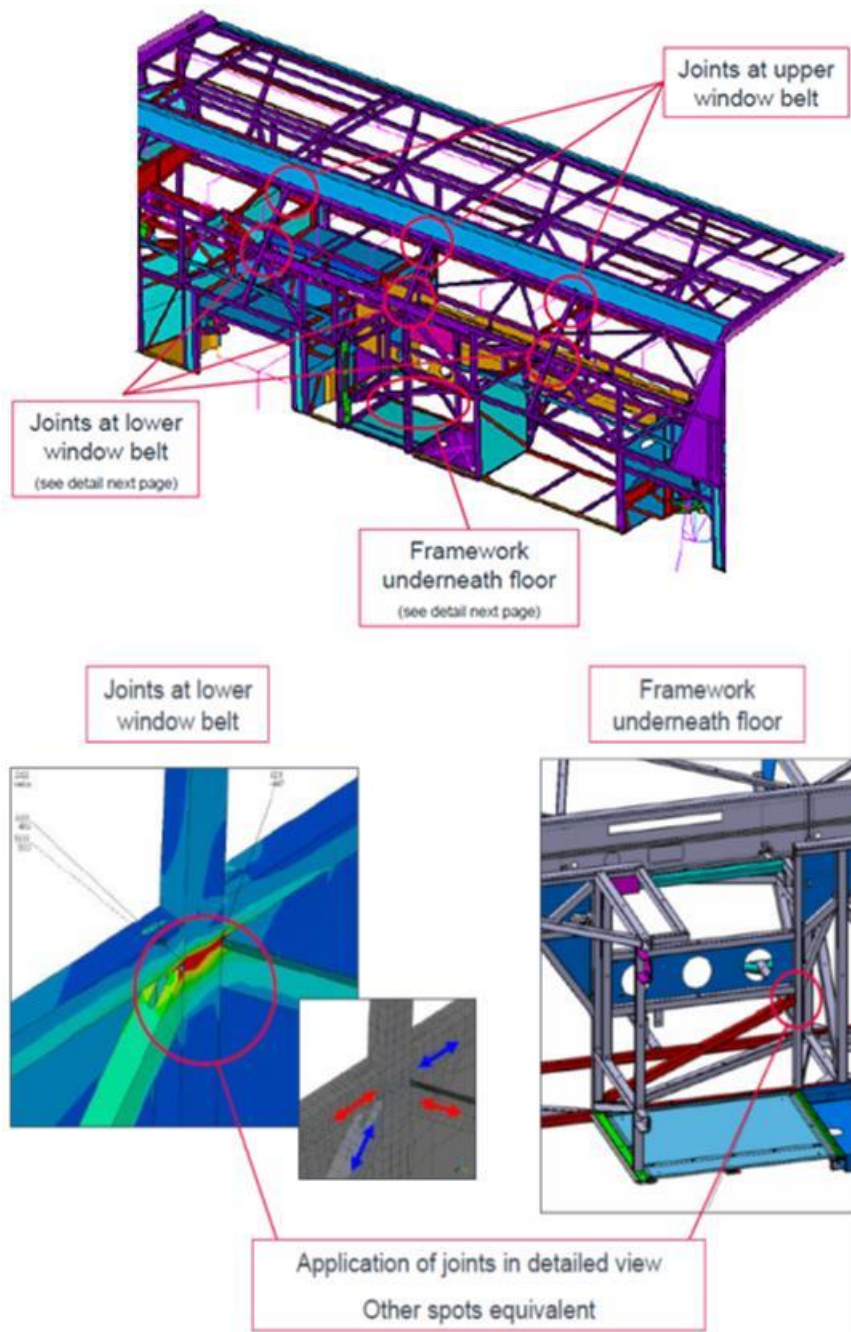


Figure 4.20 : Overview of the strain gages at the body.

4.3 Summary of the Vehicle Instrumentation Plan

4.3.1 Suspension arms

Front and rear axle suspension arms were instrumented with strain gages in order to measure tension and compression forces through the arms. After the instrumentation, the links were calibrated in order to determine the conversion factor strain – load which is explained in the previous section. At the following figure, we can see the instrumentation plan of the suspension arms.

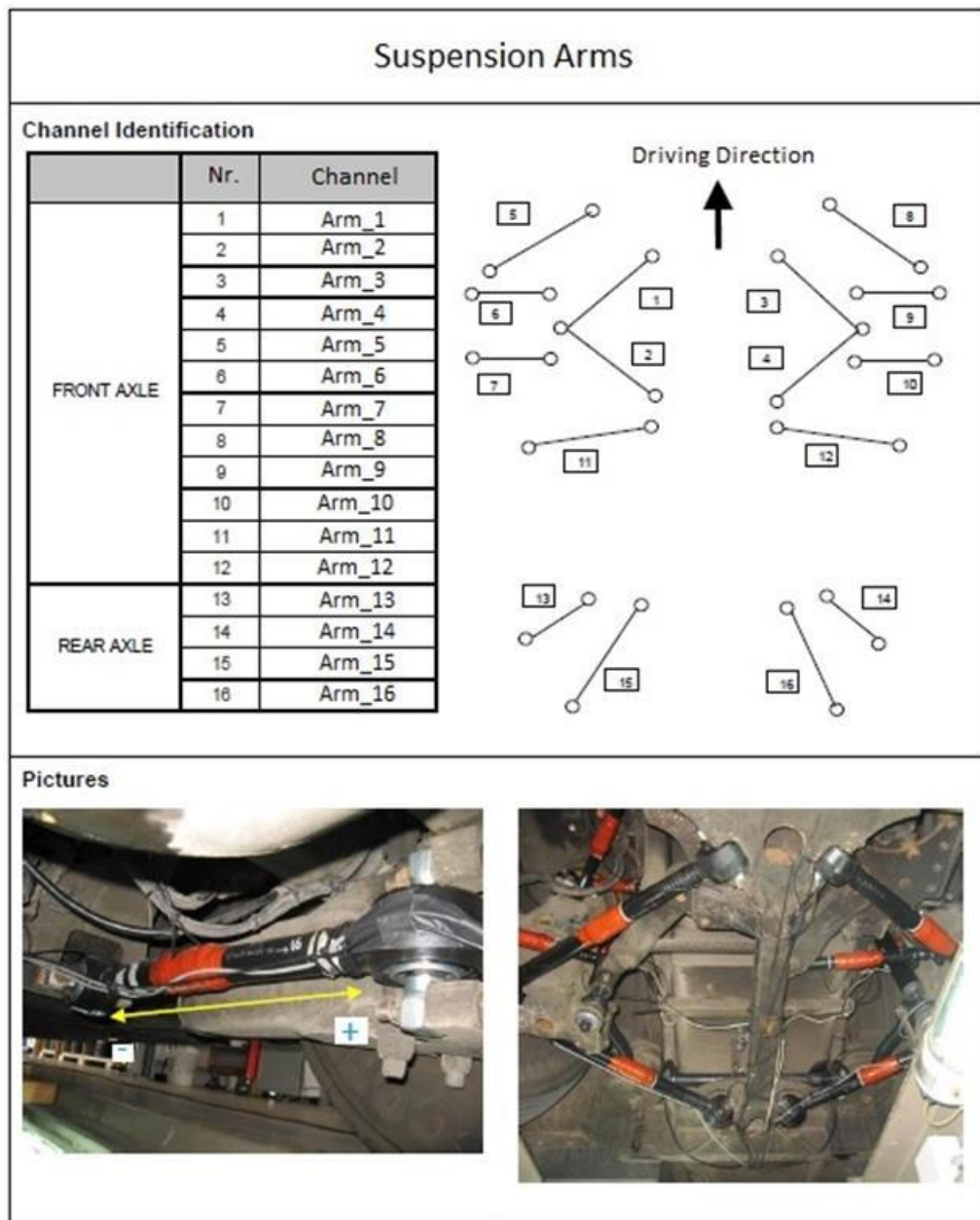


Figure 4.21 : Instrumentation plan of the suspension arms.

4.3.2 Wheel forces

Front and rear wheels were instrumented with wheel force transducers (WFT) to measure forces and moments. The model of the WFTs is Kistler S6HT. At the following figure, we can see the instrumentation plan of the wheel force transducers.

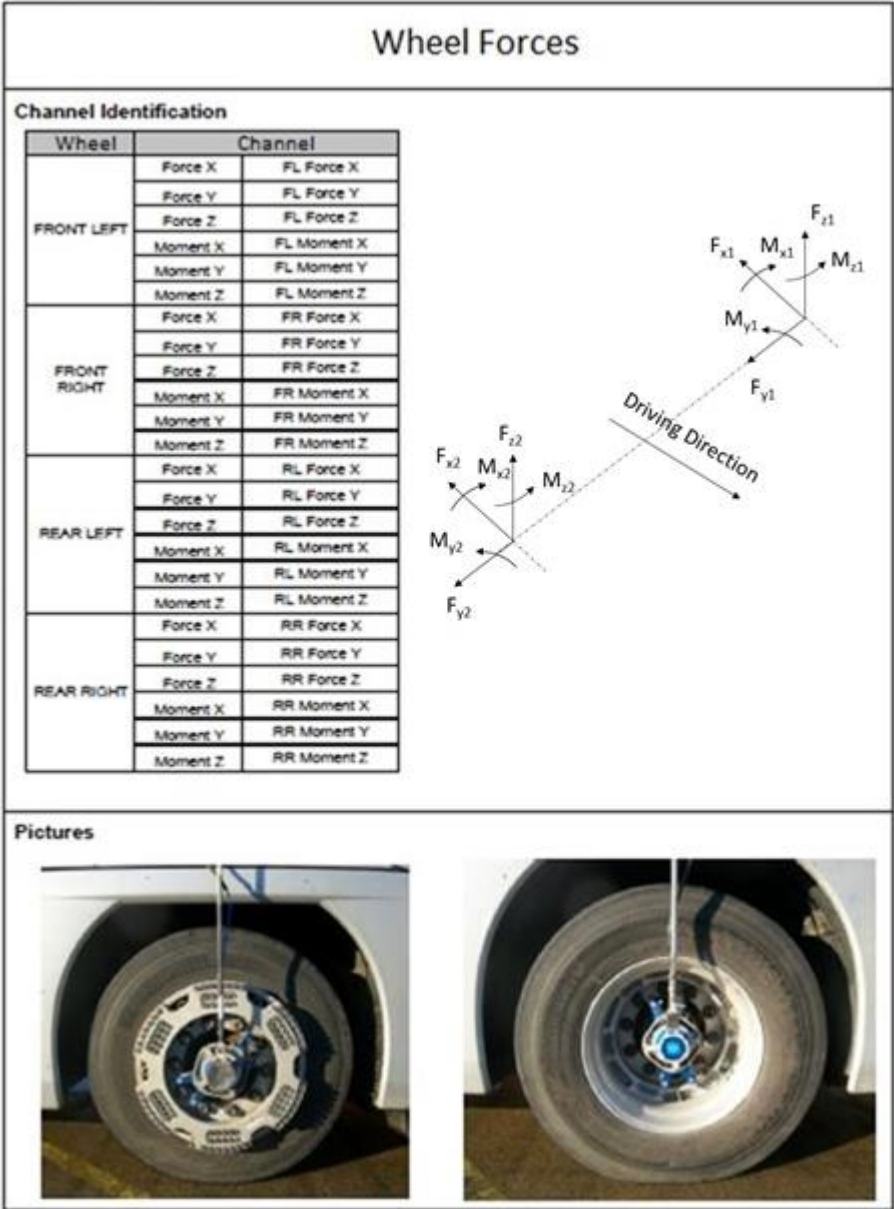


Figure 4.22 : Instrumentation plan of the wheel force transducers.

4.3.3 Shock absorbers

Front and rear axle shock absorbers were instrumented with strain gages in order to measure tension and compression forces. After the instrumentation, the shock absorbers were calibrated in order to determine the conversion factor strain – force which is explained in the previous section. At the following figure, we can see the instrumentation plan of the shock absorbers.

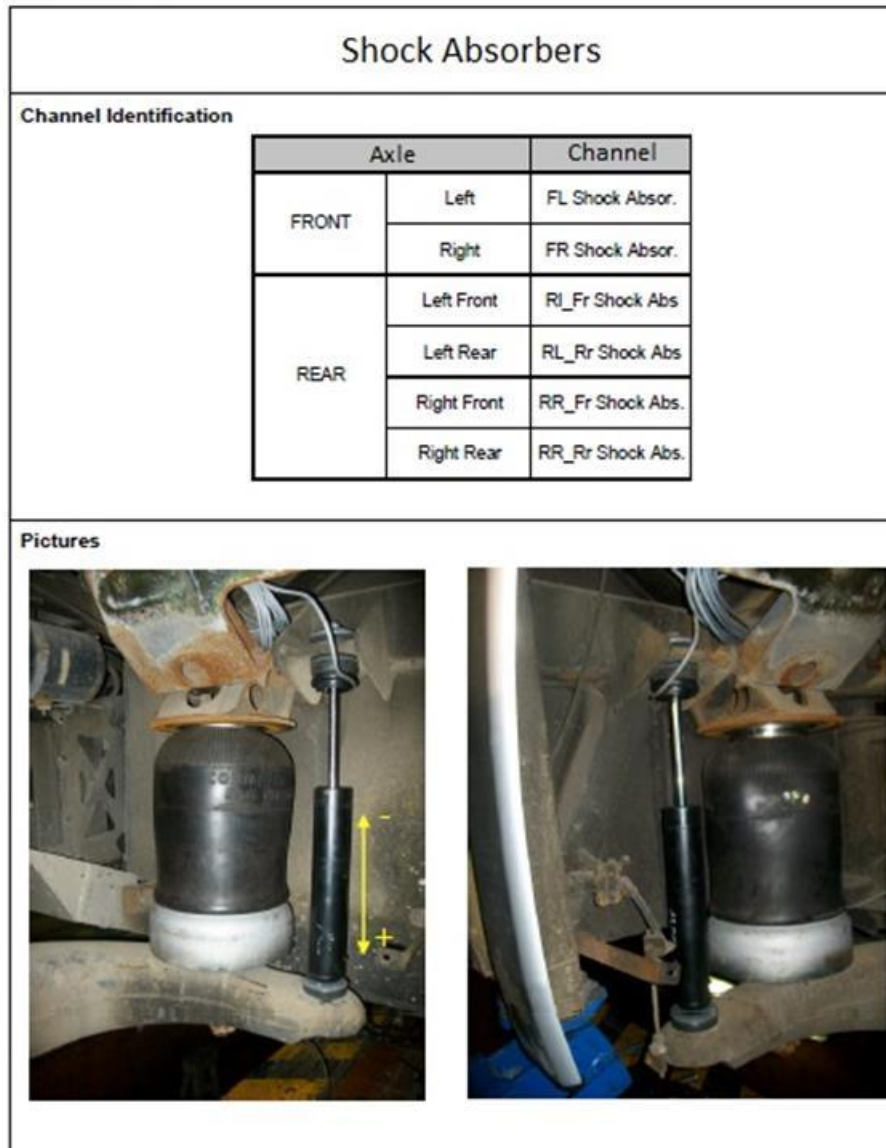


Figure 4.23 : Instrumentation plan of the shock absorbers.

4.3.4 Air spring forces

Front and rear axles air springs were instrumented with load cells in order to measure tension and compression forces. After the instrumentation, the air springs were calibrated in order to determine the sensitivity of the sensor, which is explained in the previous section. At the following figure, we can see the instrumentation plan of the air spring forces.

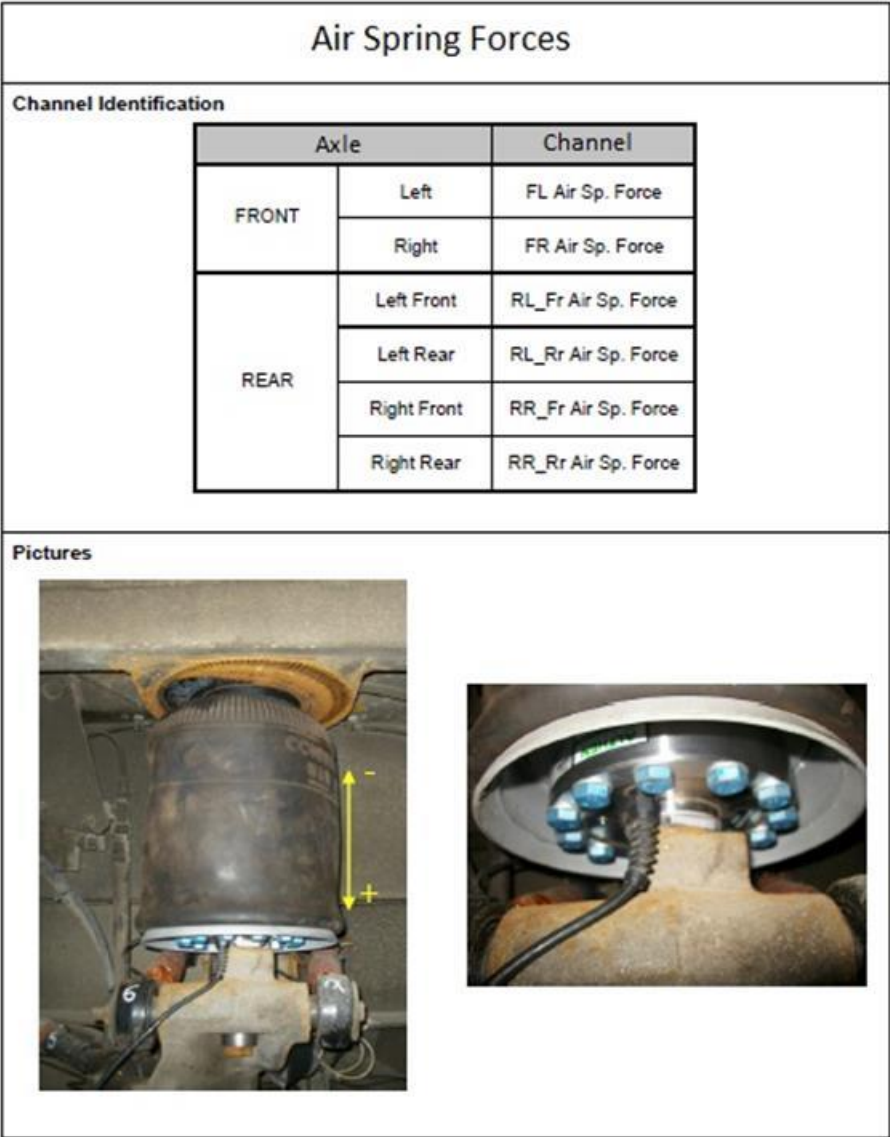


Figure 4.24 : Instrumentation plan of the air spring forces.

4.3.5 Anti-roll bar

Front axle anti-roll bar was instrumented with strain gages to measure the forces at the ends of the anti-roll bar. After the instrumentation, the anti-roll bar was calibrated in order to determine the conversion factor strain – force which is explained in the previous section. At the following figure, we can see the instrumentation plan of the anti-roll bar.

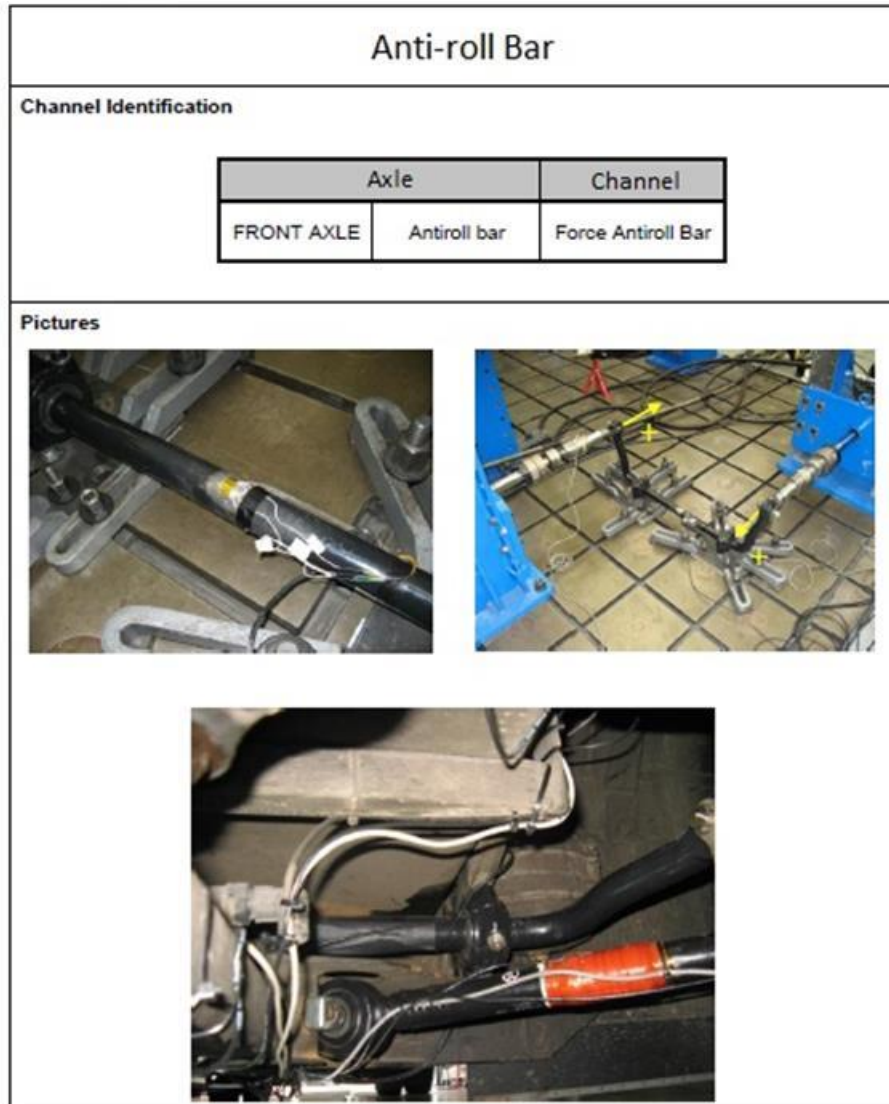


Figure 4.25 : Instrumentation plan of the anti-roll bar.

4.4 Vehicle Data and Vehicle Loading Conditions at the Measurements

The general properties of vehicle and vehicle loading conditions, which will be used for the measurement purposes, can be seen at the following tables. This vehicle is a two-axle coach that has an independent front axle and rigid rear axle.

Table 4.6 : Vehicle data.

Property	Unit	Value
Number of Axles	-	2
Wheel base	mm	6060
Overall length	mm	12240
Gross Vehicle Weight Rating (GVWR)	kg	18000
Front Axle Weight	kg	6890
Rear Axle Weight	kg	11600

Table 4.7 : Vehicle loading conditions.

Axle	Proving Ground			Customer Usage	
	empty	half-loaded	loaded	empty	loaded
Front Axle [kg]	5060	5790	6600	4929	-
Rear Axle [kg]	9900	11060	12000	9993	-
Overall [kg]	14960	16850	18600	14922	18780

Now we explain RLDA at the proving ground (PG) location.

4.5 Phase 3: RLDA at the Proving Ground Location (PG)

Product validation tests are essential at later design stages of product development. In the automotive industry, durability testing in a laboratory is an accelerated test that is specifically designed to replicate fatigue damage and failure modes from proving grounds (PG) testing. Detailed damage analysis is needed to correlate the accelerated test to PG testing. Therefore, accurate representation of PG loading is essential for laboratory-durability test development. PG loading can be measured by driving an instrumented vehicle over the PG with various test drivers. The vehicle is equipped with transducers for component loading histories and sensors for other important vehicle parameters [13]. The test track of the commercial vehicle producer is summarized at the following tables with an overview of the test programs, which are measured. The proving ground (test track) measurement campaign is performed with three different vehicle loading conditions (empty, half-loaded and loaded).

Table 4.8 : Various testing programs at proving ground - durability program I.

Program	Vehicle Speed [km/h]
Zero Balance	-
Measurement of the Motor Speed	0
small Sine Wave - out of phase	0-50
Measurement Track 07	18
Bad Highway	60
Bad Federal Road	50
Belgian Block	25
Pot-Hole Road	30
Höcker Curve	25
Bad Federal Road	30
Algerian Railroad Crossing	25
Good Highway	60
Bump Road	50
small Sine Wave - straight	0-50
Pot-Hole Road	20-50
Single Obstacle	20
Zero Balance	-

Table 4.9 : Various testing programs at proving ground - durability program II.

Program	Vehicle Speed [km/h]	Radius of the Turn [m]
Zero Balance	-	-
Eight Driving	20	-
Circular Driving left + Braking	10	-
Circular Driving right + Braking	10	-
Braking in reverse	5	-
Circular Driving left	35	30
Circular Driving right	35	30
Circular Driving left	0-max	12
Circular Driving right	0-max	12
Drive Line Change	40	-
Full Brake	30	-
Harsh Drive away with 3. Gear	-	-
Zero Balance	-	-

Table 4.10 : Reference test program at the proving ground.

Program	Vehicle Speed [km/h]
Zero Balance	-
Measurement of the Motor Speed	0
Bad Highway	50
Bump Road	50
small Sine Wave - out of phase	0-50
Bad Highway	50
Single Obstacle	25
Bad Federal Road - Acceleration	25-50
Algerian Railroad Crossing	25
Eight Driving	15
Full Brake	30
Turn the Steering by standing	0
Bad Highway	50
Measurement Track 07	20
Bad Federal Road - Acceleration	20-50
Cycle -1	-
Belgian Block	30
Pot-Hole Road	30
Höcker Curve	30
Good Highway	50
Bad Highway	50
Bad Federal Road	50
Cycle 1-7 as Cycle-1	-
Zero Balance	-

Now we have seen the test track at the following figure.

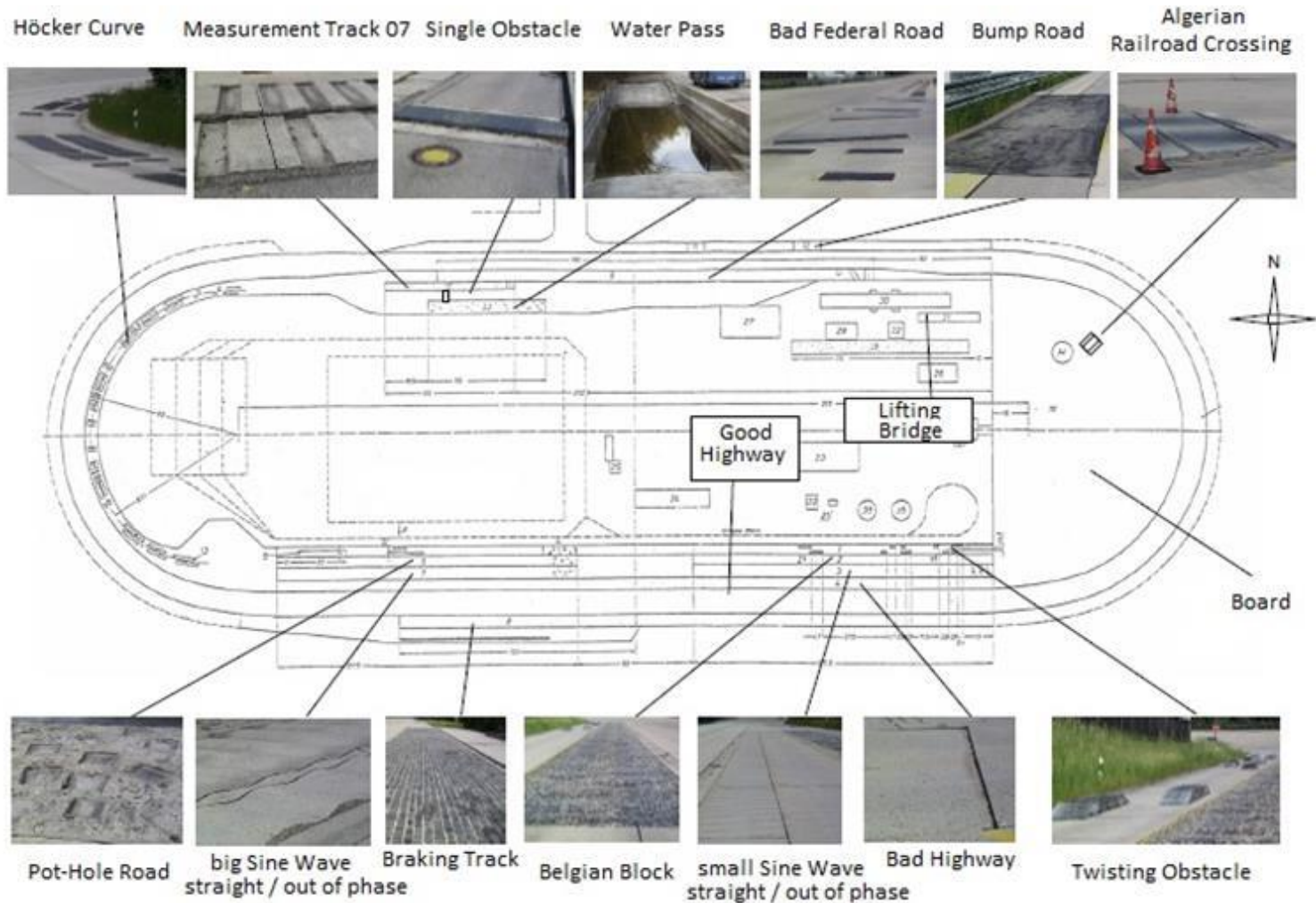


Figure 4.26 : Test track.

5. LOAD DATA ANALYSIS ON THE CUSTOMER USAGE

Lack of durability is not only a problem for commercial vehicle users also the producers suffer. Failures reduce company profitability through callbacks, warranty costs and bad-will. In other words, good durability leads to good quality and customer satisfaction. The particular loads, which affect commercial vehicle, are governed by their applications. The application decides where the commercial vehicle will be used and how it may be used.

The main factors that governing the loads are:

- The vehicle utilization that is the particular use of the truck giving the utilization profile described by for example transport mission and yearly usage.
- The operational environment that is the road conditions and other environmental conditions the commercial vehicle will experience.
- The driver's behavior that is the driver's influence on the load such as speed changes, braking, and ability to adapt to curves.
- The vehicle dynamics, for example the transfer of external road loads to local loads will be affected by the particular tires and suspension of the.
- Legislations, for example the speed limits, and allowed weight and size of commercial vehicle, in different regions and countries.

It is desirable to make a load description that is independent of the vehicle, i.e. a description of the vehicle utilization, the operational environment, the driver's behavior, and so on. It is thus necessary to describe the different load influential, preferably as simply as possible, e.g. by classifying the types of roads, or by describing each road by some few parameters.

When a component of the commercial vehicle is to be designed, the loads it is expected to meet have to be estimated. The design specification, detailing the minimum performance to be demonstrated in tests and calculations, is based on the expected vehicle usage and pertinent load estimation. The load estimation is based on several different sources. There is experience of the performance of previous designs, which has been verified on test grounds, in rig tests and/or through calculations. There have also been measurements on components of the commercial vehicles in service. The process seems satisfactory since most components function well and failures are rare. The component is rather that some parts of these commercial vehicles may become unnecessarily strong and heavy, which causes costs both for the producer in terms of material, and for the consumer in terms of permissible payload reduction. Since commercial vehicles are tested on proving grounds, it is possible that they pass tests on the proving ground of their producers but fail on the proving ground of their competitors. This test practice tends to produce over-designed commercial vehicles. A design being adequately strong for the world's most demanding customer will be over-designed for everybody else, and a design just fulfilling the median customer's expectations would be under-designed/unsatisfactory for every other customer. A truly unique commercial vehicle design for every customer is economically impossible; more than one experimental vehicle is needed to verify a completely new design. By "grouping" similar customers, an economically feasible design (without too much over-design, with reasonable production volume) may be found. The key is to understand and describe customer loads and their variation, i.e. the variation between customers, markets, transport tasks, etc. When discussing evaluation of customer loads there are two scales. In the small scale, the problem is to evaluate a specific customer or to compare the severity of two (or more) individual customers. In the large scale, the problem is to evaluate the severity of a population of customers, or to compare the severity of two different populations of customers (e.g. European customers and Brazilian customers).

In this chapter, the focus is given to the measured loads on the customer usage and at the proving ground respectively. Firstly, it is aimed to determine and describe the service loads. Service loadings in most cases display a random nature. In such cases, they can be illustrated through so-called load spectrum. The load spectrum for a

component is determined by the system behavior (stiffness, springs, dampers) of the design, its usage (driver, transport load) and environmental conditions (road roughness). The concept of loading is primarily limited to external forces (WFT Forces) which have a varying effect on the components; the loads affect the time-variable local stress in individual system points within the design [11]. Secondly, the required phase information between wheel forces will be investigated in order to create test program for the axles. For this purpose, the transfer function or frequency response function (FRF) will be used to define the phase shift between those wheel forces. Note that the methodical and systematical Approach in Section 2, which is also plotted at the following figure.

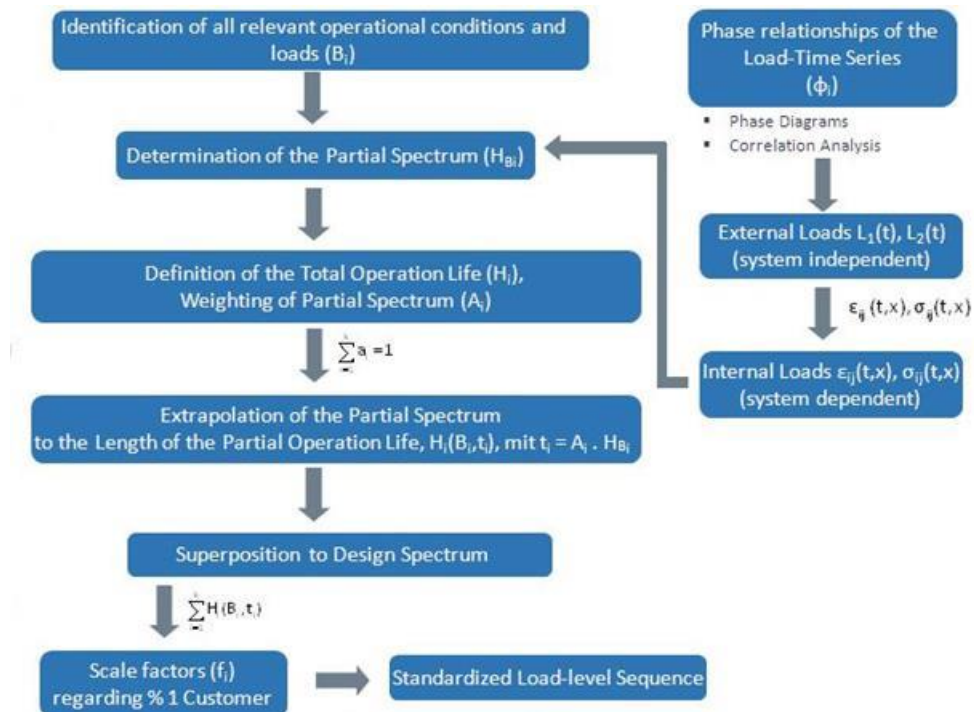


Figure 5.1 : Methodical and systematical approach.

Now in the next chapter we explain the identification of all relevant operational conditions and loads.

5.1 Step 1: Identification of All Operational Conditions and Loads (B_i)

It is necessary to use a variety of measuring sensors and measuring devices in order to determine service loads and stresses. The sequence of such a time-variable loading is depicted as the load-time-history. The service load data obtained under various operating conditions is used as a starting point to derive the relevant loading data for

dimensioning and proof-out of the individual vehicle components. It should be noted that the local stresses produced by the loadings are significant in terms of the design. In this step, all the relevant operational conditions and loads were identified by choosing characteristic roads. For this purpose, the characteristic roads are chosen as in following table.

Table 5.1 : The Characteristic roads.

Classification	Road Type
1-P	Highway
2-P Federal	Federal road
2-P National	National road
3-P	Local Connection Road
4-P	Main Traffic City
5-P	Local Traffic City

An example of the time signal of the wheel longitudinal force (front-left) from the measurement on Highway (approx. 732 km) can be seen at the following figure.

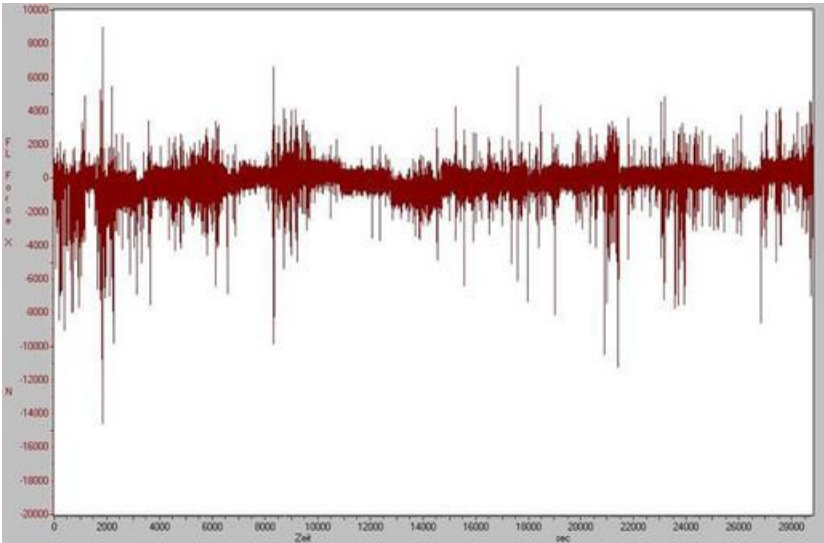


Figure 5.2 : Wheel longitudinal force front left – highway (732 km).

In the next chapter, we explain the determination of the partial spectrum $[H (B_i)]$.

5.2 Step 2: Determination of the Partial Spectrum $[H (B_i)]$

5.2.1 Pre-processing of load signals

- i. **Data Inspection and correction.** The process of acquisition of load data may contain errors. Therefore, the measured load signal needs to be inspected with

the aim to detect measurement errors, such as offsets, drifts, periodic variations, spikes, and noise. If present, these types of errors need to be corrected in order to get valuable results during later analysis. In the worst case, the results may otherwise be misleading, or simply wrong.

- ii. **Range-pair & level crossing counting.** These two methods are often used together for comparison of signals as they show somewhat complementary load information. The range-pair diagram as shown in the following figure shows the distribution of rainflow amplitudes, while the level crossing diagram gives a hint of the distribution of the mean values of the cycles, and information on the maximum and minimum of the signal. The range-pair method are used to analyze the in the next section.

The measurement campaigns result in several hundred files, each containing 97 channels. The length of the files varies from a 40 kilometers to about 100 km. Consequently, a huge amount of data has to be checked and corrected if necessary before further analysis. As explained above, this can hardly be achieved in a fully automated way. However, a semi-automatic approach could be the following:

- a. Calculate simple statistical values (min, max, mean, RMS “Root mean square” etc.) and check if these are reasonable.
- b. Pick a few measurements including the suspicious ones with respect to the simple statistics and check the data using a suitable display tool.
- c. If there are problems, apply the methods described above and tune the parameters to get reasonable results.
- d. Insofar as the tuned methods gave good results for the test measurements, apply them to the entire data set.
- e. Repeat the first step for the corrected data.

Of course, this is not a recipe for solving all the problems, but it should at least solve most of them. For the remaining issues, there is no way around a separate treatment unless the corresponding channels and measurements can be skipped in a further analysis.

Now we explain the derivation of the partial spectrum.

5.2.2 Derivation of the partial spectrum

It is necessary to use a variety of evaluation procedures in order to analyze the measured service loads or stresses. As long as the mean load remains constant, it is relatively simple to make an evaluation by counting the number of level crossings. If the mean load changes, it is necessary to resort to more complex counting methods for the structural durability evaluation. These counting procedures involve a one-parameter counting procedure with only a single parameter for the load or stress/strain selecting from range-pair, or level being counted to evaluate the cumulative frequency distribution. If mean loads/stresses are not constant, the counting of level crossing and range-pair will differ. In this step, the cumulative frequency distribution of service loads/stresses, the so-called load spectrum, can be derived based on the range-pair counting algorithm. Range pair is not sequential and only complete waves are recognized, as seen at the following figure. In addition, it counts the points in pair and suitable for fatigue life estimation [12].

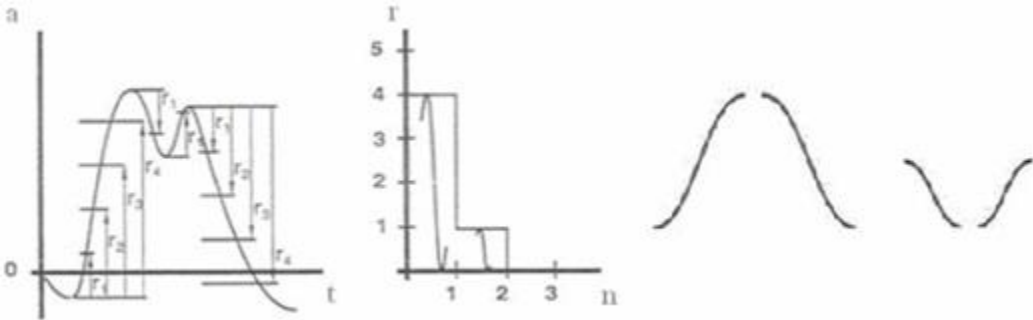


Figure 5.3 : Principal of range pair counting and wave pairs.

This method is the only one with a direct relation to hysteresis cycles. For a discretized load, it summarizes all cycles of a certain range or amplitude and forgets about the mean value. It can thus be obtained from the rainflow count by simply summing over all cycles with the same amplitude. The result is a vector, where the index indicates the range (or amplitude) and the value indicates the number of cycles. It can be plotted as a histogram. Note that the load spectrum introduced previously is the same as the range-pair count.

Apart from the counting procedures discussed above, which will be required later for durability evaluation, additional analysis procedures are also required for the structural durability testing. In the first instance, this includes an evaluation of the correlation of two functions, by which it is possible to make a determination based

on the magnitude and frequency of the values of individual loading or stress functions occurring simultaneously. However, this method and their results will be mentioned after this section.

An example of load spectrum or partial spectrum of the wheel longitudinal force (front-left) from the measurement on Highway (approx. 732 km) can be seen at the following figure.

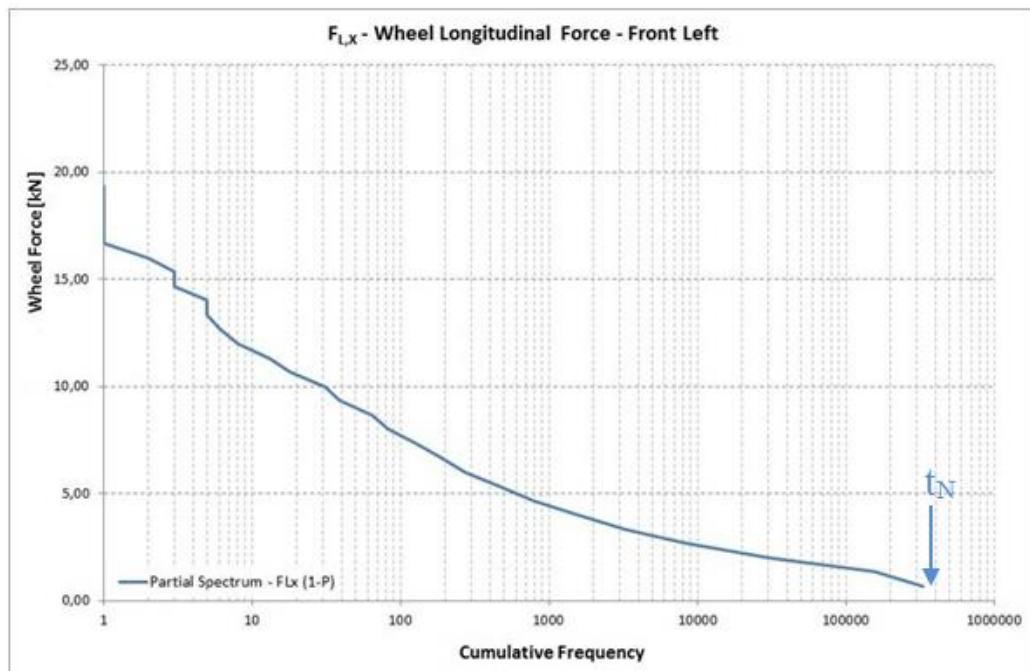


Figure 5.4 : Partial Spectrum of the wheel longitudinal force front left – highway.

In the next section, we will explain the definition of the total operation life (H_i) and weighting of partial spectrum (A_i).

5.3 Definition of Operation Life (H_i) and Weighting of Partial Spectrum (A_i)

In this step, the total operation life will be defined. In order to achieve this, each operational condition (e.g. each road type) will be multiplied with the weighting factors. The total operation life is a description, which is determined from the vehicle manufacturers. Each vehicle manufacturer defines differently for each customer usage. Considering the commercial vehicle axles (in our case study), the total operation life is plotted in the following table.

Table 5.2 : Definition of the total operation life on the customer usage.

Route Classification, Different Road Classes		Target Customer Usage Profiles [%]	Target Customer Usage [km]
1-P	Highway	10	100000
2-PF	Federal Road	20	200000
2-PN	National Road	30	300000
3-P	Local Connection	20	200000
4-P	Through Road	15	150000
5-P	Main Road	5	50000
Total		100	1000000

After defining the total operating life, it is simple to calculate the weighting factors (5.10).

$$A_i \rightarrow a_i \text{ Extrapolation factors} \quad (5.10)$$

Each weighting factor is the ratio of the measurement campaign to the target customer usage. In literature, the factors are also called extrapolation factors, which are plotted in the following Table.

Table 5.3 : The Extrapolation factors based on customer usage.

Route Classification, Different Road Classes		Target Customer Usage [km]	Measured Mileages on Customer [km]	Extrapolation Factors (a_i)
1-P	Highway	100000	732	137
2-PF	Federal Road	200000	2165	92
2-PN	National Road	300000	406	739
3-P	Local Connection	200000	258	775
4-P	Through Road	150000	76	1974
5-P	Main Road	50000	27	1852
Total		1000000	3664	$A_i = 273$

In the next section, we explain extrapolation of the partial spectrum to the length of the partial operation life $H_i (B_i, t_i)$.

5.4 Step 4: Extrapolation of Partial Spectrum to the Operation Life $H_i (B_i, t_i)$

It is necessary to extrapolate the partial spectrums with the help of the extrapolation factors, which were derived at the previous steps, to the length of the partial operation life. In order to achieve this, the extrapolation factors will be used to extend the cumulative frequency of the partial spectrum to the desired length of the partial operation life (5.11). At the following figure, we see the extrapolation of the partial spectrum to the length of the partial operation life of the wheel longitudinal force front left – highway (100000 km).

$$H_i (B, t_i), \quad t_i = a_i \cdot t_N \quad (5.11)$$

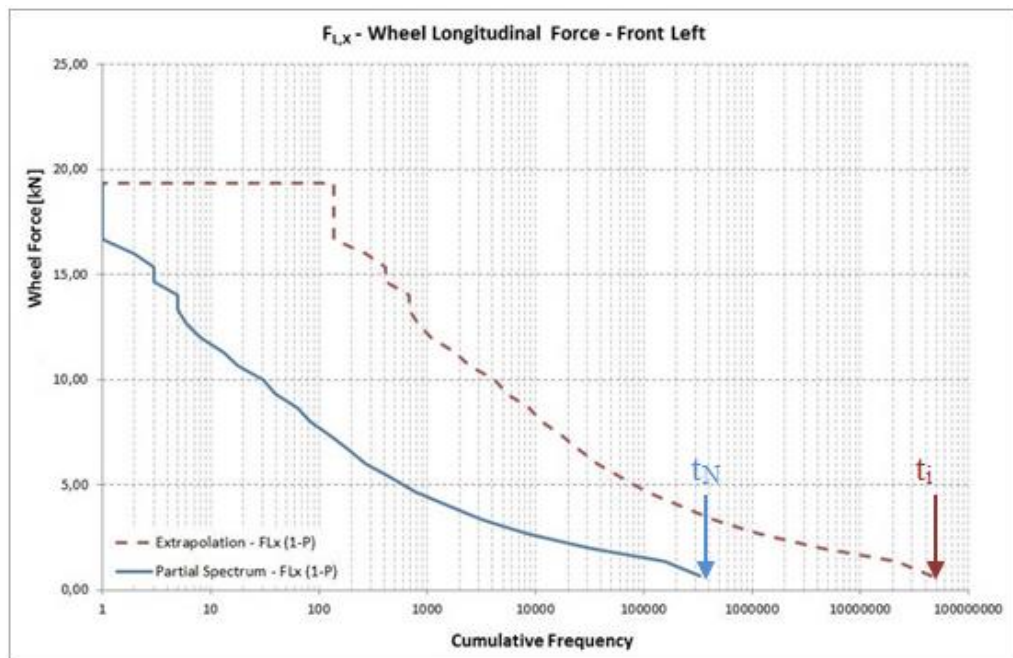


Figure 5.5 : Extrapolation of the partial spectrum – highway (100000 km).

After the extrapolation, it is hard to estimate the maximum amplitude of the investigated components because of their probability of occurrence at the short-term measurement. That is why some methods are developed to find better the maximum amplitude, which can be seen at the whole service life of the vehicle. One of these methods is also used in this study. However, the method and their results will be explained lately.

5.5 Step 5: Superposition to Design Spectrum H (B, t_N)

The term superposition means here to combine the individual derived extrapolated spectrums. Thus it can be derived a spectrum, that called design spectrum. This spectrum has a significant role to service life of the investigated component. A design spectrum includes all the relevant operating conditions and loads of the investigated component. In this study, the commercial vehicle axles are investigated. As long as the external forces (F_x, F_y and F_z) are measured on the characteristic proads, it is relatively simple to make assumptions about the testing program of these commercial vehicle axles. At the following figure, we see design spectrum of the wheel longitudinal force front left (10⁶ km).

To achieve this, the following equation is used to derive those design spectrums (5.12).

$$H(B, t_N) = \sum_{i=1}^k H_i(B, t_i) \tag{5.12}$$

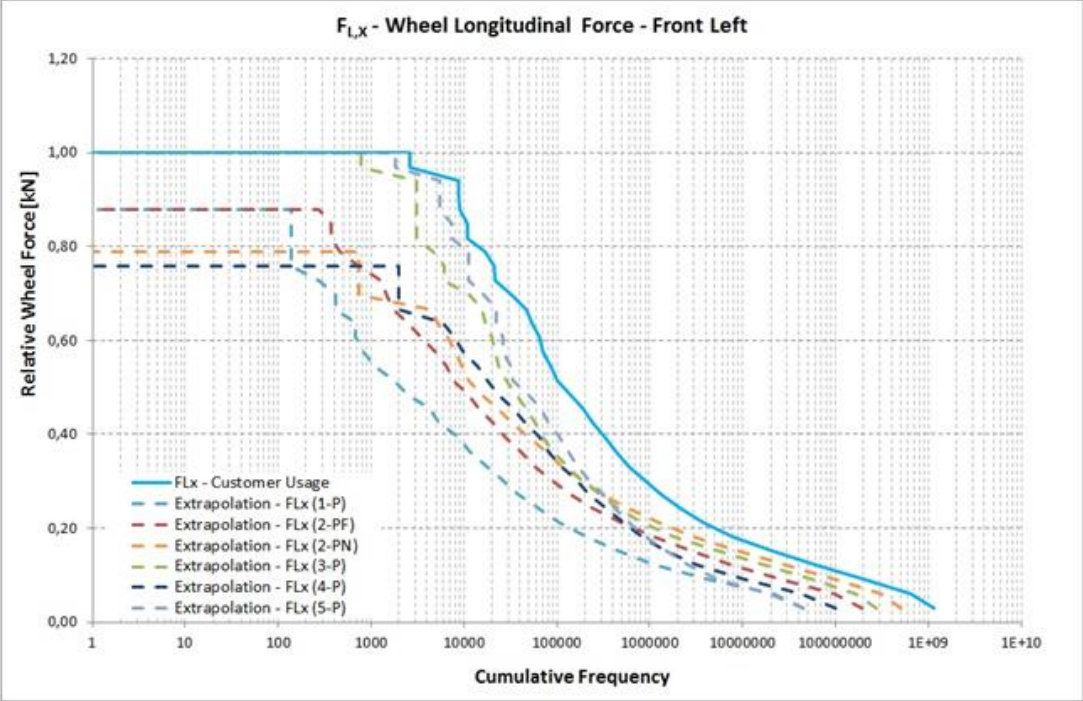


Figure 5.6 : Design spectrum of the wheel longitudinal force front left (10⁶ km).

5.6 Step 6: Scaling Factors of Wheel Forces (f_i)

It is also necessary to standardize these spectrums in order to derive the test program of the investigated components (commercial vehicle axles) by means of scaling factors. The idea behind of this, it is a factor, which helps us to scale the wheel forces in one direction to another direction. For example, the measured wheel vertical forces (front left) are normalized to the maximum range of the vertical force. The result of this normalization is one. After that, some procedure will be used again to the wheel lateral forces. For example, the measured wheel lateral forces are normalized again to the maximum range of the vertical force. This time, the result can be 0.3. This means, if we scale the spectrum of the lateral forces (front left) with a factor of 3.3, we can obtain the vertical forces at the service life of the vehicle. This helps us lately to derive the other components of wheel forces by using only wheel vertical forces, as long as these spectrums are almost same shape values.

In other words, the mathematical formula is summarized in the following equation (5.13).

$$\frac{H(B, t_N)_{FL,i}}{H(B, t_N)_{Fzmax}} = f_{i_{FL}} \quad (5.13)$$

Now the scaling of the wheel lateral forces to the wheel max. vertical force (front left) (5.14);

$$\frac{H(B, t_N)_{FL,y}}{H(B, t_N)_{Fzmax}} = 0,3 \rightarrow f_{y_{FL}} \quad (5.14)$$

At the following figure, we see normalized design spectrums of the wheel forces to the maximal vertical force – front left.

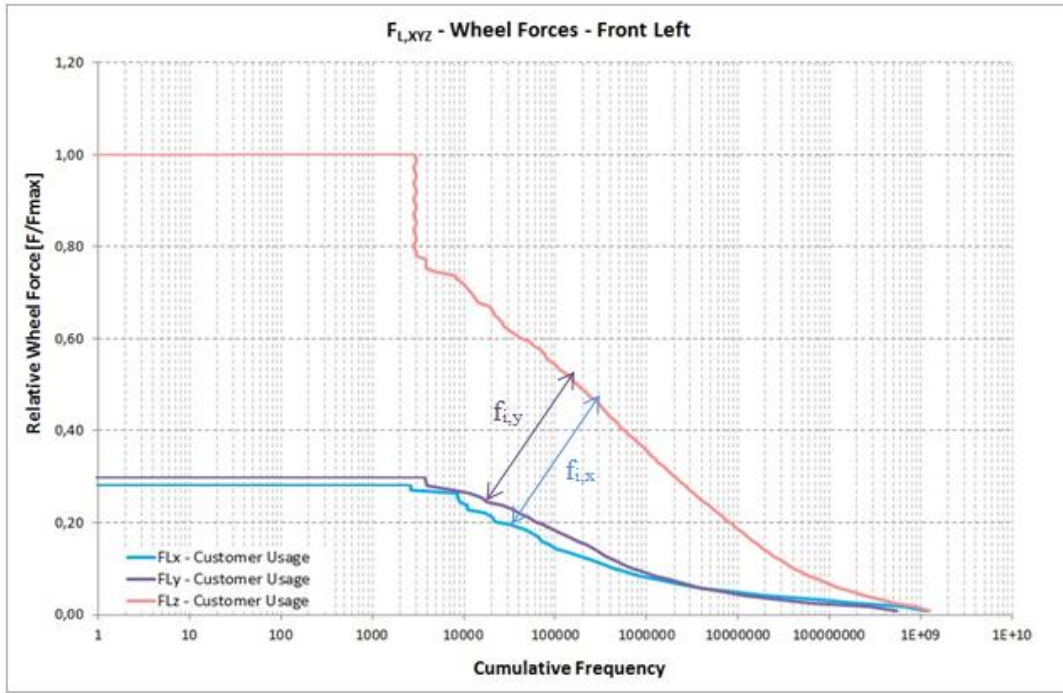


Figure 5.7 : Normalized design spectrums of the wheel forces to the max force.

At the following figure, we see scaled design spectrums of the wheel forces based on vertical force – front left.

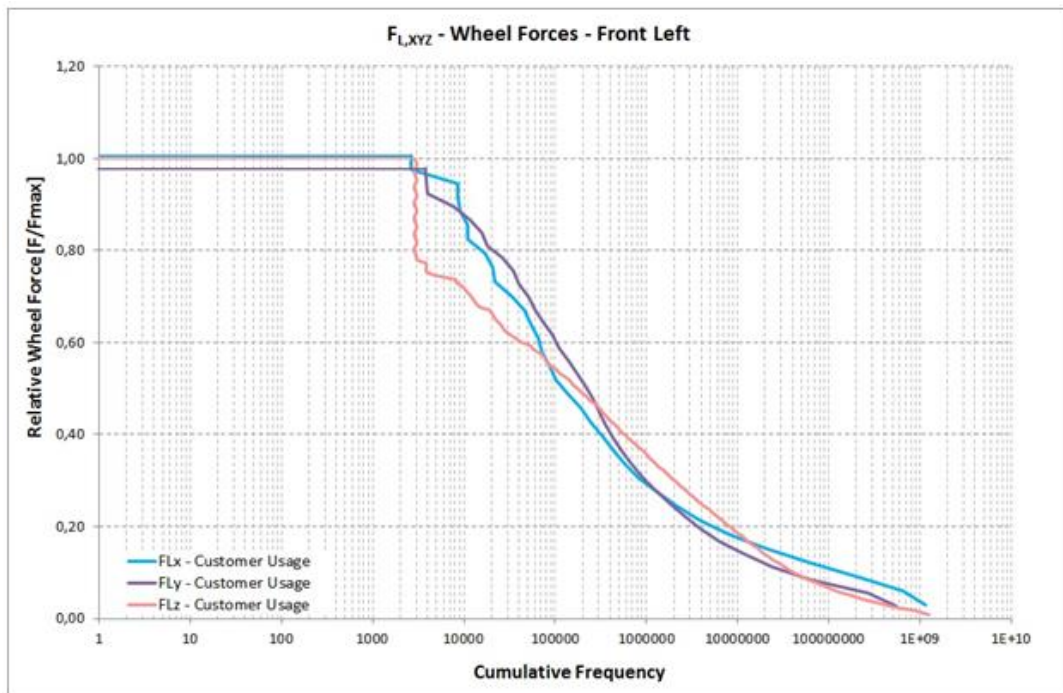


Figure 5.8 : Scaled design spectrums of the wheel forces based on vertical force.

After these analyses, the scaling factors are determined for each force direction and plotted in the following table.

Table 5.4 : Scaling factors of wheel forces on the customer usage [f_i].

Scaling Factors on the Customer Usage [f_i]		
f_{zFL}	$H(B, t_N)_{FL,z}/H(B, t_N)_{FL,zmax}$	1,00
f_{yFL}	$H(B, t_N)_{FL,y}/H(B, t_N)_{FL,zmax}$	0,30
f_{xFL}	$H(B, t_N)_{FL,x}/H(B, t_N)_{FL,zmax}$	0,28
f_{zFR}	$H(B, t_N)_{FR,z}/H(B, t_N)_{FR,zmax}$	1,00
f_{yFR}	$H(B, t_N)_{FR,y}/H(B, t_N)_{FR,zmax}$	0,32
f_{xFR}	$H(B, t_N)_{FR,x}/H(B, t_N)_{FR,zmax}$	0,28
f_{zRL}	$H(B, t_N)_{RL,z}/H(B, t_N)_{RL,zmax}$	1,00
f_{yRL}	$H(B, t_N)_{RL,y}/H(B, t_N)_{RL,zmax}$	0,32
f_{xRL}	$H(B, t_N)_{RL,x}/H(B, t_N)_{RL,zmax}$	0,40
f_{zRR}	$H(B, t_N)_{RR,z}/H(B, t_N)_{RR,zmax}$	1,00
f_{yRR}	$H(B, t_N)_{RR,y}/H(B, t_N)_{RR,zmax}$	0,29
f_{xRR}	$H(B, t_N)_{RR,x}/H(B, t_N)_{RR,zmax}$	0,40

In the next section, we summarize the first 6 steps on customer usage.

5.7 Summary of the first 6 Steps on the customer usage (CU)

It is also very helpful to summarize these entire steps as flow chart in the figure in order to make a better overview for the analysis of the loads.

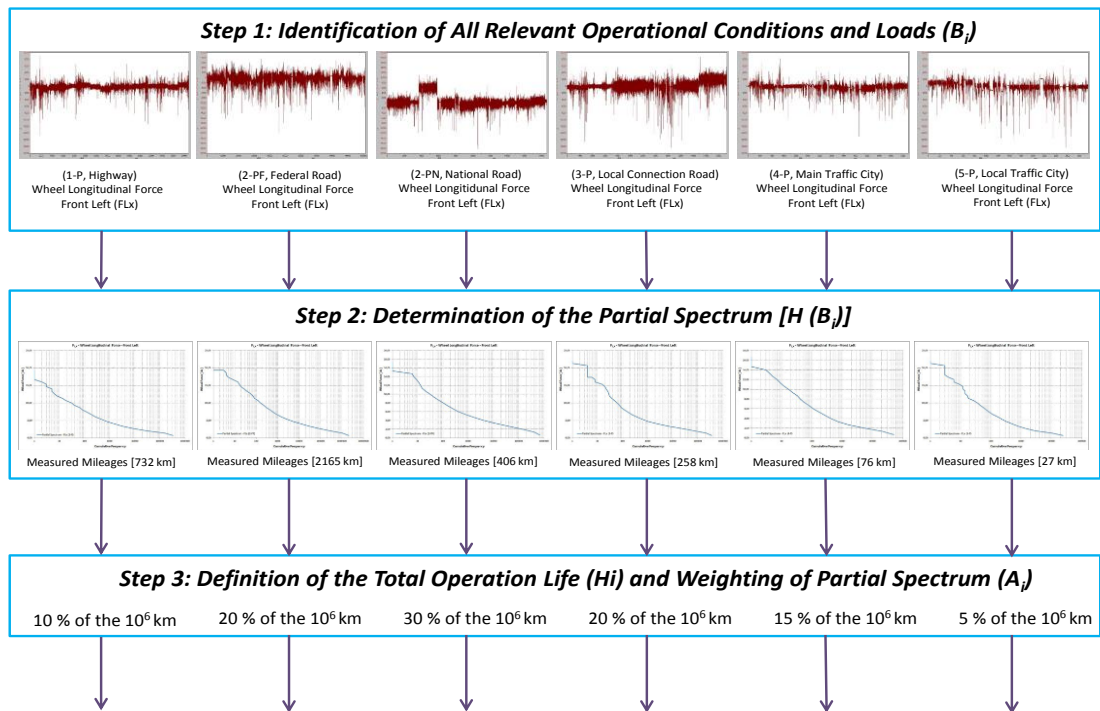


Figure 5.9 : Summary of the six steps of the load data analysis on the CU.

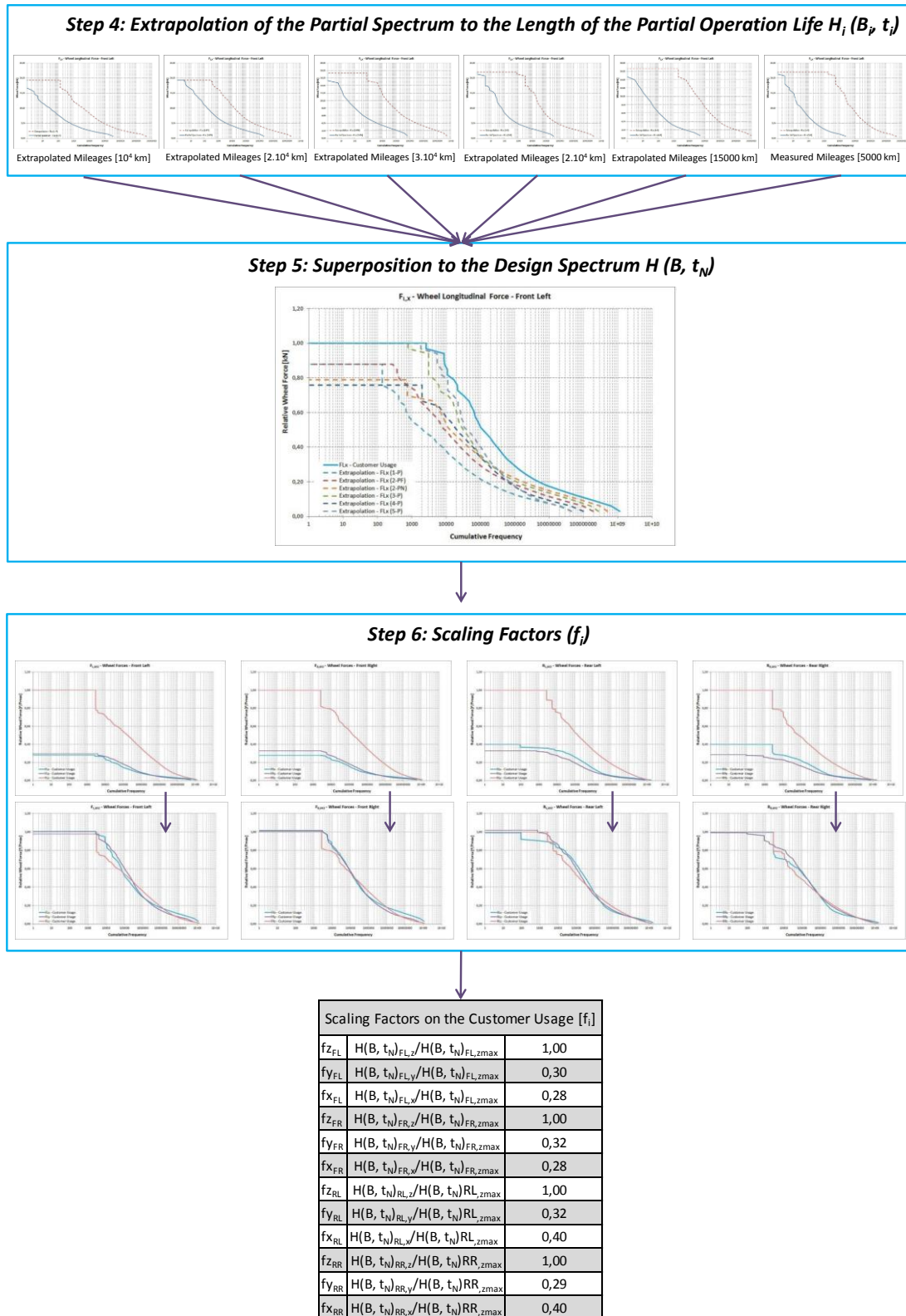


Figure 5.9 (continued): Summary of the six steps of the load data analysis on CU.

6. LOAD DATA ANALYSIS AT THE PROVING GROUND

The design loads are often defined through a test track. Existing driving schedules for the proving ground may be based on empirical knowledge about the relation between the loads on the test track and the expected service loads. A typical rule might read as follows:

“A unit of the proving ground load is defined as a certain set of lanes and maneuvers with a total length of 5 km. It has to be repeated 1000 times. The corresponding load is supposed to cover 1.000.000 km of Western Europe customer usage.”

The rule might depend on the target market as well as on the type of truck. There are two ways of defining a schedule:

1. By long-term experience. In that case, it is only known from previous results that the proving ground load is enough demanding to cover the customer usage. The relation between the customer load and the design load is not given explicitly. However, in this case it can be back calculated from the customer load distribution and measured test track loads.
2. A proving ground schedule can also be derived from the description of the design load in terms of pseudo damage values or rainflow matrices (or range-pair spectrum) for all channels under consideration. The target (i.e. the design load) needs to be derived from load data in customer service as explained in the previous section. Often, the target load represents a certain quantile of the customer loading. Since the strength requirement essentially is the design load times the safety factor, we can equally well use the strength requirement as the target for the optimization.

In the latter case, the mapping of the proving ground to the load targets (design loads or strength requirements) can be done using optimization techniques, which take into account all interesting spots (channels or sensors). However, this topic will be not discussed in this study.

6.1 Step 1: Measurement at Various Vehicle Loading Conditions

If we consider the same procedure, which is discussed in detail in the previous chapter, we could obtain the scaling factors. Before the results of these analyses are explained, firstly it is mentioned about the definition of the total operation life at the proving ground. The following table enables us to make it easier to understand the idea behind of this.

At the following table, we see the definition of the total operation life and the extrapolation factors at the proving ground.

Table 6.1 : Definition of the total operation life and the extrapolation factors.

Proving Ground	Vehicle Loading Condition			
	empty	half-loaded	loaded	Total
Percentages [%]	33,3	33,3	33,3	100
Mileages on the PG [km]	10000	10000	10000	30000
Measured Mileages on PG	18,5	18,5	18,5	55,5
Extrapolation Factors	$A_i = 541$			

The measurements were executed at the proving ground with three different vehicle-loading conditions. The percentages of these loading conditions are previously determined according to the long-time vehicle measurements at the customer usage.

The proving ground measurement campaign includes three different measurement programs, which are durability program I-II, reference test program. The reference the program is only suitable to derive the test spectrums. Others can only be used to analyze the critical points of the components by some extreme driving usage.

An example of the time signal of the wheel longitudinal force (rear-right) from the measurement at the proving ground with a loaded vehicle (approx. 18.5 km) can be seen at the following figure.

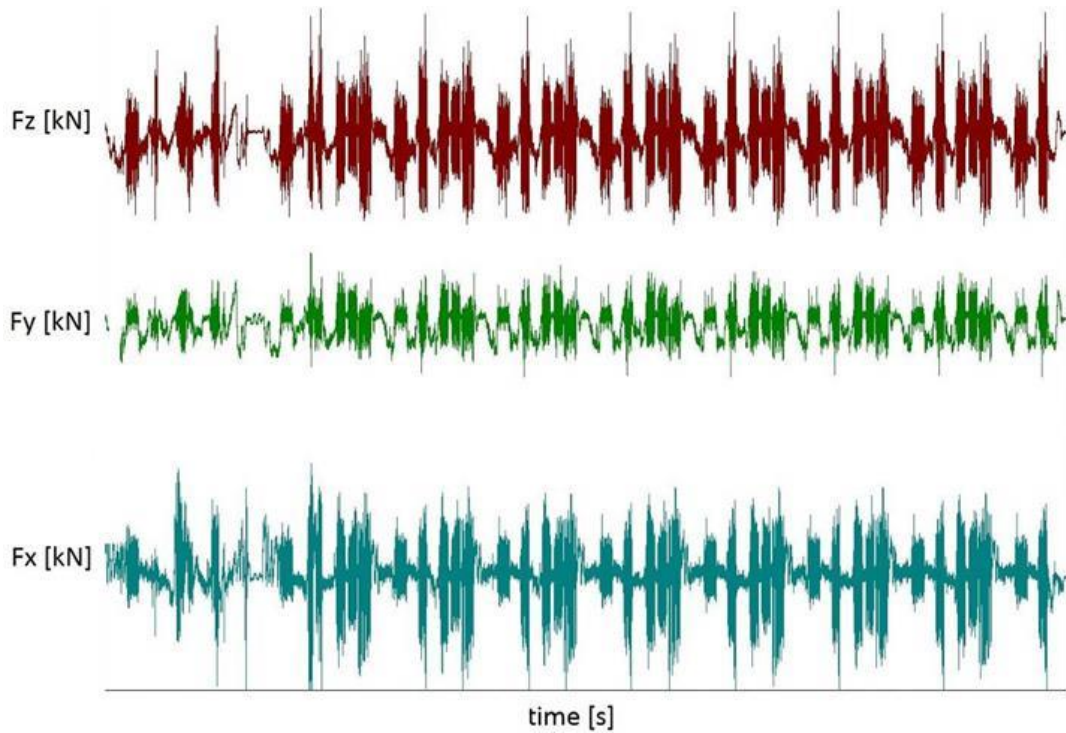


Figure 6.1 : Measured WFT forces from the reference test program.

In the next section, we summarize the first 6 steps at proving ground.

6.2 Summary of the first 6 Steps at the proving ground (PG)

As in the previous chapter explained, the steps from two to six are used to derive load spectrums and the scaling factors for the analysis of the measurement of the test track. It is also very helpful to summarize these entire steps as flow chart in order to make a better overview for the analysis of the loads.

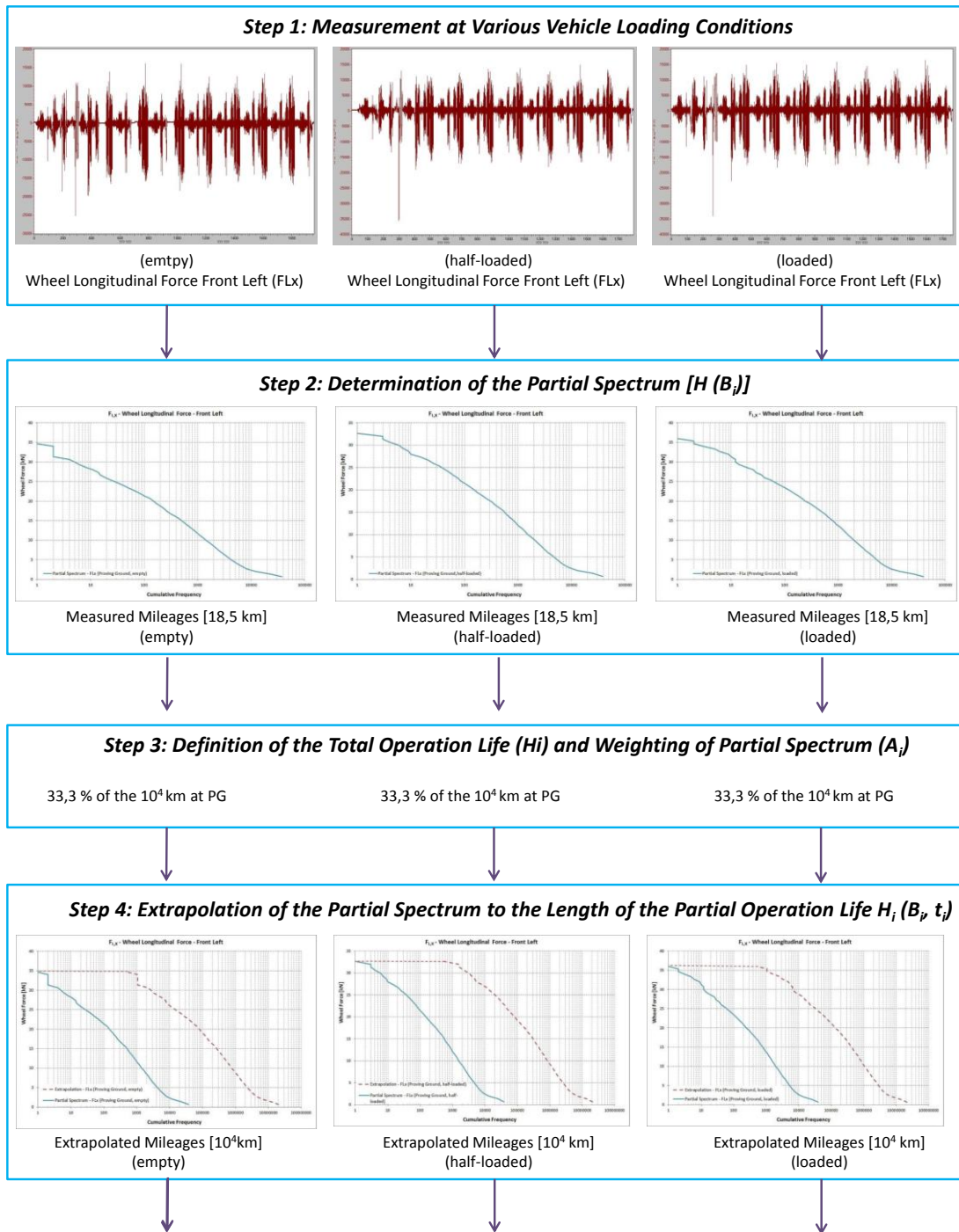
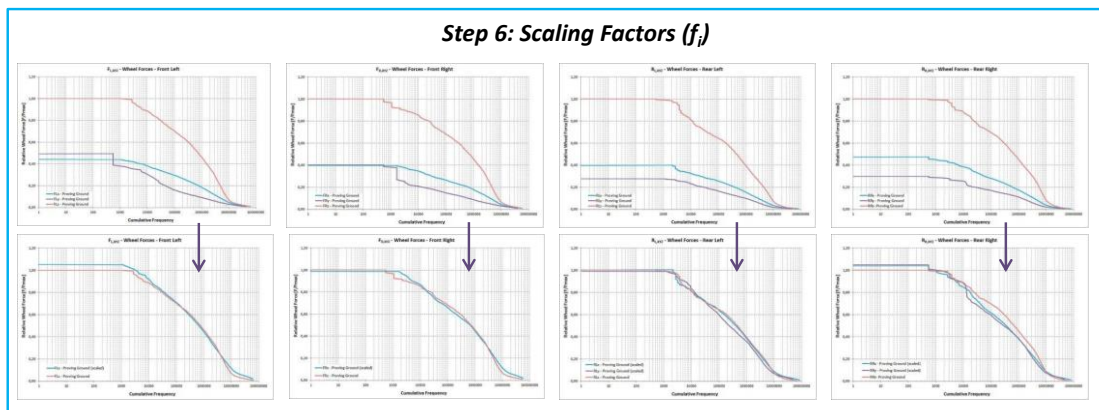
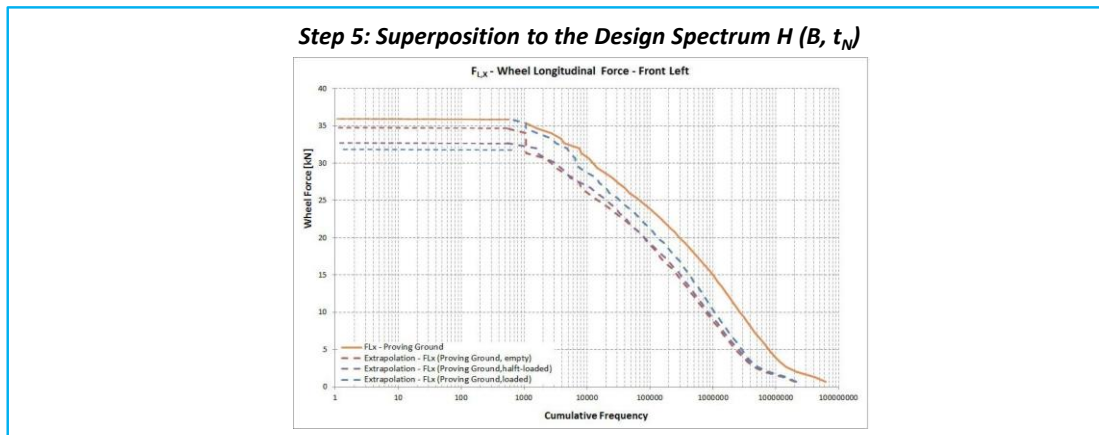


Figure 6.2 : Summary of the first six steps of the load data analysis at the PG.



Scaling Factors on the Proving Ground [f_i]		
$f_{z_{FL}}$	$H(B, t_N)_{FL,z} / H(B, t_N)_{FL,zmax}$	1,00
$f_{y_{FL}}$	$H(B, t_N)_{FL,y} / H(B, t_N)_{FL,zmax}$	-
$f_{x_{FL}}$	$H(B, t_N)_{FL,w} / H(B, t_N)_{FL,zmax}$	0,42
$f_{z_{FR}}$	$H(B, t_N)_{FR,z} / H(B, t_N)_{FR,zmax}$	1,00
$f_{y_{FR}}$	$H(B, t_N)_{FR,y} / H(B, t_N)_{FR,zmax}$	-
$f_{x_{FR}}$	$H(B, t_N)_{FR,w} / H(B, t_N)_{FR,zmax}$	0,40
$f_{z_{RL}}$	$H(B, t_N)_{RL,z} / H(B, t_N)_{RL,zmax}$	1,00
$f_{y_{RL}}$	$H(B, t_N)_{RL,y} / H(B, t_N)_{RL,zmax}$	0,28
$f_{x_{RL}}$	$H(B, t_N)_{RL,w} / H(B, t_N)_{RL,zmax}$	0,40
$f_{z_{RR}}$	$H(B, t_N)_{RR,z} / H(B, t_N)_{RR,zmax}$	1,00
$f_{y_{RR}}$	$H(B, t_N)_{RR,y} / H(B, t_N)_{RR,zmax}$	0,29
$f_{x_{RR}}$	$H(B, t_N)_{RR,w} / H(B, t_N)_{RR,zmax}$	0,45

Figure 6.2 (continued): Summary of the first six steps of load data analysis at PG.

As mentioned above, first five steps are used to derive the normalized design spectrum of suspension arms, air spring forces and shock absorbers at the proving ground. See the following figures for the results.

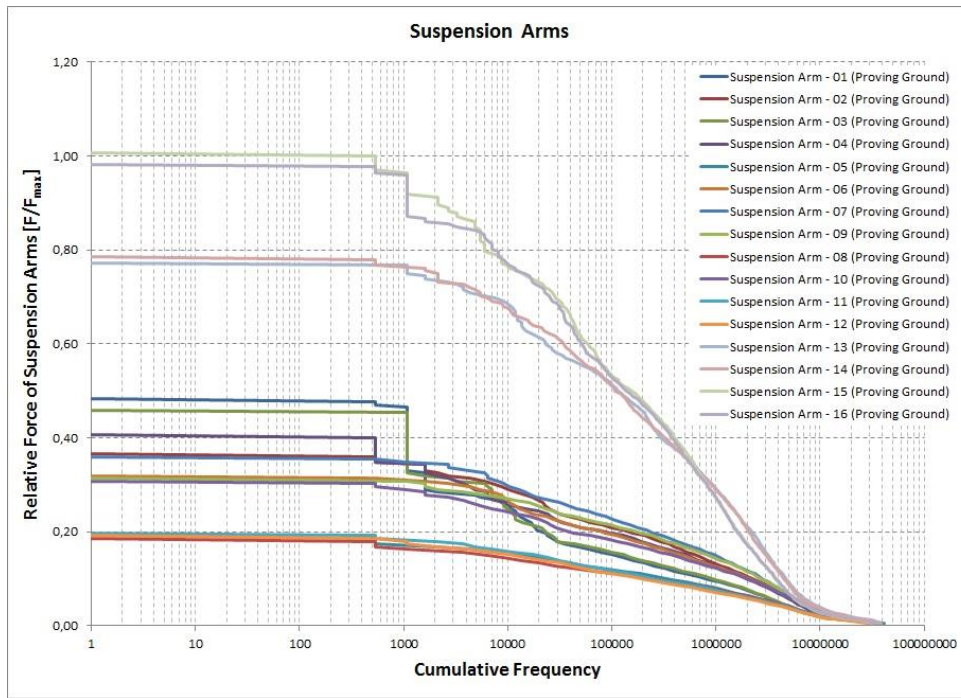


Figure 6.3 : Normalized design spectrum of suspension arms at the PG.

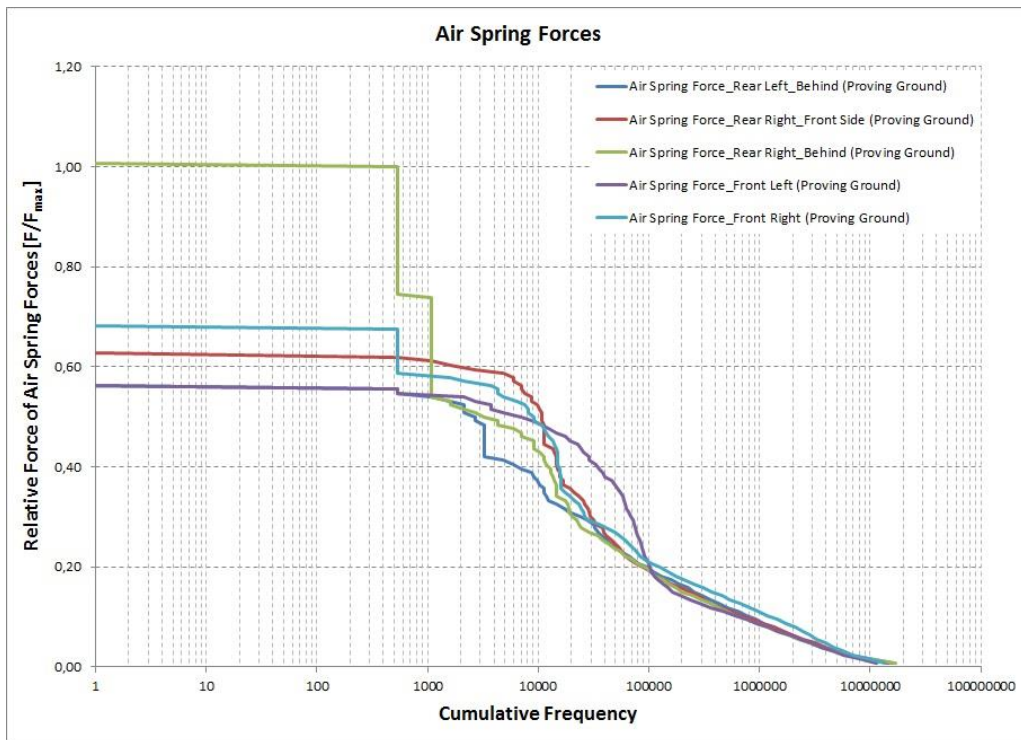


Figure 6.4 : Normalized design spectrum of air spring forces at the PG.

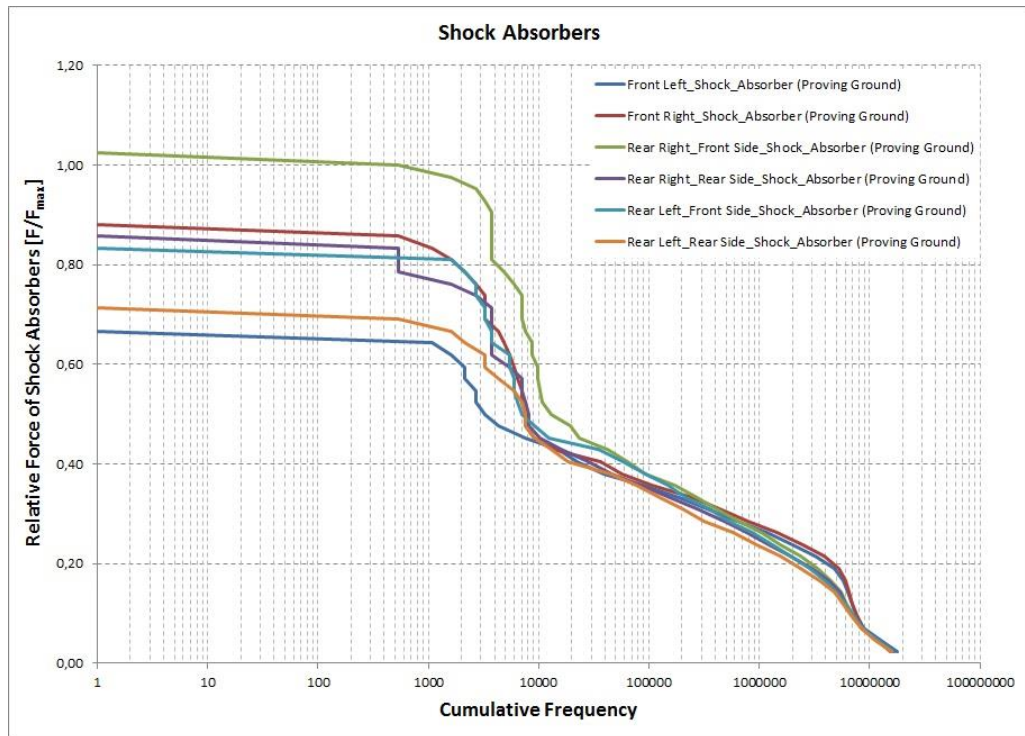


Figure 6.5 : Normalized design spectrum of shock absorbers at the PG.

In the next section, we explain the scaling factors of suspension arms (f_i).

6.3 Scaling Factors of Suspension Arms (f_i)

It is obvious to see that the rear suspension arms, which are 13, 14, 15 and 16, are relatively high loaded compared to others. The air spring forces at the rear right side of the vehicle (behind) are also higher than the other air spring forces. If we look at the shock absorber, the right of the vehicle is always more loaded compared to the left side of the vehicle. As explained in the previous section, the scaling factors are determined for each suspension arms and plotted the scaled design spectrums in the following figure. However the scaling factors for the suspension arms 3 and 4 couldn't be calculated at the proving ground because of the different shape of spectrum distributions.

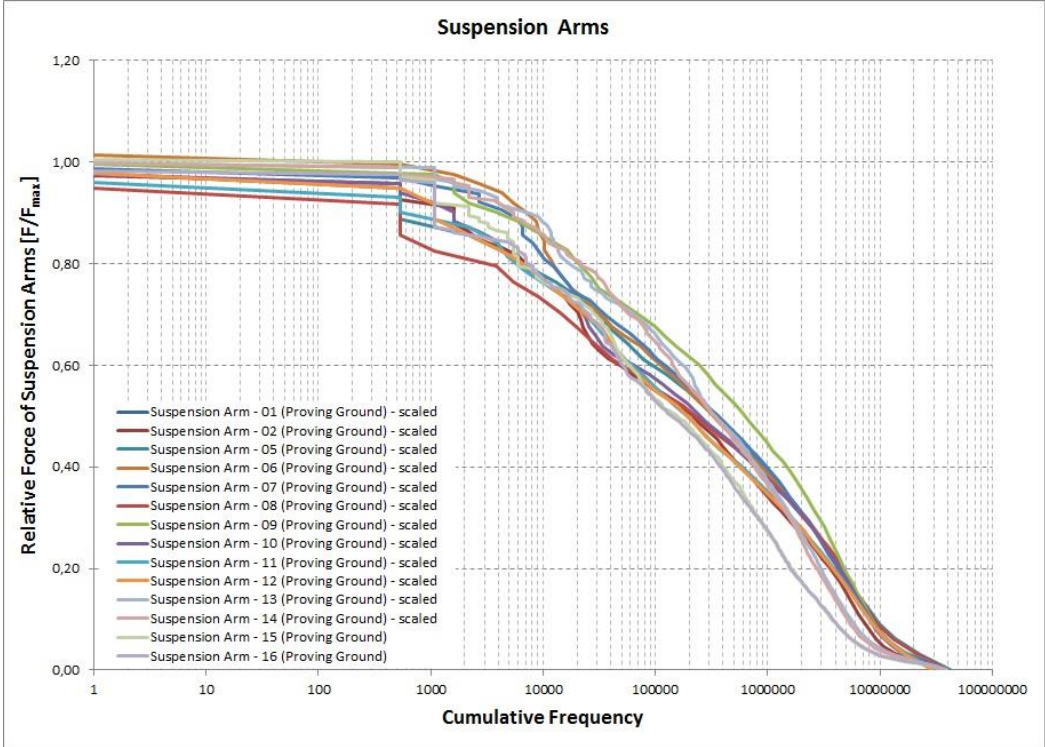


Figure 6.6 : Scaled design spectrums of the suspension arms.

At the following table, we see the scaling factors of suspension arms at the proving ground [f_i].

Table 6.2 : Scaling factors of suspension arms at the proving ground [fi].

Axle	Channels	Scaling Factors at the Proving Ground [f_i]
Front Axle	Suspension Arm - 01 (Proving Ground)	0,48
	Suspension Arm - 02 (Proving Ground)	0,37
	Suspension Arm - 05 (Proving Ground)	0,19
	Suspension Arm - 06 (Proving Ground)	0,31
	Suspension Arm - 07 (Proving Ground)	0,36
	Suspension Arm - 08 (Proving Ground)	0,19
	Suspension Arm - 09 (Proving Ground)	0,31
	Suspension Arm - 10 (Proving Ground)	0,31
	Suspension Arm - 11 (Proving Ground)	0,20
	Suspension Arm - 12 (Proving Ground)	0,19
Rear Axle	Suspension Arm - 13 (Proving Ground)	0,77
	Suspension Arm - 14 (Proving Ground)	0,78
	Suspension Arm - 15 (Proving Ground)	1,00
	Suspension Arm - 16 (Proving Ground)	1,00

7. COMPARISON OF SCALING FACTORS (f_i) OF WHEEL FORCES

The scaling factors that are calculated for the customer usage and the proving ground are compared. The main object of this comparison is to standardize the wheel loads that are acting on the axles, as long as the conformity of the factors for each measurement campaign exists. It is obvious to see that the scaling factors are almost same for each measurement. However, the scaling factors for the longitudinal direction, which are calculated at the proving ground measurements, are always slightly higher than the factors that are obtained from the measurement on the customer usage. Another point is that, the scaling factors for the lateral direction couldn't be calculated at the proving ground because of the different shape of vertical and lateral spectrum distributions of the forces at the front axle. In addition, the scaling factors in lateral direction for each axle and wheel are always same as on the customer usage, the factor is approx. 0.3. That means, the load spectrum of the vertical forces are always 3.3 times higher than the lateral forces. Besides, the scaling factors in lateral direction for each wheel at the rear axle are always around 0.29 on the customer usage. In other words, the load spectrums of the vertical forces are always approx. 3.5 times higher than the lateral forces at the rear axle on the customer usage. The scaling factors for the longitudinal direction are around 0.42 at each axle and wheel at the proving ground. That is why; the vertical forces acting the wheels are 2.4 times higher than the longitudinal forces at the proving ground. On the customer usage, at the front axle and rear axle the scaling factors for the longitudinal direction are 0.28 and 0.4 respectively. An overview of the scaling factors can be seen at the following figure.

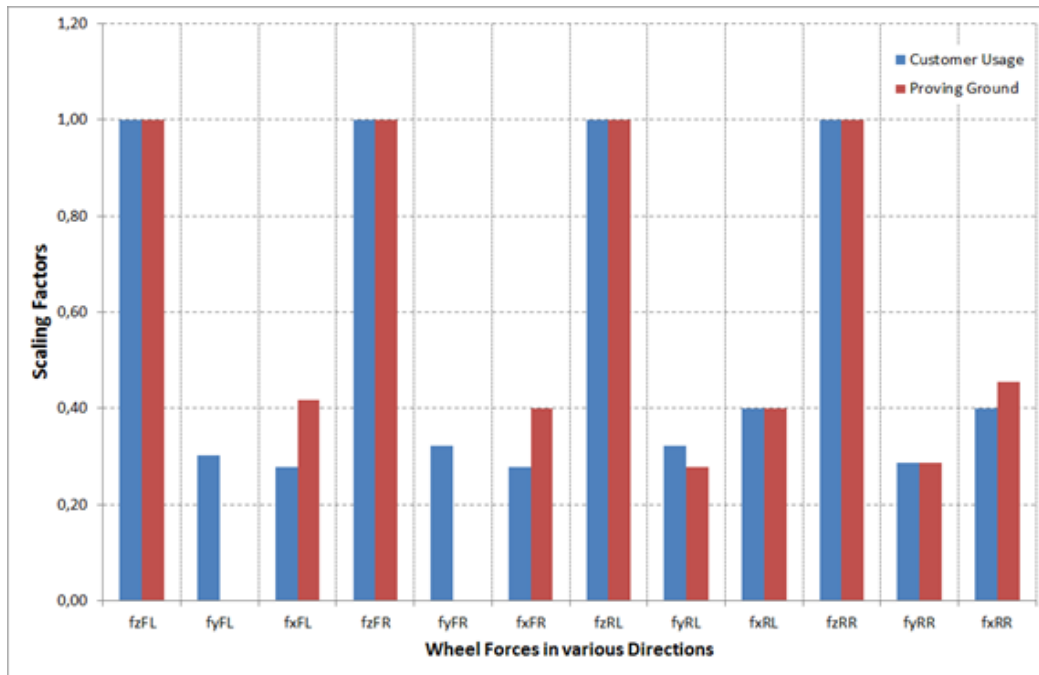


Figure 7.1 : Comparison of the scaling factors between the CU and the PG.

8. DERIVATION OF EXTREME LOADS

The load cycle distributions derived from sample measurements have to be extrapolated according to the requirements of the operating profile. The simplest way is the plain repetition (factor for the cumulative frequency of every loading element) without extrapolation of the maximum load levels as explained in the previous sections. This may be sufficient when the maximum loads are well defined and already covered by the customer usage and proving ground with extreme values measurements. If only segments of a random load sequence are available, generally extrapolation up to physical limits will be necessary. A simple, but well-suited approach for continuous loading environments would rely on extrapolation based on an approximation of the respective sample load spectra by exponential distributions, [14]. However, for loading environments with discontinuous single loading events the above-mentioned method may fail. In this case, the distribution of extreme values originating from consistent physical causes has to be considered. According to experience, the extreme value distributions can be well approximated by Weibull- or log-normal distributions. An additional advantage is the possibility to determine certain probabilities for extrapolated extreme values and the confidence level of the approximation [15].

High loads in the driving are considered as extreme loads. The probability of these loads rises with the increasing mileage, which means that these are single events with low occurrences relevant to customers. These extreme loads are closely related to the dimensioning consideration of the components. Therefore, the derivation of reliable extreme load assumptions is necessary.

The aim of this method is to derive the extreme loads from the short-term measurement, which can be expected after 1 million km. The point of concern is the Turkey measurement with fully loaded case with 3664 km mileages. This measurement is split into 100 intervals with almost equal distances. The extreme values of these 100 customer measurement intervals are investigated with respect to their probability of occurrence. In the first step, the maximum and minimum values

for each measurement interval are obtained. Then, the ranges of each interval are calculated. These values (Xdata) are ranked according to their magnitude. This called as rank in the following equation. Z-scores are calculated based on this equation (8.15).

$$Z - Score = NORMSINV \left(\frac{rank - 05}{count\ rank} \right) \tag{8.15}$$

NORMSINV is a Microsoft Excel function that delivers the inverse of the cumulative standardized normal distribution. You enter the “probability that a value Z is up to...” and it returns that value Z in terms of sigma, because it is the standardized distribution with average 0 and sigma 1. The calculated Z-Scores are shown in the following table in the second column as Yrank.

Table 8.1 : Z-Scores or Yrank.

Xdata	Rank	Yrank
21,89	1	-2,58
18,14	2	-2,17
18,14	3	-1,96
17,78	4	-1,81
17,59	5	-1,70
16,66	6	-1,60
16,48	7	-1,51
16,14	8	-1,44
16,13	9	-1,37
15,37	10	-1,31

Z-scores are a special application of the transformation rules. The Z score for an item indicates how far and in what direction, that item deviates from its distribution's mean, expressed in units of its distribution's standard deviation. The mathematics of the z-score transformation is such that if every item in a distribution is converted to its z score, the transformed scores will necessarily have a mean of zero and a standard deviation of one. Z-scores are sometimes called "standard scores". The z-score transformation is especially useful when seeking to compare the relative standings of items from distributions with different means and/or different standard deviations [16].

At the following figure, it can be seen the compares the various grading methods in a normal distribution, which includes standard deviations, cumulative percentages, percentile equivalents, Z-scores, T-scores.

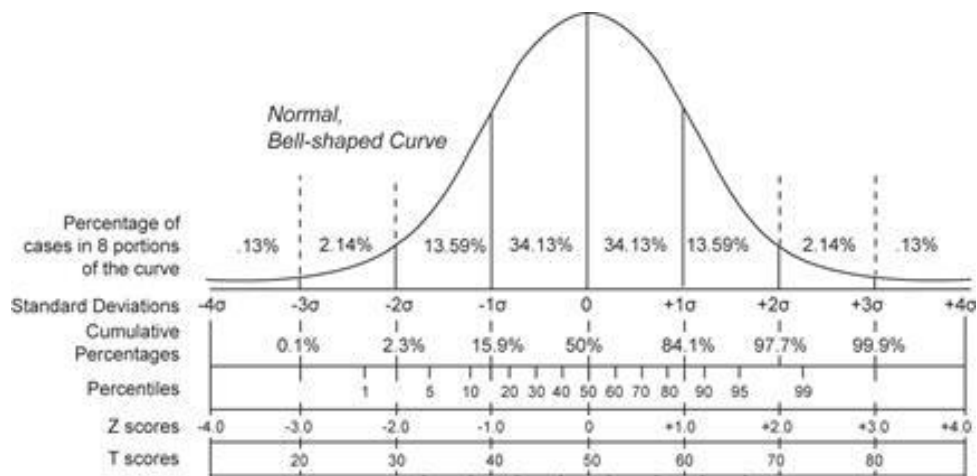


Figure 8.1 : Comparison of the various grading methods in a normal distribution.

After that, the probability of the each rank value is calculated based on this formula (8.16) [17].

$$Probability [P] = \left(\frac{3 \cdot (rank - 1)}{3 \cdot (count rank + 1)} \right) \quad (8.16)$$

Finally, YLabel returns the inverse of the standard normal cumulative distribution. Probability is a probability corresponding to the normal distribution. P = a probability value (0 < P < 1).

For this purpose, the Excel function is “=NORMSINV (probability)”. In other words, the cumulative distribution function (CDF) of the standard normal distribution, usually denoted with the Φ is the integral as seen at the following equation (8.17). This function is defined as Ylabel in the following table.

$$\Phi(x) = \frac{1}{\sqrt{2 \cdot \pi}} \int_{-\infty}^x e^{-t^2/2} dt \quad (8.17)$$

Table 8.2 : Calculated Ylabel values corresponding to the probability values.

P [Probability]	Ylabel
0,01	-2,32634787
0,10	-1,28155157
0,50	0
0,90	1,28155157
0,99	2,32634787

To sum up, the points in the following figure show the extreme values of the measured variables for each interval. They are depicted on a cumulative normal probability distribution plot. Based on Gumbel's approximation which is shown in the following equation (8.18), where P is Probability, a_N is the extrapolation factor (explained in the chapter-5), the measured values are extrapolated from the short-term measurement to the customer usage.

$$P = \frac{1}{2 A_i} \cdot \% 100 \quad (8.18)$$

In this case, $a_N = 10^6$ (km) / 3664 \rightarrow 273. Thus, the expected extreme values are calculated for the duration of 1 million kilometers. These expected extreme values are represented in the probability diagrams. Most measured variables appeared normally distributed along the straight-line approximation, which fit to the Gaussian distribution curve. The equation of this straight-line approximation is the logarithmic trendline as follows (8.19).

$$y = [c \cdot \ln(x)] + b \quad (8.19)$$

In this equation, c and b are trendline coefficients. A logarithmic trendline is a best-fit curved line that is used when the rate of change in the data increases or decreases quickly and then levels out. A logarithmic trendline can use both negative and positive values. These extrapolated extreme values are only valid and plausible, when the physical limits of components, such as displacement of springs, are larger than the calculated extrapolated values. Higher or smaller values can occur depending on the extrapolation factor. 3664 km is extrapolated to 1 million km by a factor 273. When all calculated extreme values are considered, the averaged probabilities of occurrence for these values stay around 0.1%. As an example, the extreme load assumption of the front wheel longitudinal forces at the left side can be seen based on the extreme value distribution as the following figure.

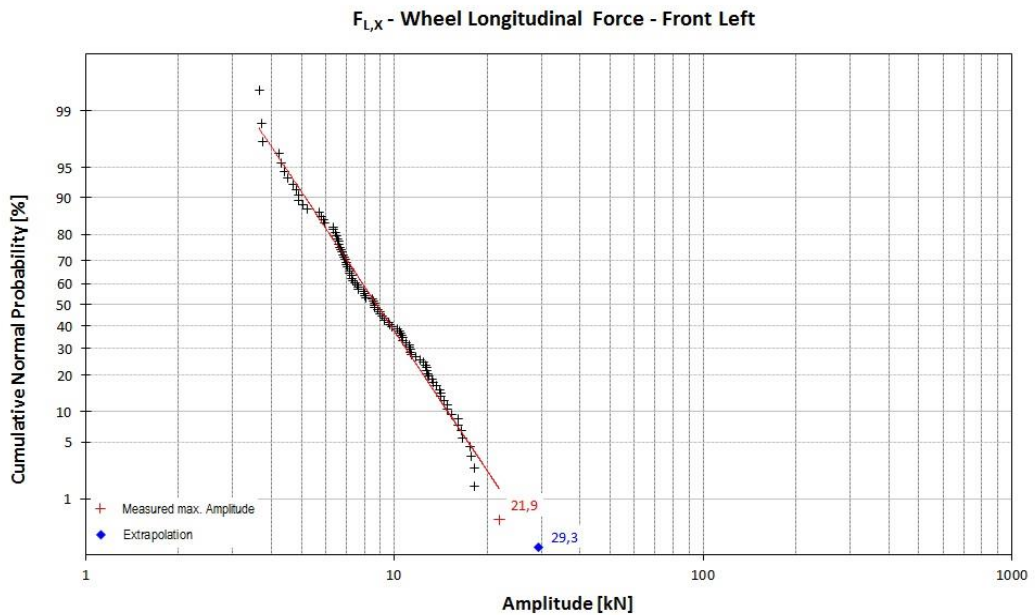


Figure 8.2 : Cumulative normal probability of the wheel longitudinal force.

The extreme load assumptions are executed for the other channels such as suspension arms, air spring and anti-roll bar forces by means of the extreme value distributions that are plotted in the following figure. These derived extreme loads that are expected after 1 million km on the customer usage will be used in the next chapters to derivation of the testing program for the commercial vehicle axles.

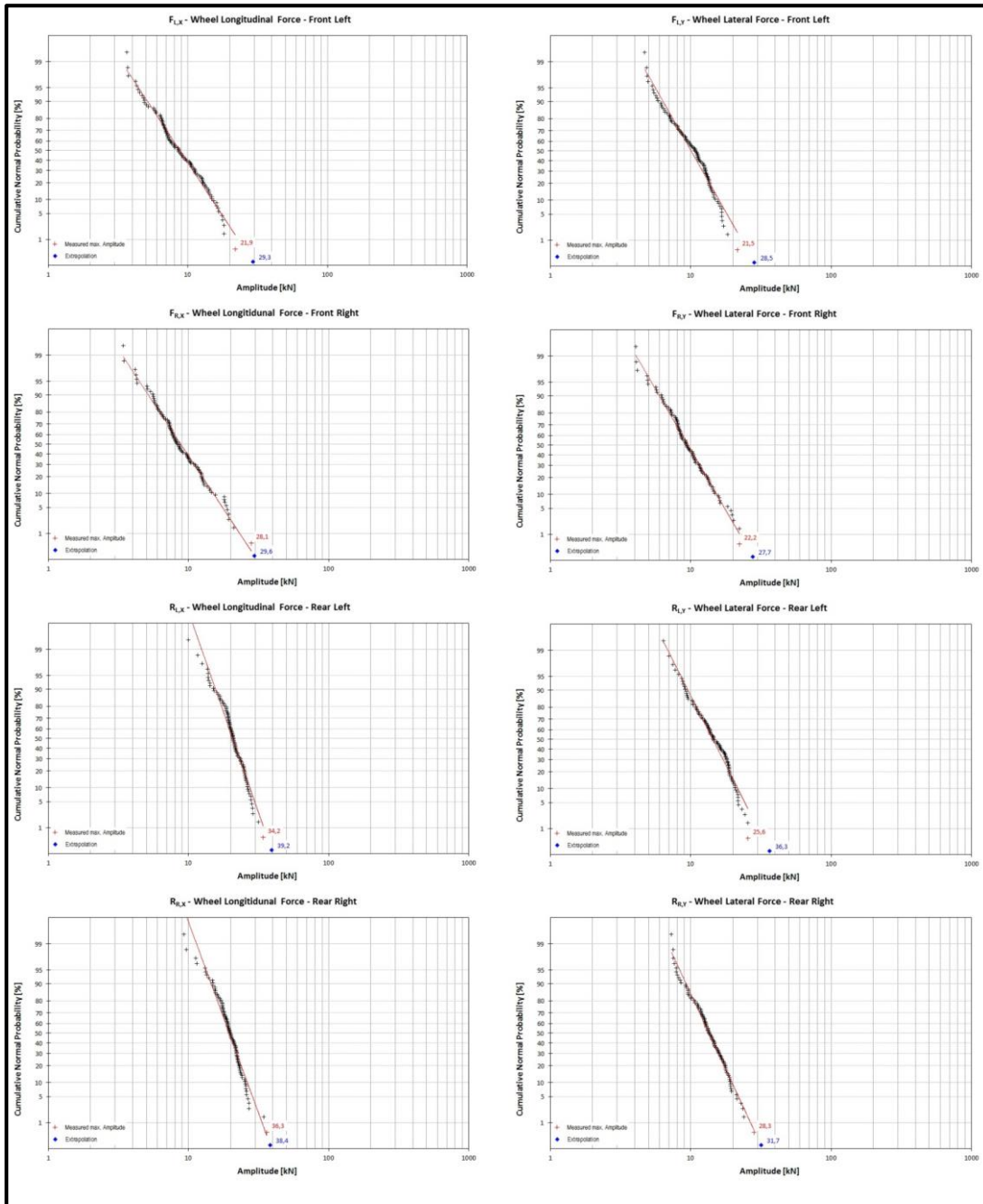


Figure 8.3 : Extreme load for the suspension arms, air spring and anti-roll bar.

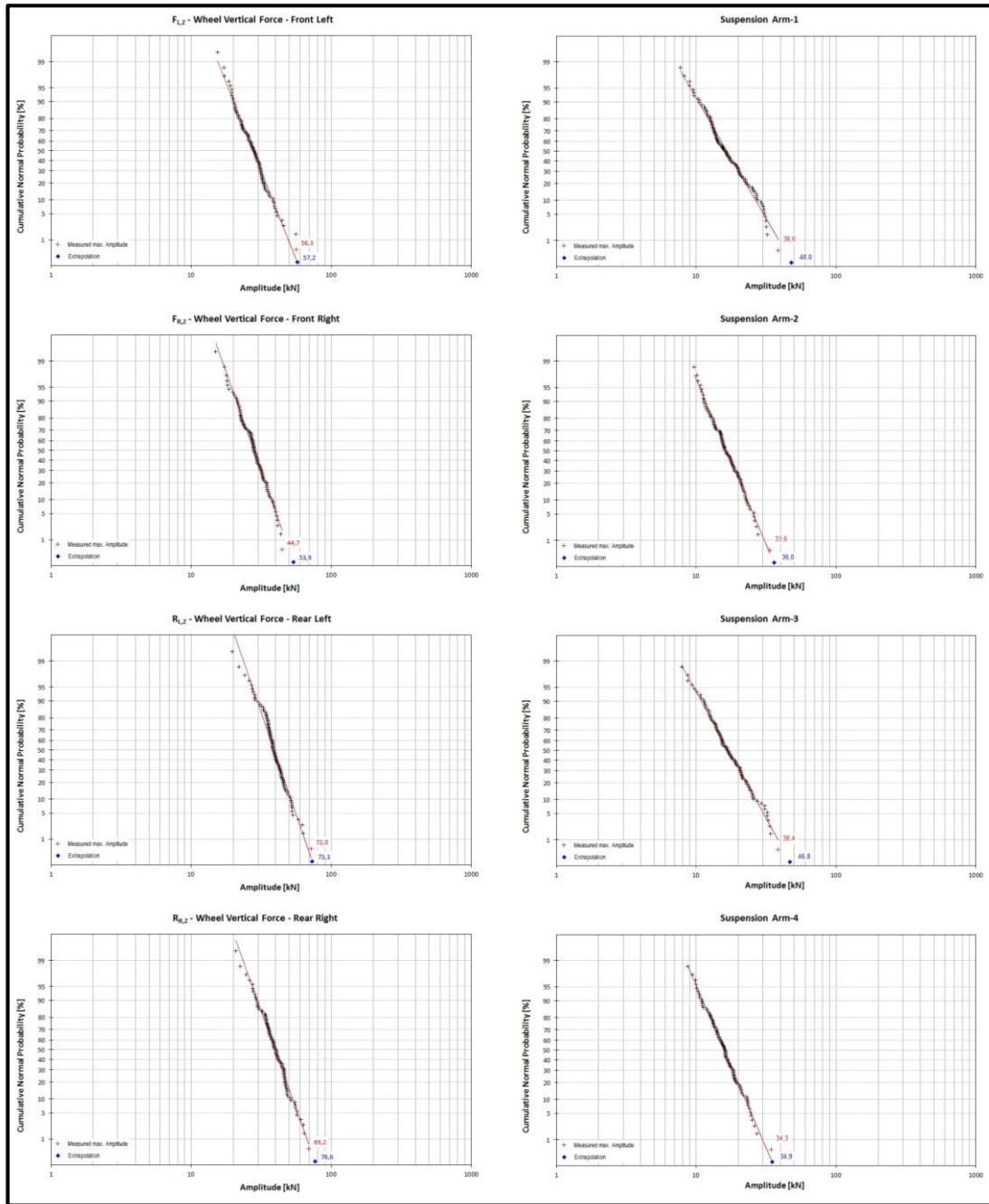


Figure 8.3 (continued): Extreme load for suspension arms, air spring, anti-roll bar.

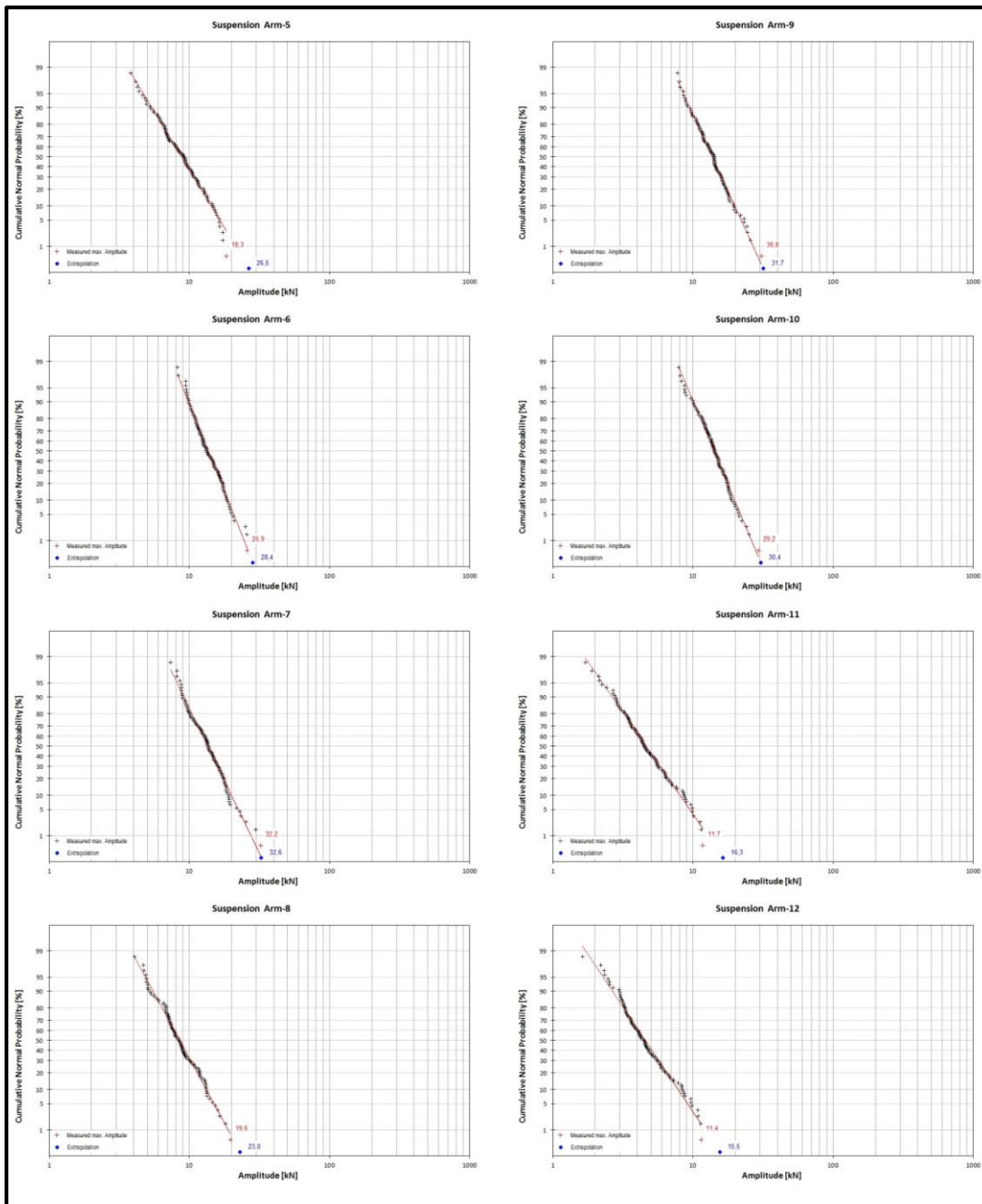


Figure 8.3 (continued): Extreme load for suspension arms, air spring, anti-roll bar.

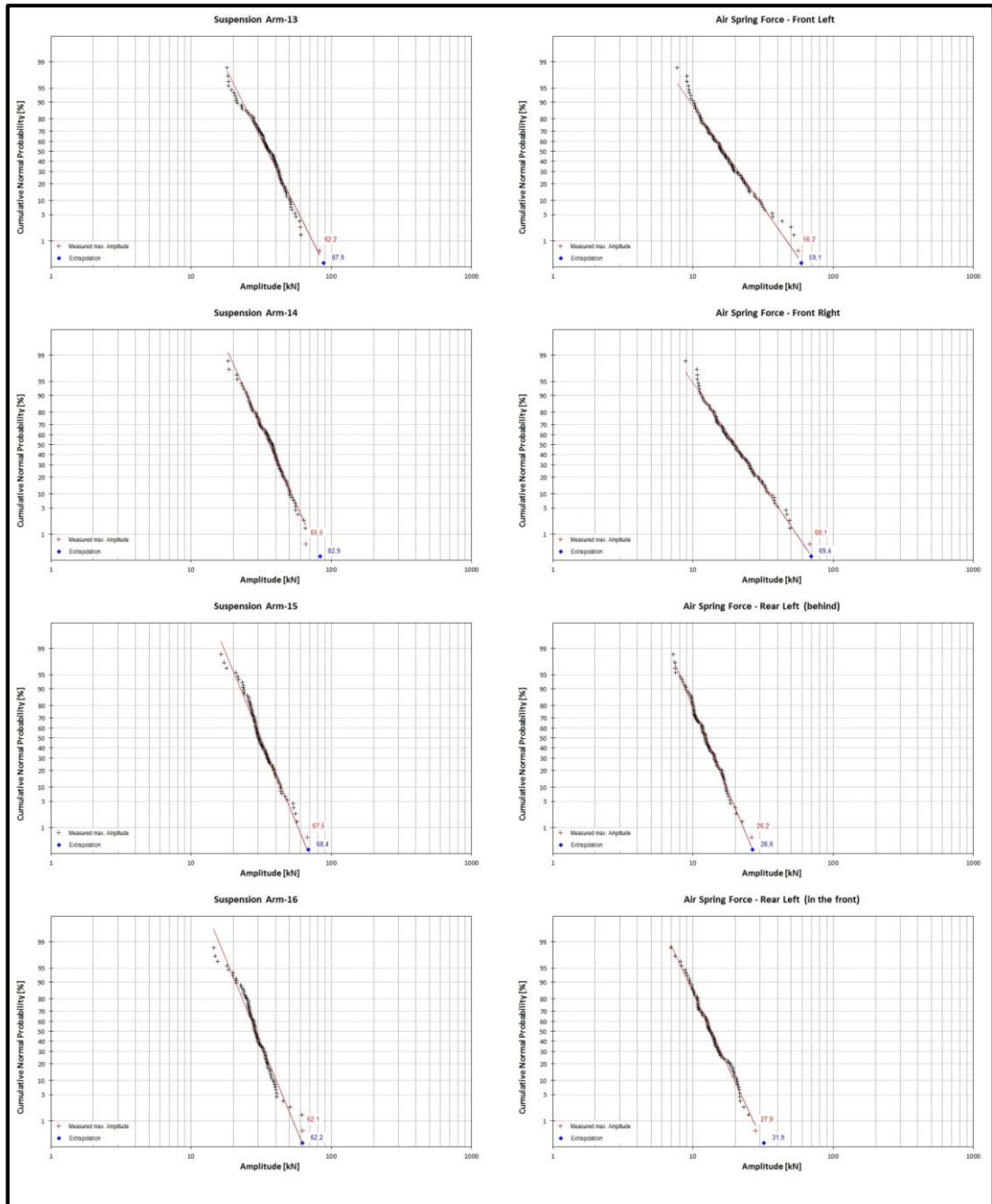


Figure 8.3 (continued): Extreme load for suspension arms, air spring, anti-roll bar.

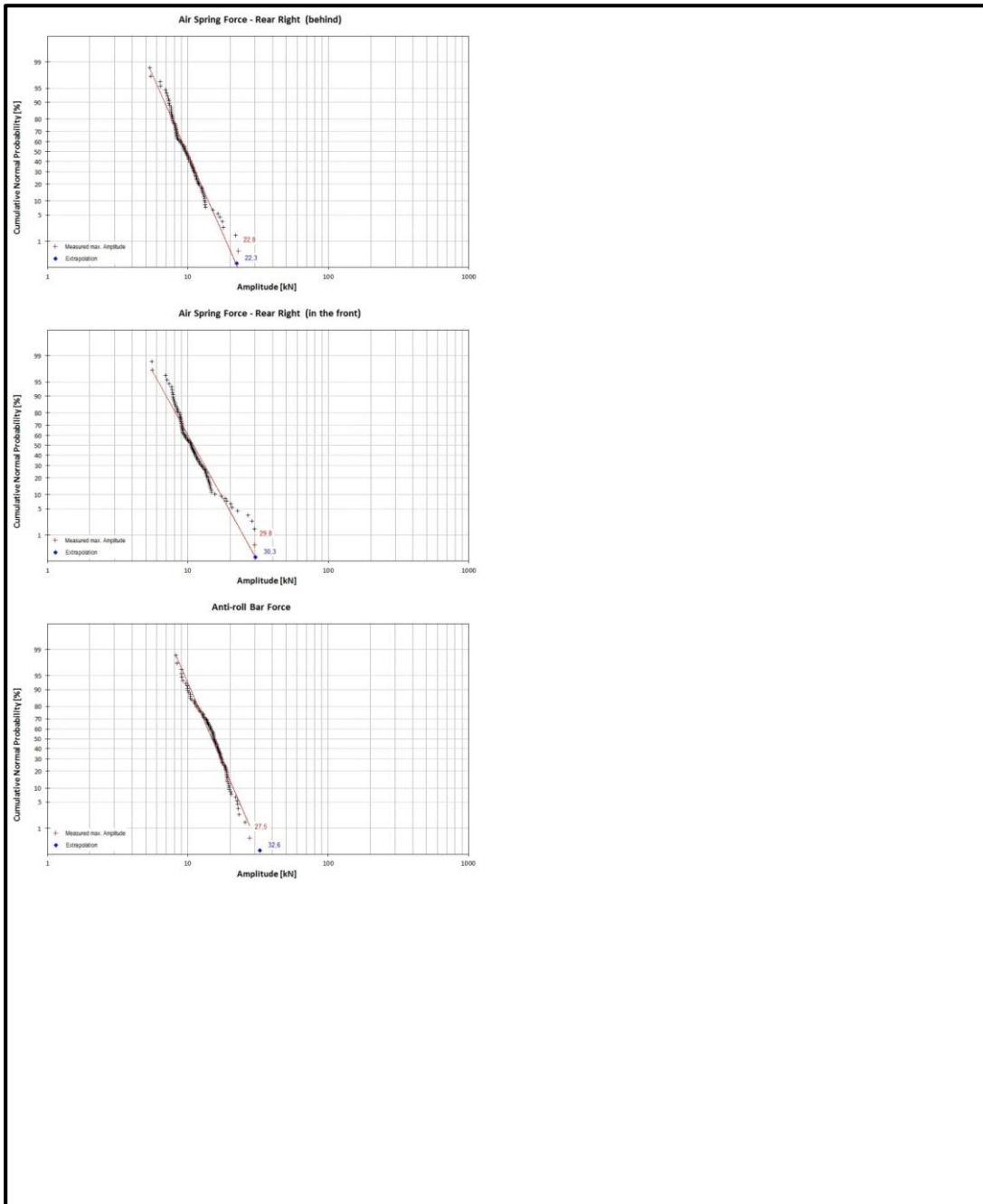


Figure 8.3 (continued): Extreme load for suspension arms, air spring, anti-roll bar.

9. DETERMINATION OF THE PHASE RELATIONSHIP

The phase relationship of the different wheel forces are investigated systematically. Due to the missing phase information (phase effect), it could be not determined if the high loads occur simultaneously or chronologically in the each channel of the wheel forces. Thus, the damage content of the applied test program could not be optimal in terms of the structural durability approval of the commercial vehicle axles. In addition to this, because of the missing phase information it is also possible to change the damage mechanism of the component through the applied test program. Some methods are practical to define the correlation of the wheel forces; however, the exact phase information between two non-sinusoidal signals is not easy to find out with the help of the existing methods. Two methods are used to calculate the phase shift between non-sinusoidal signals, which are the frequency response analysis (FRA) of signals and the direct determination of zero crossing method with the help of linear interpolation of the examined signals.

However, it is necessary to make a review about types of signals. A distinction between stationary signals and non-stationary signals has to be made. Stationary signals can again be divided into deterministic signals and random signals, and non-stationary signals into continuous and transient signals. Stationary deterministic signals are made up entirely of sinusoidal components at discrete frequencies. Random signals are characterized by being signals where the instantaneous value cannot be predicted, but where the values can be characterized by a certain probability density function, i.e. we can measure its average value. Random signals have a frequency spectrum, which is continuously distributed with frequency. The continuous non-stationary signal has some similarities with both transient and stationary signals. During analysis, continuous non-stationary signals should normally be treated as random signals or separated into the individual transient and treated as transients. Transient signals are defined as signals, which commence and finish at a constant level, normally zero, within the analysis time [18]. At the following figure we see types of the signals.

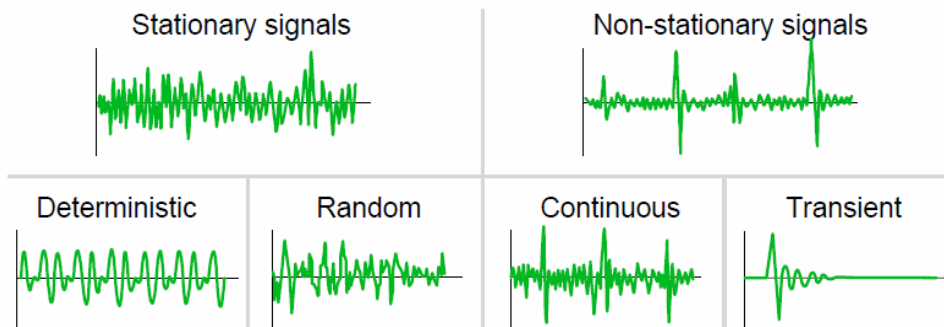


Figure 9.1 : Types of the signals.

In order to make a proper frequency analysis of signals it is necessary to know the characteristics of the different types of signals. As illustrated here, all signals have characteristics, which lie between the two extremes: a sine wave and an ideal impulse. An ideal sine wave, which in theory has infinite duration in time (from $-\infty$ to $+\infty$), will in the frequency domain be represented by a single infinitely narrow value. In contrast to this, an ideal pulse, which is infinitely narrow in time, will have in the frequency domain a value at all frequencies. At the following figure, we see time and frequency domain of the signals.

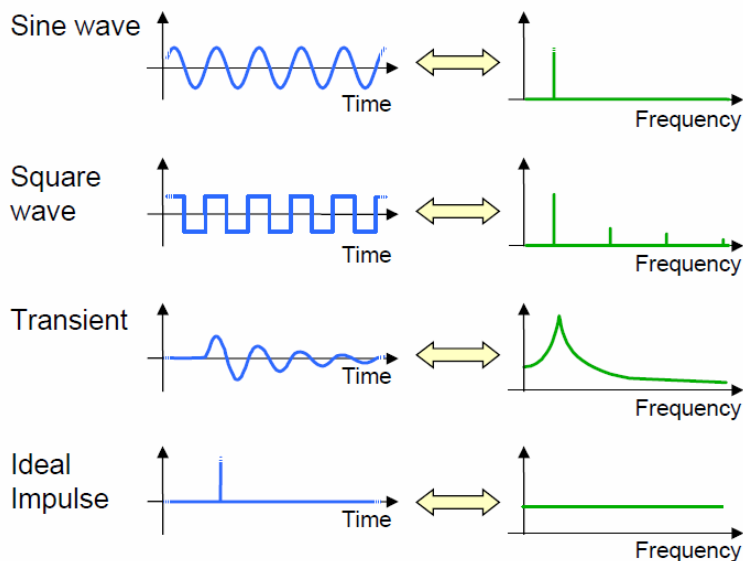


Figure 9.2 : Time and frequency domain of the signals.

Here, a square wave, which is periodic in time, will have its energy concentrated at specific frequencies and a transient response of a Single Degree of Freedom system, which, because of its periodic nature, has most of its energy concentrated at one frequency and, because it is limited in time, has energy over a wide frequency range [19].

9.1 Amplitude, Frequency, and Phase of a Sinusoidal Signal

Firstly, it is useful to mention quite a bit about the term phase. The notion of “phase” is usually associated with periodic or repeating signals. With these signals, the wave shape perfectly repeats itself every time the period of repetition elapses. For periodic signals, one can think of the phase at a given time as the fractional portion of the period that has been completed. This is commonly expressed in degrees or radians, with full cycle completion corresponding to 360° or 2π radians. Thus, when the cycle is just beginning, the phase is zero. When the cycle is half completed, the phase is half of 360° , or 180° as seen in the following Figure [20].

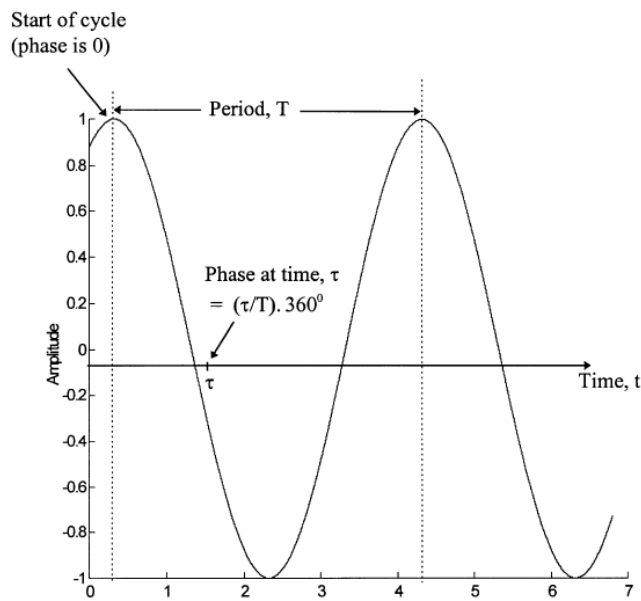


Figure 9.3 : The Phase of a periodic sinusoidal signal (the time scale is arbitrary).

It is important to note that if phase is defined as the portion of a cycle that is completed, the phase depends on where the beginning of the cycle is taken to be. There is no universal agreement on how to specify this beginning. For a sinusoidal signal, probably the two most common assumptions are that the start of the cycle is (1) the point at which the maximum value is achieved, and (2) the point at which the negative to positive zero crossing occurs. Assumption (1) is common in many theoretical treatments of phase. It should be noted, however, that assumption (2) has some benefits from a determination perspective, because the zero-crossing position is easier to define than the maximum. Frequently what is needed in practice is a determination of the phase difference between two signals of the same frequency;

that is, it is necessary to define the relative phase between two signals rather than the absolute phase of either one as seen at the following figure.

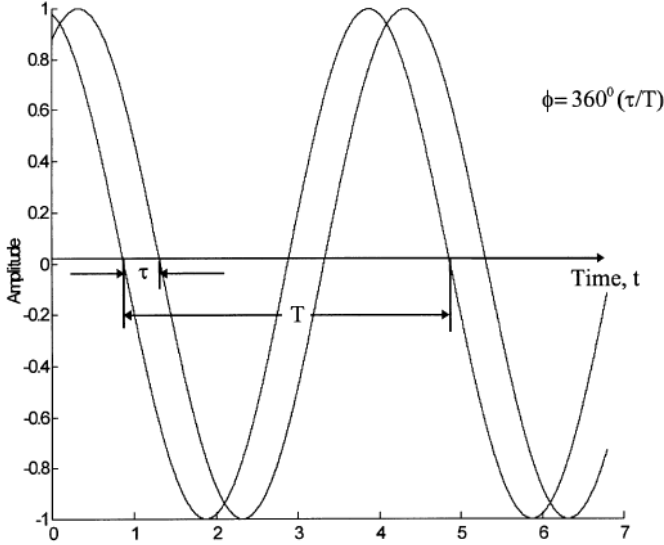


Figure 9.4 : Two Signals with a relative phase difference of ϕ between them.

An arbitrary sinusoidal signal can be written in the form of the following equation (9.20).

$$s(t) = A \cos(2\pi f t + \phi_o) = A \cos(\omega t + \phi_o) \tag{9.20}$$

where, A = Peak amplitude; f = Frequency; ω = Angular frequency; ϕ_o = Phase at time $t = 0$. This signal can be thought of as being the real part of a complex phasor that has amplitude, A , and which rotates at a constant angular velocity $\omega = 2\pi f$ in the complex plane as seen at the following figure. Mathematically, then, $s(t)$ can be written as the following equation (9.21).

$$s(t) = \text{Re} \{ A e^{j2\pi f t + \phi_o} \} = \text{Re} \{ z(t) \} \tag{9.21}$$

where, $z(t)$ is the complex phasor associated with $s(t)$, and $\text{Re}\{.\}$ denotes the real part. The “phase” of a signal at any point in time corresponds to the angle that the rotating phasor makes with the real axis. The initial phase (i.e., the phase at time $t = 0$) is ϕ_o . The “frequency” f of the signal is $\frac{1}{2} \pi$ times the phasor’s angular velocity. As the following figure we see a complex rotation phasor.

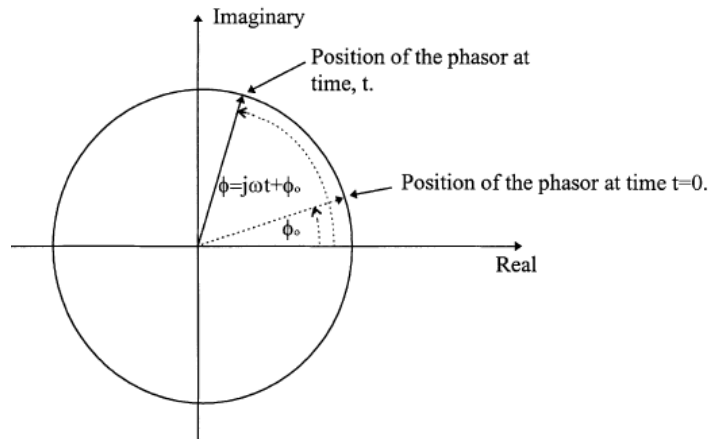


Figure 9.5 : A Complex rotating phasor, $A\exp(j\omega t + \phi_0)$.

9.2 Determination of a Phase Angle of a Periodic Non-Sinusoidal Signal

It is possible to define “phase” for signals other than sinusoidal signals. If the signal has harmonic distortion components present in addition to the fundamental, the signal will still be periodic, but it will no longer be sinusoidal. The phase can still be considered to be the fraction of the period completed. The “start” of the period is commonly taken to be the point at which the initial phase of the fundamental component is 0, or at a zero-crossing. This approach is equivalent to just considering the phase of the fundamental, and ignoring the other components.

9.2.1 Zero-crossing methods

Firstly, it is meaningful to define the term zero-crossings method. In mathematical terms, a "zero-crossing" is a point where the sign of a function changes (e.g. from positive to negative), represented by a crossing of the axis (zero value) in the graph of the function. At the following figure, we see zero crossing in a waveform representing amplitude vs. time.

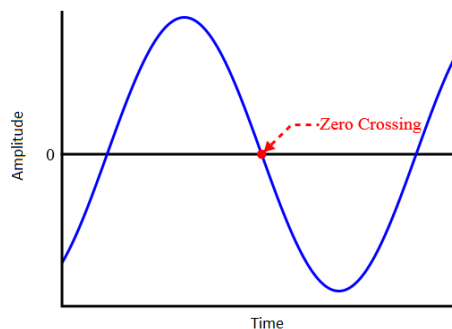


Figure 9.6 : Zero-crossing in a waveform representing amplitude vs. time.

This method is currently one of the most popular methods for determining phase difference, largely because of the high accuracy achievable. In the simplest case when signals are sinusoidal, the phase shift between them is constant and is defined by the initial phase difference between the examined signals. For multi-frequency complex signals, they must be expressed as the sum of harmonic components, where each component is characterized by its own amplitude and phase. Then the phase shift between the analyzed signals is conventionally defined as the phase difference between the first harmonics of these signals [21].

In practice, to estimate the phase shift between two non-sinusoidal signals represented by digital counts, the phase difference between the signal harmonics with the greatest amplitudes is used. The methods based on the interpolation procedures used to determine zero crossing points for the main harmonics are also well known. By analogy with sinusoidal signals, phase shift between periodic non-sinusoidal signals are characterized by the difference between time moments the signals cross zero level.

This method is based on the widespread approach – measuring the phase shift by its reduction to the time interval. To determine the phase of any arbitrary signal $a(t_j)$ shown in the figure below, a pair of counts $a(t_w)$ and $a(t_i)$ at which the signal polarity changes is calculated. To increase the accuracy of determining the time the signal $a(t_j)$ crosses zero level, it is interpolated on the interval $[t_w; t_i]$. At the following figure we see a pair of counts $a(t_w)$ and $a(t_i)$ at which the signal polarity changes.

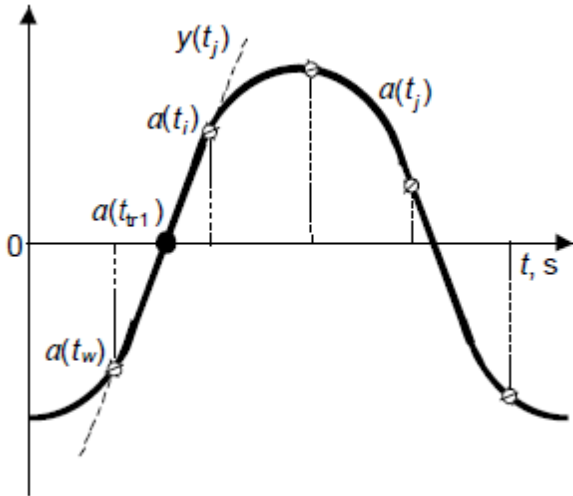


Figure 9.7 : A Pair of counts $a(t_w)$ and $a(t_i)$ at which the signal polarity changes.

For linear interpolation, we have the following equations (9.22).

$$y(t_j) = r \cdot t_j + h \rightarrow r = \frac{a(t_w) - a(t_i)}{t_w - t_i} \rightarrow h = a(t_i) - r \cdot t_i \quad (9.22)$$

The moment of time t_{tr1} corresponding to the first transition of signal $a(t_j)$ through zero level is determined by the following equation (9.23).

$$t_{tr1} = \frac{t_i \cdot a(t_w) - a(t_i) \cdot t_w}{a(t_w) - a(t_i)} \quad (9.23)$$

Then analogous procedure can be used to determine the signal period, and the phase of the signal ϕ_a is calculated as follows (9.24).

$$\phi_a = 360 \cdot \frac{t_{tr1}}{t_{tr2} - t_{tr1}} \quad (9.24)$$

The phase ϕ_b of the second signal is determined analogously. The phase shift between signals $a(t)$ and $b(t)$ is then calculated as a difference between ϕ_a and ϕ_b values. This method was applied to the measured signals of the wheel forces and suspension arms at the proving ground. The analysis was executed for a specific test program, which is small sine wave - out of phase. The periodic non-sinusoidal time signal of the measurement can be seen at the following figure.

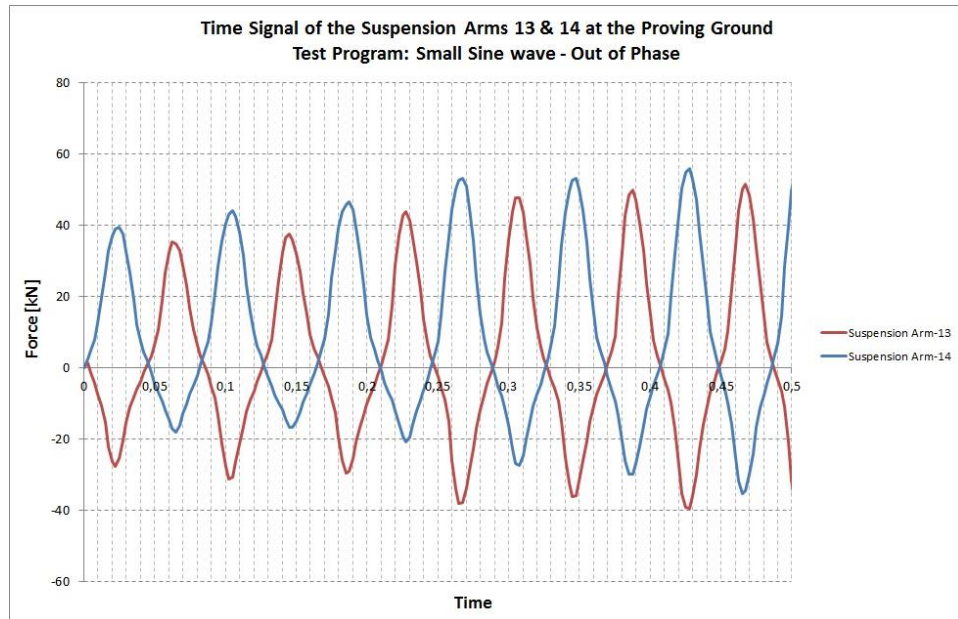


Figure 9.8 : Time signal of the suspension arms 13 & 14 at the proving ground.

The analysis was done with the help of the Microsoft Excel. All the equations are integrated to the Microsoft Excel as seen the following figures.

t	Amplitude	Zero Crossing	t at Zero Crossing	t-tr1	Amplitude	Zero Crossing	t at Zero Crossing	t-tr2
0	0	0	0	0	0	0	0	0
0,0025	1,430636764	0		0,003739819	2,471083641	0		0,000100817
0,005	-1,454133391	1	0,005	0,003747518	5,046005726	0		0,000760821
0,0075	-4,356637001	1		0,003831019	8,021821022	0		0,002987282
0,01	-7,32519722	1		0,004418659	12,4658289	0		0,005751911
0,0125	-10,60630703	1		0,006814639	19,80196762	0		0,005370843
0,015	-15,27017403	1		0,009458103	26,74597549	0		0,004109998
0,0175	-22,15868759	1		0,003994274	-32,8860054	0		-0,001941313
0,02	-26,2604084	1		-0,022960559	37,11488724	0		-0,031352365
0,0225	-27,78857803	1		0,051664801	38,92176056	0		-0,167806748
0,025	-25,40654755	1		0,037658597	39,43306351	0		0,074055523
0,0275	-20,38890076	1		0,03742019	37,42508698	0		0,046989603
0,03	-15,25066757	1		0,039115963	32,62443924	0		0,043382819
0,0325	-11,06826019	1		0,04230289	26,52997589	0		0,041537612
0,035	-8,245556831	1		0,044081544	19,19120789	0		0,041715213
0,0375	-5,975690365	1		0,044117734	12,04653263	0		0,044055795
0,04	-3,718236923	1		0,044032987	7,452683449	0		0,046197172
0,0425	-1,413346767	1		0,043988051	4,446197987	0		0,046725516
0,045	0,961146712	2	0,045	0,044010407	1,815633178	0		0,046439489
0,0475	3,389283419	2		0,044443956	-1,337627411	1	0,0475	0,04636184
0,05	6,16189003	2		0,046512696	-4,275763512	1		0,045823061
0,0525	10,57926369	2		0,049343518	-6,8349123	1		0,045355833
0,055	18,9582634	2		0,048675236	-9,226693153	1		0,046184277
0,0575	26,45192719	2		0,046228653	-11,84323788	1		0,04603453
0,06	32,31900024	2		0,033055885	-14,42560863	1		0,045955897
0,0625	35,31770706	2		0,280162665	-16,99352074	1		0,022332165
0,065	34,91205978	2		0,107111713	-18,05117798	1		0,088366625
0,0675	32,83947372	2		0,088344785	-16,11987877	1		0,079624964
0,07	28,9009179	2		0,08215687	-12,79618263	1		0,081702996
0,0725	22,95757484	2		0,081578541	-10,06265545	1		0,082112842
0,075	16,6356411	2		0,08204385	-7,445672989	1		0,08226612
0,0775	10,73132706	2		0,083537011	-4,883895397	1		0,082034988
0,08	6,287353516	2		0,085213971	-2,191553354	1		0,081821824
0,0825	3,27268672	2		0,085794359	0,815808117	2	0,0825	0,081859521
0,085	0,78913337	2		0,085701008	4,00017643	2		0,082008127
0,0875	-2,025146723	3	0,0875	0,085907475	7,342711449	2		0,083895293

Figure 9.9 : Excel sheet for the application of the method, step-1.

t	The moment of time t-tr1	t	The moment of time t-tr2	ϕ_1 [°]	ϕ_2 [°]	$\Delta\phi$ [°]
0,005	0,003747518	0,0475	0,04636184	16,4204868	205,097299	188,6768123
0,045	0,044010407	0,0825	0,081859521	192,908522	358,673777	165,7652546
0,0875	0,085907475	0,13	0,12773913	377,380901	563,433133	186,0522326
0,1275	0,126141287	0,165	0,164021724	545,816837	724,418971	178,6021338
0,17	0,167858339	0,21	0,209356778	753,489352	953,953557	200,4642047
0,21	0,209339275	0,2475	0,245532318	949,84404	1095,41893	145,5748889
0,25	0,248057218	0,29	0,288363182	1127,70919	1297,43411	169,7249132
0,29	0,288680868	0,3275	0,326224401	1291,47964	1461,15673	169,6770948
0,3275	0,327244831	0,37	0,368375527	1465,26306	1652,09308	186,8300222
0,37	0,369150672	0,4075	0,406599614	1668,85301	1847,53308	178,6800701
0,41	0,407645506	0,45	0,448646543	1839,10962	2050,88521	211,7755911
0,45	0,448782755	0,4875	0,485827349	2034,89962	2185,2816	150,3819777
0,4875	0,487440849	0,53	0,527399247	2197,63347	2364,44293	166,8094654
0,53	0,528178215	0,5675	0,565861815	2382,70978	2537,86279	155,1530064
0,5675	0,56728979	0,61	0,607698808	2615,02128	2800,64115	185,6198743
0,61	0,607979859	0,6475	0,646130242	2759,43736	2930,2007	170,7633371
0,6475	0,64538641	0,6875	0,685813625	2971,13384	3155,73393	184,600089
0,6875	0,687297749	0,7275	0,725512821	3153,66223	3338,71973	185,0575002
0,725	0,723585213	0,765	0,764049911	3354,35283	3476,19477	121,8419382
0,7675	0,765754848	0,805	0,803741794	3518,05437	-360	-3878,054373
0,8025	0,801242719	0,845	0,843176079	-360	-360	0
0,845	0,844113997					

Figure 9.10 : Excel sheet for the application of the method, step-2.

As a result, the calculated phase angle ($\Delta\phi$) can be seen at the following table.

Table 9.1 : Arithmetic mean of the calculated phase angle with error percentage.

Calculated $\Delta\phi$ [°]	Arithmetic mean of the Calculated $\Delta\phi$ [°]	Error [%]
188,68	173,79	3,45
165,77		
186,05		
178,60		
200,46		
145,57		
169,72		
169,68		
186,83		
178,68		
211,78		
150,38		
166,81		
155,15		
185,62		
170,76		
184,60		
185,06		
121,84		

As seen on the table above, the calculated phase angles are nearly around 180°. Considering the time signal, it is obvious to mention a phase shift between two periodic non-sinusoidal signals. The expected or real phase angle between those signals is 180°. The error between calculated phase angle and the real phase angle is about 3.45 %. Same methodology are also applied another time series. Another example is the time signal of the wheel forces at the proving ground. At the following figure, we see time signal of the wheel forces (rear right) in vertical and in lateral direction at the proving ground (test program: small sine wave - out of phase).

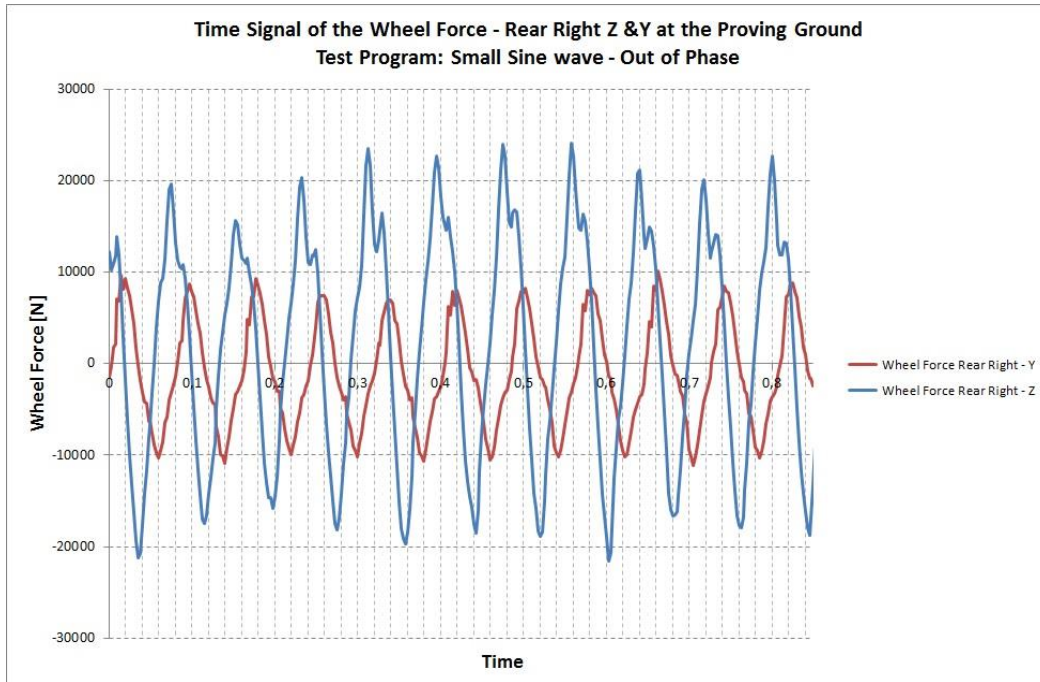


Figure 9.11 : Time signal of the wheel forces rear right Z&Y at the RG.

If we consider the same procedure, which is discussed previously in detail, we could obtain the calculated phase angles. Considering the time signal, it is obvious to mention a phase shift between two periodic non-sinusoidal signals. The expected or real phase angle between those signals is around 90° . The error between calculated phase angle and the real phase angle is about 0.70 %. At the following table, we see arithmetic mean of the calculated phase angle with error percentage.

Table 9.2 : Arithmetic mean of the calculated phase angle with error percentage.

Calculated $\Delta\phi$ [°]	Arithmetic mean of the Calculated $\Delta\phi$ [°]	Error [%]
121,77	90,63	-0,70
96,80		
82,09		
90,07		
77,08		
61,32		
28,22		
64,65		
76,99		
1,07		
109,26		
212,97		
16,66		
-312,52		
146,16		
624,28		
94,47		
116,12		
148,99		
-43,88		

It is obvious that, the phase angle between two periodic non-sinusoidal time signals can be calculated well with the help of this method. The error percentages of both examples are less than 5 %, which means the accuracy of calculations is also high. The disadvantage of this method is that, the time signals must be periodic. Otherwise, we could not talk about a dominant phase angle.

9.3 Determination of a Phase Angle of a Non-Sinusoidal Signal

9.3.1 Frequency response analysis (FRA)

Frequency response analysis (sometimes called FRA) is a key analysis tool for control of some dynamic systems. This analysis is based on the fact that if the input to a stable process is oscillated at a frequency, the long-time output from the process will also oscillate at a frequency, though with a different amplitude and phase. Advanced control techniques related to frequency response are crucial to the

performance of devices in the communications industry and other facets of electrical engineering. The frequency response technique can also be valuable to mechanical engineers studying things like airplane wing dynamics or chemical engineers studying diffusion or process dynamics [22].

9.3.1.1 Fourier-series and fourier transforms

Fourier-Series

Fourier series are a method to express any function that is continuous on a given interval as a sum of sine's and cosines on that interval. Fourier supposed, and later proved, that if a function $f(x)$ is continuous on the interval $(0, L)$, then one can write as the following equation (9.25).

$$f(x) = \sum_{n=-\infty}^{\infty} a_n \sin(k_n x) + b_n \cos(k_n x) \quad (9.25)$$

where $k_n = n\pi/L$; this makes for the following properties (9.26):

$$\begin{aligned} \int_{-\infty}^{\infty} \sin(k_n x) \sin(k_m x) dx &= \frac{L}{2} \delta[n - m] \\ \rightarrow \int_{-\infty}^{\infty} \cos(k_n x) \cos(k_m x) dx &= \frac{L}{2} \delta[n - m] \\ \rightarrow \int_{-\infty}^{\infty} \sin(k_n x) \cos(k_m x) dx &= 0 \end{aligned} \quad (9.26)$$

Therefore if we multiply both sides by $\sin(m\pi x/L)$ or $\cos(m\pi x/L)$ and integrate, we obtain the following equation (9.27);

$$a_m = \frac{2}{L} \int_0^L f(x) \sin\left(\frac{m\pi x}{L}\right) \rightarrow b_m = \frac{2}{L} \int_0^L f(x) \cos\left(\frac{m\pi x}{L}\right) \quad (9.27)$$

Some people call this equation (9.27) the definition of the Finite Fourier Transform or the Discrete Fourier Transform.

The Fourier transform

The purpose of the Fourier transform is similar to that of the Laplace transform in that it seeks to transform a differential equation into an algebraic equation. However, whereas the Laplace transform uses the complex variable s (which has units of inverse time but is otherwise difficult to interpret), the Fourier transform uses complex waves of the form e^{ikx} or some variation on that form to write the transformed function as a sum of waves of all frequencies (represented here by the frequency ν or wave number $\bar{\nu}$, or their angular equivalents ω and k).

The Fourier transform can be defined by several integral pairs, depending on the units of the quantity to be transformed and the desired units of the transformed variable. If f is a function of displacement x , with units of length, then the resulting variable can be defined to have units of wave number ($\bar{\nu}$,) or angular wave number (k). In wave number units, we can define as the following equation (9.28),

$$\begin{aligned}\mathcal{F}[f(x)] = F(\bar{\nu}) &= \int_{-\infty}^{\infty} e^{-2\pi i x \bar{\nu}} f(x) dx \rightarrow \mathcal{F}^{-1}[F(\bar{\nu})] = f(x) \\ &= \int_{-\infty}^{\infty} e^{2\pi i x \bar{\nu}} f(\bar{\nu}) d\bar{\nu}\end{aligned}\tag{9.28}$$

In this form, x has units of length, and $\bar{\nu}$, has units of inverse length (wavenumbers). A similar form that is more common is as follows (9.29):

$$\begin{aligned}\mathcal{F}[f(x)] = F(k) &= \int_{-\infty}^{\infty} e^{-ikx} f(x) dx \rightarrow \mathcal{F}^{-1}[F(k)] = f(x) \\ &= \frac{1}{2\pi} \int_{-\infty}^{\infty} e^{ikx} f(k) dk\end{aligned}\tag{9.29}$$

where, k is an angular wave number (radians/unit length). The factor of 2π is sometimes moved to the forward transform; the only important part is that the entire transform have a factor of $1/2\pi$ somewhere in this form. In fact, some authors (especially physicists); define the transform with these units as follows (9.30):

$$\begin{aligned}\mathcal{F}[f(x)] = F(k) &= \frac{1}{\sqrt{2\pi}} \int_{-\infty}^{\infty} e^{-ikx} f(x) dx \rightarrow \mathcal{F}^{-1}[F(k)] = f(x) \\ &= \frac{1}{\sqrt{2\pi}} \int_{-\infty}^{\infty} e^{ikx} f(k) dk\end{aligned}\tag{9.30}$$

Which you use is largely a matter of preference, provided you remember that the factor of 2π is to cancel the units of k , which is in radians per unit length. The form defined by (9.30) would therefore have a transformed function with the somewhat awkward units of radians. They are analogous to the spatial forms, except that the transformed variable has units of frequency instead of wave number. For frequencies in Hz (cycles/second) and analogous units as follows (9.31):

$$\begin{aligned}\mathcal{F}[f(t)] = F(v) &= \int_{-\infty}^{\infty} e^{-2\pi i vt} f(t) dt \rightarrow \mathcal{F}^{-1}[F(v)] = f(t) \\ &= \int_{-\infty}^{\infty} e^{2\pi i vt} f(v) dv\end{aligned}\tag{9.31}$$

Similarly, for angular frequencies as follows (9.32):

$$\begin{aligned}\mathcal{F}[f(t)] = F(\omega) &= \int_{-\infty}^{\infty} e^{-i\omega t} f(t) dt \rightarrow \mathcal{F}^{-1}[F(\omega)] = f(t) \\ &= \frac{1}{2\pi} \int_{-\infty}^{\infty} e^{i\omega t} f(\omega) d\omega\end{aligned}\tag{9.32}$$

We will define (9.32) as the definition of the Fourier Transform, for elements in the time domain.

Frequency from the transfer function

The open-loop transfer function $G(s) = P(s)C(s)$, where $C(s)$ is the transfer function of the controller (from error to input, as it were). The transfer function is the Laplace transform of the impulse response. The transfer function can thus be found by the definition of the Laplace transform (9.33):

$$G(s) = \mathcal{L}[g(t)] = \int_0^{\infty} e^{-st} g(t) dt\tag{9.33}$$

Strictly speaking, this is the unilateral Laplace transform; the bilateral Laplace transform is integrated over the entire real axis. Since outputs are assumed to be at steady-state (or at least unknown) prior to time $t = 0$, these are equivalent for our purposes. If we restrict s to be purely imaginary, we can let $s = i\omega$ and (9.33) becomes (9.34)

$$G(i\omega) = \int_0^{\infty} e^{-i\omega t} g(t) dt = \mathcal{F}[g(t)] \quad (9.34)$$

Comparing this to (9.32) leads us to the equality on the right. In short, $G(i\omega)$ is the Fourier transform of the impulse response: the value of $G(i\omega)$ at each value of ω represents the contribution of a wave of frequency ω to the value of $g(t)$. If we eliminate the contributions from all other waves (say, by exciting at that frequency and allowing the other states to relax away), the Fourier transform tells us the final response of the system to that oscillation, including its magnitude and phase-shift.

To obtain the magnitude and phase directly from the transfer function $G(s)$ (the open-loop transfer function), we separate $G(i\omega)$ into real and imaginary parts as seen on the following equation (9.35).

$$G(i\omega) = R(\omega) + iI(\omega) \quad (9.35)$$

The amplitude response (AR) or gain and phase response (ϕ) or phase shift of the long-time oscillations are then (9.36),

$$AR = |G(i\omega)| = \sqrt{R^2 + I^2} \rightarrow \phi = \tan^{-1}\left(\frac{I}{R}\right) \quad (9.36)$$

At the following figure, we see the explanation of the gain and phase.

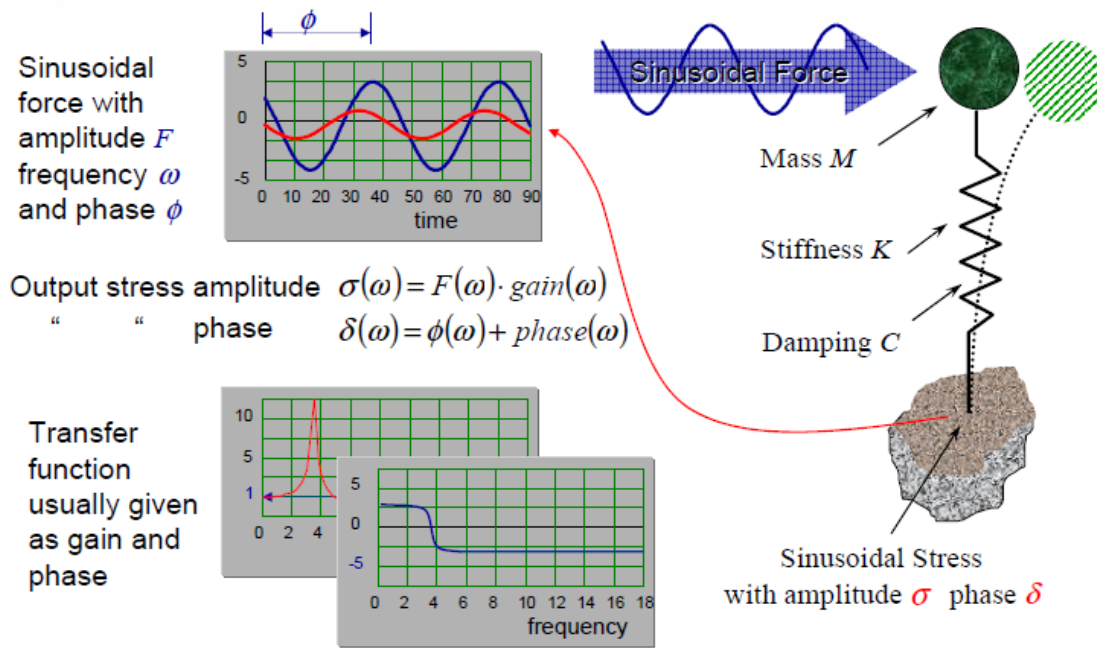


Figure 9.12 : Explanation of the gain and phase.

Note that the magnitude of the actual oscillation will be aAR , where a is the amplitude of the exciting oscillation (see the figure above). This method was executed using measured signals by means of software called MGraph (Stiegele Datensysteme GmbH). MGraph is graphical evaluation software for technical data that makes it possible to analyze even very large data set volumes going up to the gigabyte range, and still work effectively. Its special strength is quick and intuitive evaluation of large data volumes. This includes processing, illustrating, and presenting the data through easily accessible mechanisms.

To sum up, this tool, which is integrated in the software of MGraph, performs frequency response analysis using two time series, one of which is the input and the second is the response. The program calculates the transfer function between the data sets and from that creates a number of outputs that inform the user of the relationship between the data sets in the frequency domain. If we want to summarize how works frequency response analysis (FRA), we can explain as follows [23]. At the following figure, we see the explanation of the frequency response analysis.

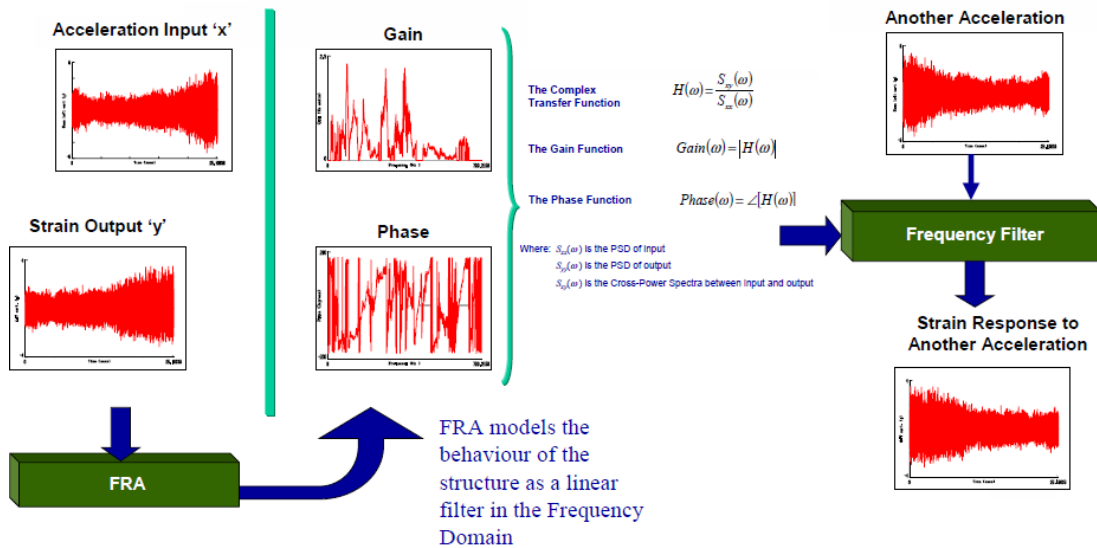


Figure 9.13 : Explanation of the frequency response analysis.

Filter – signal processing

It is also helpful to mention about the filter of a signal in order to understand the frequency filter, which is also used in the previous section to perform a frequency response analysis. In signal processing, a filter is a device or process that removes from a signal some unwanted component or feature. Filtering is a class of signal processing, the defining feature of filters being the complete or partial suppression of some aspect of the signal. Most often, this means removing some frequencies and not others in order to suppress interfering signals and reduce background noise.

There are many different bases of classifying filters and these overlap in many different ways; there is no simple hierarchical classification. Filters may be:

- linear or non-linear
- time-invariant or time-variant, also known as shift invariance. If the filter operates in a spatial domain then the characterization is space invariance.
- causal or not-causal: depending if present output depends or not on "future" input; of course, for time related signals processed in real-time all the filters are causal; it is not necessarily so for filters acting on space-related signals or for deferred-time processing of time-related signals.
- analog or digital
- discrete-time (sampled) or continuous-time
- passive or active type of continuous-time filter

- infinite impulse response (IIR) or finite impulse response (FIR) type of discrete-time or digital filter.

Terminology of the filter functions

Some terms used to describe and classify linear filters:

The frequency response can be classified into a number of different bandforms describing which frequencies the filter passes (the passband) and which it rejects (the stopband):

- Low-pass filter – low frequencies are passed, high frequencies are attenuated.
- High-pass filter – high frequencies are passed, low frequencies are attenuated.
- Band-pass filter – only frequencies in a frequency band are passed.
- Band-stop filter or band-reject filter – only frequencies in a frequency band are attenuated.
- Notch filter – rejects just one specific frequency - an extreme band-stop filter.
- Comb filter – has multiple regularly spaced narrow pass bands giving the band form the appearance of a comb.
- All-pass filter – all frequencies are passed, but the phase of the output is modified.

Cutoff frequency is the frequency beyond which the filter will not pass signals. It is usually measured at a specific attenuation such as 3dB. Roll-off is the rate at which attenuation increases beyond the cut-off frequency. Transition band, the (usually narrow) band of frequencies between a pass band and stop band. Ripple is the variation of the filter's insertion loss in the pass band. The order of a filter is the degree of the approximating polynomial and in passive filters corresponds to the number of elements required to build it. Increasing order increases roll-off and brings the filter closer to the ideal response. The two types of filter in the time domain can be seen at the following figure [23].

- **FIR (Finite Impulse Response)** also known as a non-recursive filter

$$y_n = \sum_{k=0}^M c_k \cdot x_{n-k}$$

Output at a given time depends on current and previous inputs

- **IIR (Infinite Impulse Response)** also known as a recursive filter

$$y_n = \sum_{k=0}^M c_k \cdot x_{n-k} + \sum_{j=0}^N d_j \cdot y_{n-j}$$

Output at a given time depends both on current and previous inputs and previous outputs

y_n = nth output

x_n = nth input

c_k and d_k are the kth filter constants

M and N are the number of filter constants used

Figure 9.14 : Time domain filters.

The filtering in the frequency domain can be explained as the following figure.

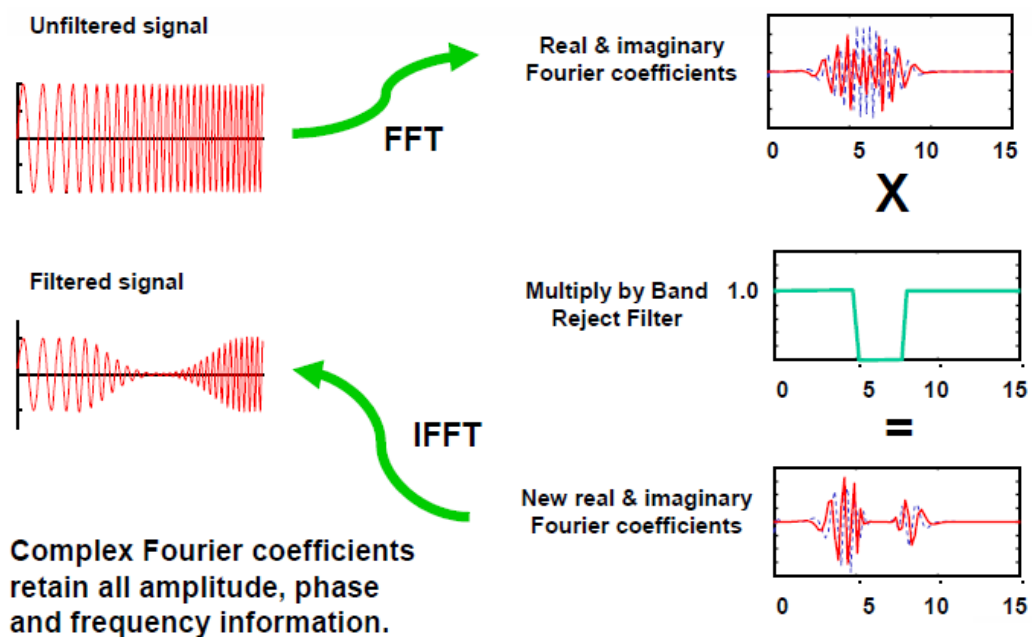


Figure 9.15 : Filtering in the frequency domain.

At the next section we explain coherence – signal processing (C_{xy}).

9.3.2 Coherence – Signal Processing (C_{xy})

This analysis method is also performed by evaluating the phase angle of the two non-sinusoidal measured signals. Certainly, it is helpful to mention about the coherence to make a better understanding for the evaluation of the data.

The spectral coherence is a statistic that can be used to examine the relation between two signals or data sets. It is commonly used to estimate the power transfer between input and output of a linear system. If the system function linear is, it can be used to estimate the causality between the input and output.

9.3.2.1 Definition and formulation of the coherence

The coherence (sometimes called magnitude-squared coherence) between two signals $x(t)$ and $y(t)$ is a real-valued function that is defined as (9.37): [24,25]

$$C_{xy} = \frac{|G_{xy}|^2}{G_{xx}G_{yy}} \quad (9.37)$$

where G_{xy} is the cross-spectral density between x and y , and G_{xx} and G_{yy} the autospectral density of x and y respectively. The magnitude of the spectral density is denoted as $|G|$. Given the restrictions noted above (linearity) the coherence function estimates the extent to which $y(t)$ may be predicted from $x(t)$ by an optimum linear least squares function. Values of coherence will always satisfy as the following equation (9.38).

$$0 \leq C_{xy} \leq 1 \quad (9.38)$$

For an ideal constant parameter linear system with a single input $x(t)$ and single output $y(t)$, the coherence will be equal to one. To see this, consider a linear system with an impulse response $h(t)$ defined as the following equation (9.39).

$$y(t) = h(t) * x(t) \quad (9.39)$$

where $*$ denotes convolution. In mathematics and, in particular, functional analysis, convolution is a mathematical operation on two functions f and g , producing a third function that is typically viewed as a modified version of one of the original functions, giving the area overlap between the two functions as a function of the amount that one of the original functions is translated. Convolution is similar to cross-correlation. In the Fourier domain, this equation becomes as the following equation (9.40).

$$Y(f) = H(f)X(f) \quad (9.40)$$

where, $Y(f)$ is the Fourier transform of $y(t)$ and $H(f)$ is the linear system transfer function. Since, for an ideal linear system (9.41):

$$G_{yy} = |H(f)|^2 G_{xx}(f) \quad (9.41)$$

and (9.42);

$$G_{xy} = H(f)G_{xx}(f) \quad (9.42)$$

and since $G_{xx}(f)$ is real, the following identity holds (9.43):

$$C_{xy} = \frac{|H(f)G_{xx}(f)|^2}{G_{xx}G_{yy}} = \frac{|H(f)G_{xx}(f)|^2}{G_{xx}^2|H(f)|^2} = \frac{|G_{xx}|^2}{G_{xx}^2} = 1 \quad (9.43)$$

However, in the physical world an ideal linear system is rarely realized, noise is an inherent component of system measurement, and it is likely that a single input, single output linear system is insufficient to capture the complete system dynamics. In cases where the ideal linear system assumptions are insufficient, the Cauchy–Schwarz inequality guarantees a value of $C_{xy} \leq 1$.

If C_{xy} is less than one but greater than zero it is an indication that either: noise is entering the measurements, that the assumed function relating $x(t)$ and $y(t)$ is not linear, or that $y(t)$ is producing output due to input $x(t)$ as well as other inputs. If the coherence is equal to zero, it is an indication that $x(t)$ and $y(t)$ are completely unrelated, given the constraints mentioned above.

The coherence of a linear system therefore represents the fractional part of the output signal power that is produced by the input at that frequency. We can also view the quantity $1-C_{xy}$ as an estimate of the fractional power of the output that is not contributed by the input at a particular frequency. This leads naturally to definition of the coherent output spectrum (9.44):

$$G_{vv} = C_{xy}G_{yy} \quad (9.44)$$

G_{vv} provides a spectral quantification of the output power that is uncorrelated with noise or other inputs.

9.3.3 Application of the Frequency Response Analysis (FRA)

All the necessary methods were explained in order to perform some analysis for the determining the phase angles of two non-sinusoidal signals. First, the coherence functions of the wheel forces are plotted from all the measurement intervals. This analysis gives us an idea about the relation between two wheel forces. After that the phase response of the wheel forces are also obtained to examine the characteristic or dominant phase angle. Finally, the FRA method is used to investigate the possibility of reproduction of the other wheel forces using only wheel vertical forces. The reproduced wheel forces from wheel vertical forces must be retained all the amplitude, phase and frequency information compared to the measured wheel forces. Therefore, it is aimed to calculate all other wheel forces (lateral and longitudinal) considering the vertical forces. The coherence function and phase responses of the measured wheel forces from all the measurement intervals can be seen as follows.

9.3.3.1 The Coherence functions of the wheel forces

At the following figure can be seen the results of the coherence analysis of wheel forces from the all measurement intervals.

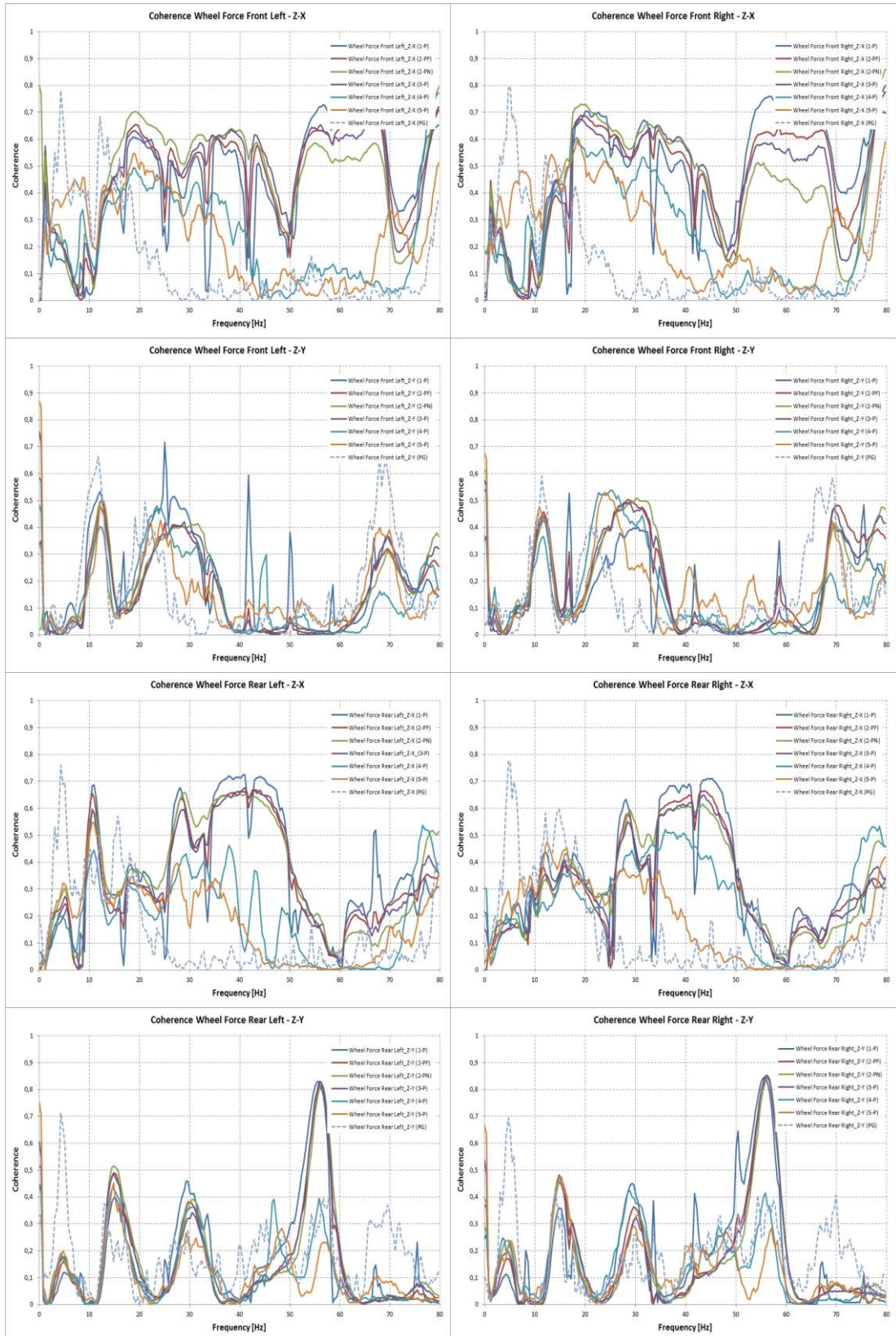


Figure 9.16 : The Coherence functions of the wheel forces.

9.3.3.2 The Phase responses of the wheel forces

At the following figure can be seen the results of the phase response analysis of wheel forces from the all measurement intervals.

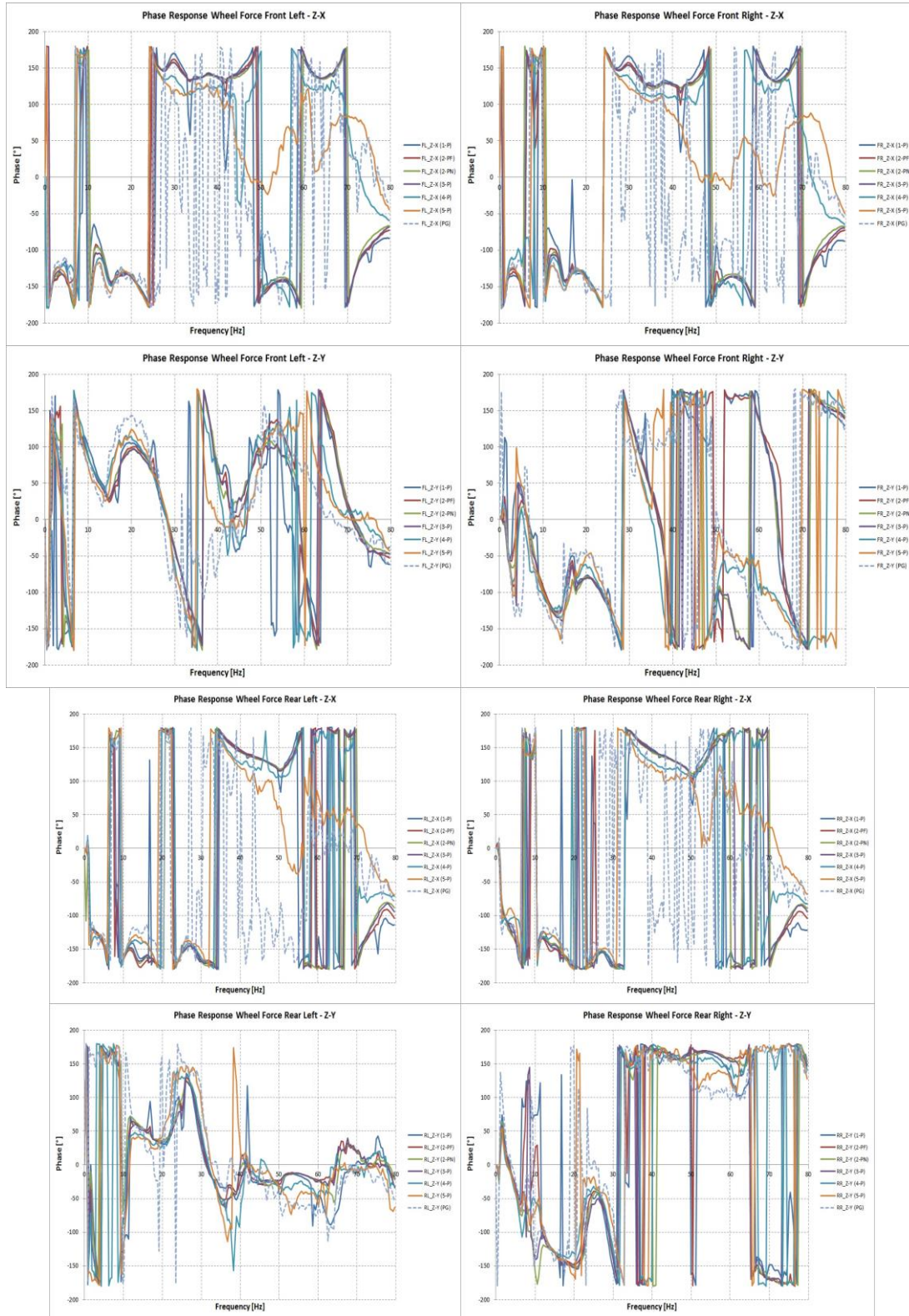


Figure 9.17 : The Phase responses of the wheel forces.

Because of the coherence functions, we can say that all road types on the customer usage have same causality between the longitudinal and vertical wheel forces. This is also valid for the relation between lateral and vertical wheel forces. However, the magnitude of the coherence value differs in road types. These coherence values are lower for the relation between lateral and vertical wheel forces than longitudinal and vertical forces. Besides, the coherence values are approximately 0.65 from 20 to 80 Hz considering the relation of longitudinal and vertical front wheel forces. In addition, the road types of four and 5-P, which are main and local traffic cities respectively, have lower coherence values for the wheel forces above 25 Hz compared to other road types. There is also a negligible difference between the right and left side of the vehicle considering the coherence functions of the wheel forces.

Apart from this, the coherence values from the proving ground measurements differ largely in customer usage considering the relation or function between longitudinal and vertical wheel forces. Except from the relation between lateral and vertical front wheel forces, it is obvious to see that the coherence values below 10 Hz are the highest.

In summary, C_{xy} is less than one and maximum value is 0.7 under 20 Hz which is an important frequency area to examine the relation of the wheel forces. It is an indication that either: noise is entering the measurements, that the assumed function relating $X(t)$ and $Z(t)$ of wheel forces is not linear, or that $Z(t)$ is producing output due to input $X(t)$ as well as other inputs. If the coherence is equal to zero, it is an indication that $X(t)$ and $Z(t)$ are completely unrelated, given the constraints mentioned above. It is obvious to see that there is not a certain relation or causality between the wheel forces. Therefore is also difficult to mention about a dominant phase relation and/or angle between the wheel forces taking into account of the phase responses.

The reproduction of the longitudinal and lateral wheel forces from the vertical forces is only possible when we have enough coherence function or values (above 0.7 constantly for a certain frequency area) between them. Therefore, by using the FRA method is not imaginable to reproduce the wheel forces from vertical measured wheel forces. However, in the next section we investigate this possibility considering

a certain measurement interval called small sine wave - out of phase at the proving ground measurements.

9.3.3.3 Reproduction of the longitudinal and lateral wheel forces

In this section, it is aimed to reproduce the longitudinal and lateral wheel forces from the vertical forces based on the frequency response analysis. The reproduced signals must be contained all the amplitude, phase and frequency information compared to the measured wheel forces. To achieve this, all the measurement intervals at the proving ground are examined. The measurement interval, which is small sine wave – out of phase at the proving ground, gives us good results taking into account of the similarity of the reproduced signals compared to the measured ones. However, it is necessary to summarize the approach that can be seen at the following figure

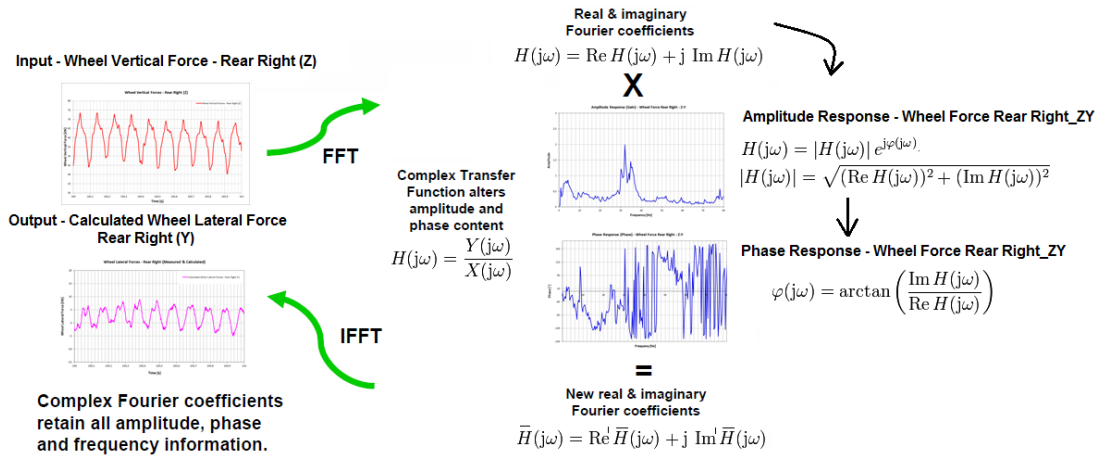


Figure 9.18 : Reproduction of longitudinal and lateral wheel force.

The calculated wheel forces are compared with the measured forces and plotted as follows.

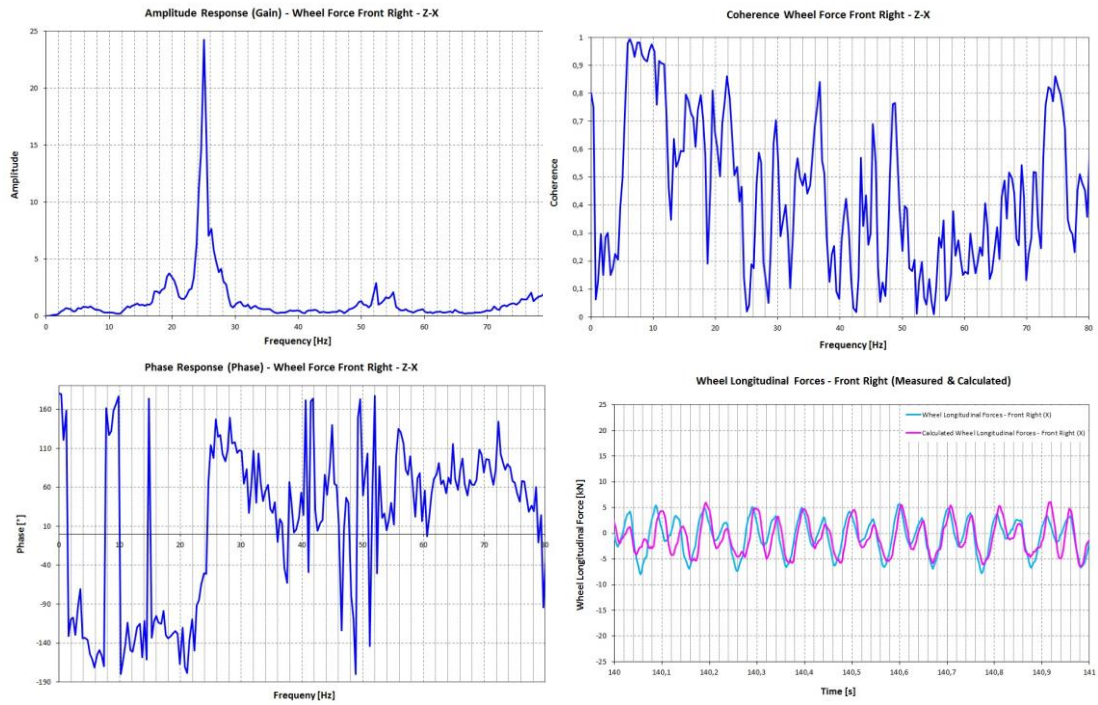


Figure 9.19 : Wheel longitudinal forces-front right (measured & calculated).

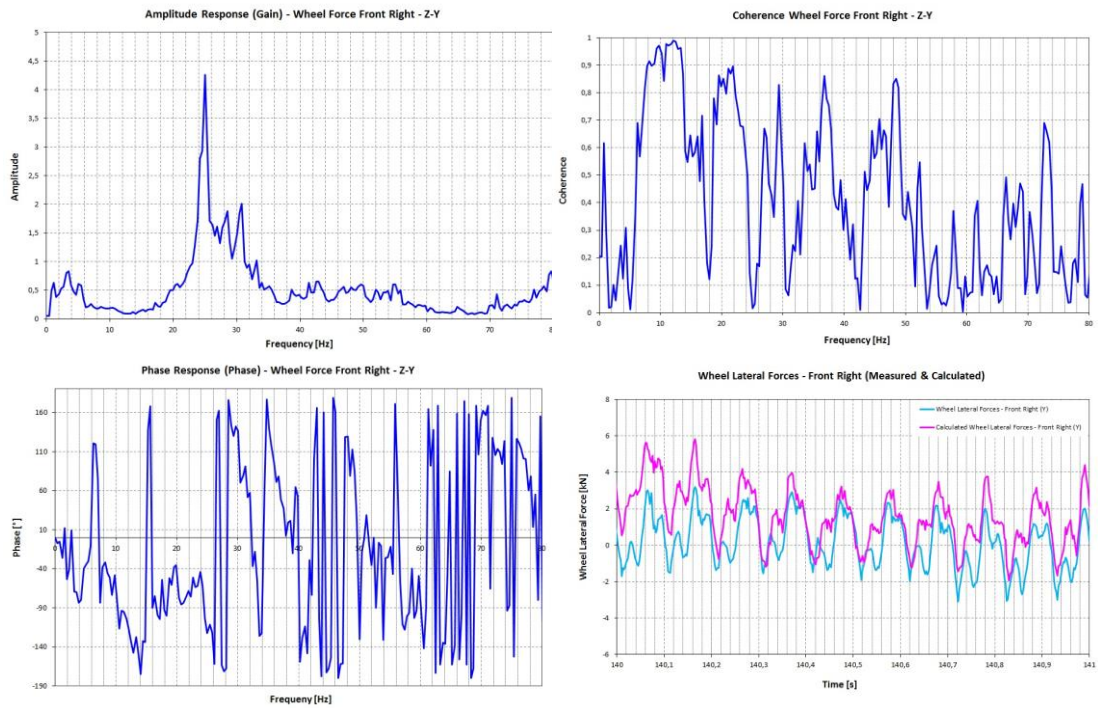


Figure 9.20 : Wheel lateral forces-front right (measured & calculated).

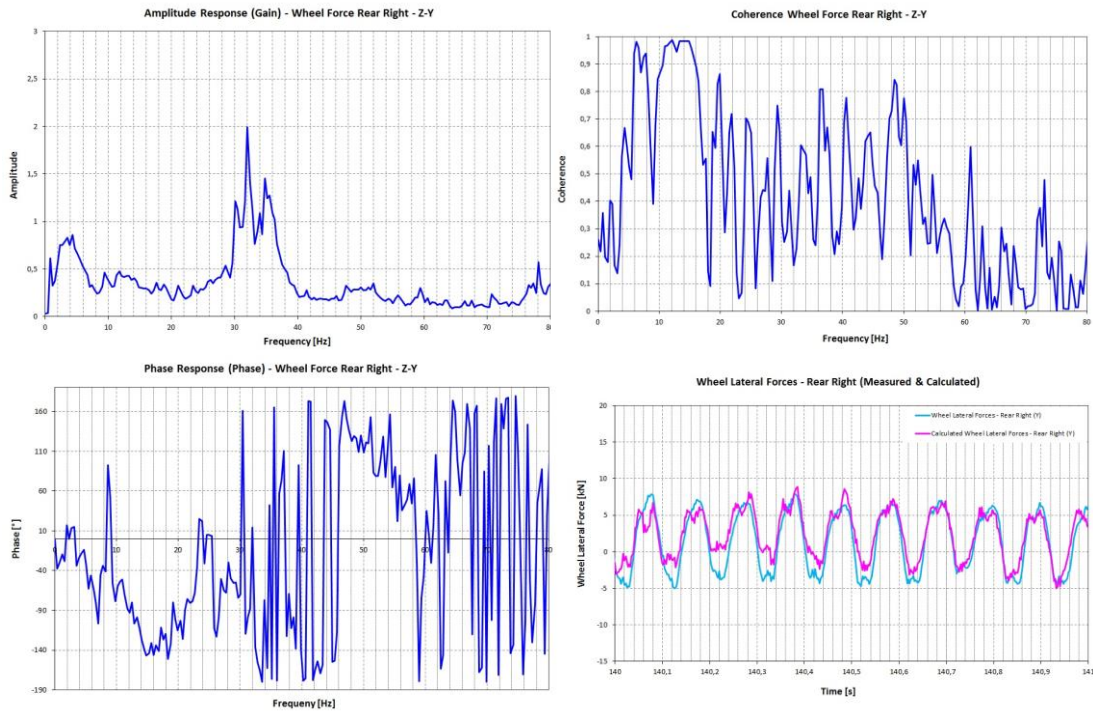


Figure 9.21 : Wheel lateral forces-rear right (measured & calculated).

As we seen on the results, as long as the coherence function well is, it is always possible to reproduce lateral or longitudinal wheel forces from vertical forces based on frequency response function. However, the coherence function of the examined wheel forces (e.g. lateral, longitudinal and vertical) gives us good results only for a specific measurement interval at the proving ground. As we explained previous section, this measurement interval is called small sine wave – out of phase. When we look at the time signal to compare the measured and calculated signals, it is obvious to see that both of them are almost same in terms of the amplitude, frequency and phase information. Because of the characteristics of stationary deterministic signals that are made up entirely of sinusoidal components at discrete frequencies it is possible to mention of the reproduction of the lateral and longitudinal forces from the vertical wheel forces. However, in reality, measured time signals of the wheel forces at the customer usage are mostly stationary random signals where we can hardly obtain good coherence function. Due to the nature of excitation of the roads at the customer usage, this method is not working with the stationary random signals.

9.3.4 Correlation Analysis with Cross Plots – Lissajous Curve

In mathematics, a Lissajous curve, also known as, Lissajous figure or Bowditch curve is the graph of a system of parametric equations (9.45).

$$x = A \sin(at + \delta), \quad y = B \sin(bt) \quad (9.45)$$

which describe complex harmonic motion. The appearance of the figure is highly sensitive to the ratio a/b . For a ratio of one, the figure is an ellipse, with special cases including circles ($A = B$, $\delta = \pi/2$ radians) and lines ($\delta = 0$). Another simple Lissajous figure is the parabola ($a/b = \text{two}$, $\delta = \pi/2$). Other ratios produce more complicated curves, which are closed only if a/b is rational.

9.3.4.1 Cross Plots of the normalized wheel forces (for case of $a = b$)

When the input to an LTI (Linear Time-Invariant Theory) system is sinusoidal, the output is sinusoidal with the same frequency, but it may have different amplitude and some phase shift. We can plot one signal against another (as opposed to one signal against time) to plot the output of an LTI system against the input to the LTI system produces an ellipse that is a Lissajous figure for the special case of $a = b$. The aspect ratio of the resulting ellipse is a function of the phase shift between the input and output, with an aspect ratio of 1 (perfect circle) corresponding to a phase shift of $\pm 90^\circ$ and an aspect ratio of ∞ (a line) corresponding to a phase shift of 0 or 180 degrees. The figure below summarizes how the Lissajous figure changes over different phase shifts. The phase shifts are all negative so that delay semantics can be used with a causal LTI system (note that a -270 degree is equivalent to $+90$ degrees). The arrows show the direction of rotation of the Lissajous figure.

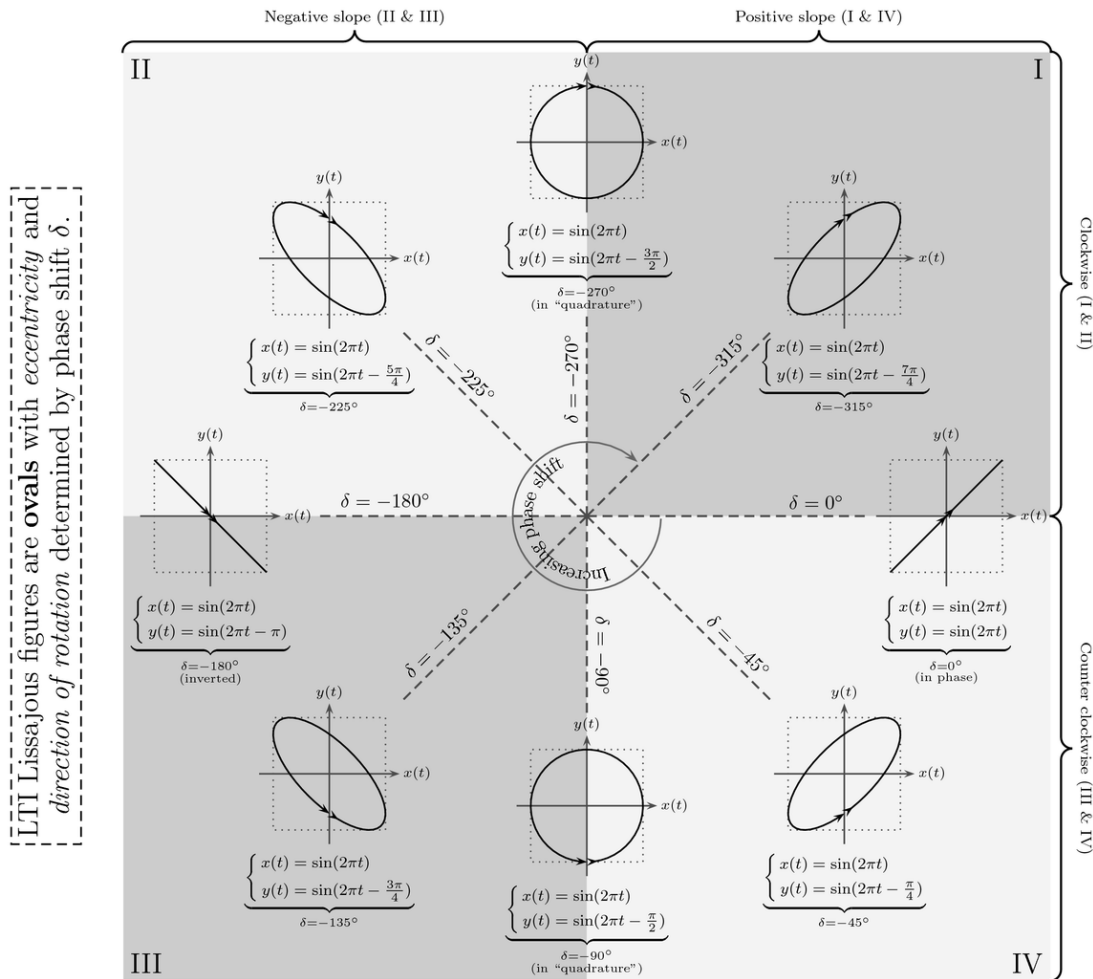


Figure 9.22 : A Pure Phase Shift affects the eccentricity of the lissajous oval.

In other words, if the two signals have the same frequency, then the Lissajous figure will assume the shape of an ellipse. The ellipse's shape will vary according to the phase difference between the two signals, and according to the ratio of the amplitudes of the two signals. The following figure shows some figures for two signals with synchronized frequency and equal amplitudes, but different phase relationships. The formula as follows (9.46) used for determining the phase is:

$$\sin(\Phi) = \pm \frac{Y}{H} \tag{9.46}$$

where H is half the maximum vertical height of the ellipse and Y is the intercept on the y-axis.

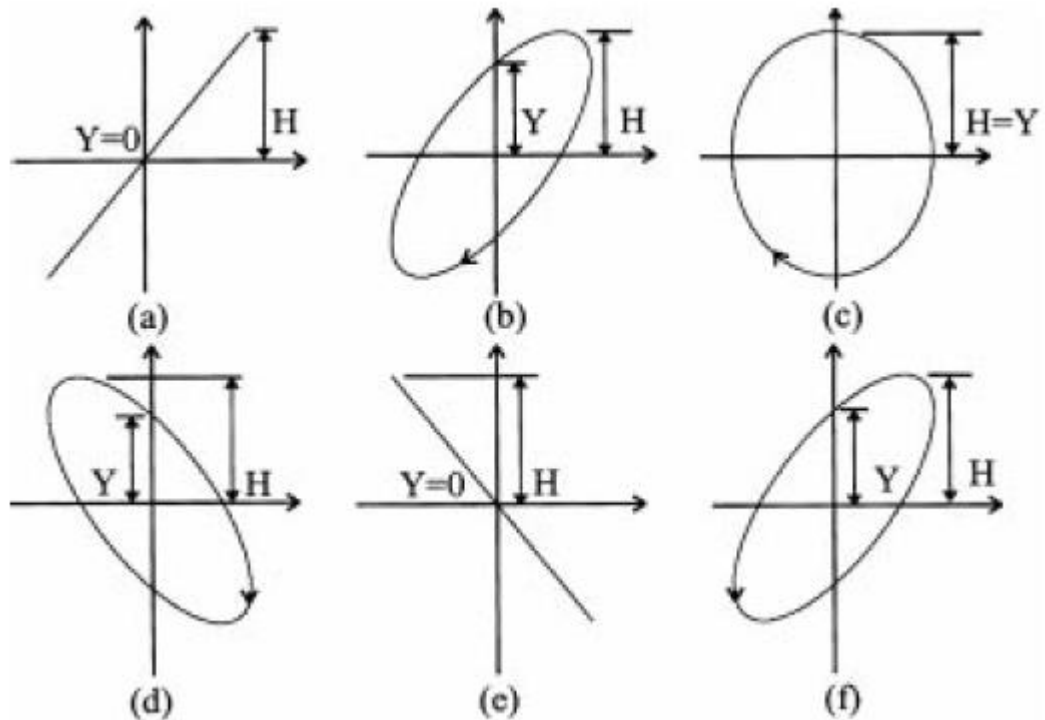


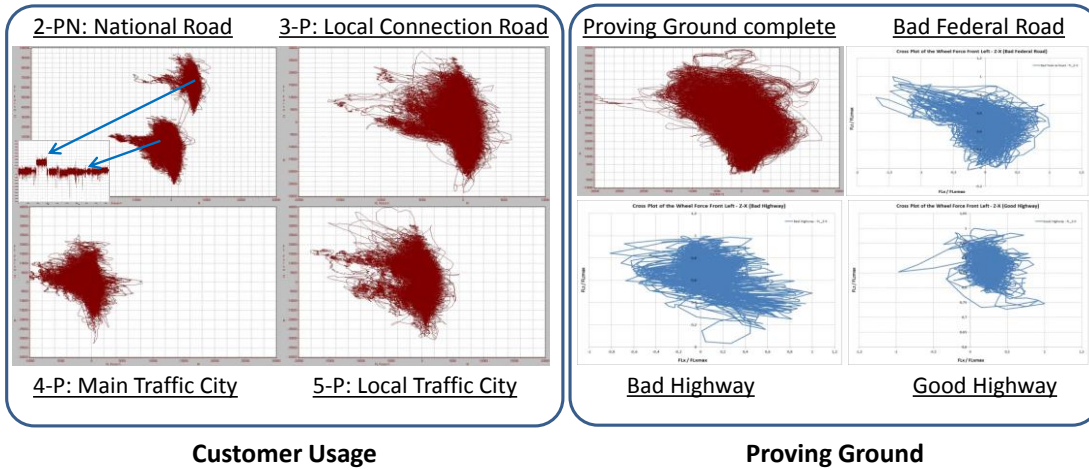
Figure 9.23 : Lissajous figures for two signals.

with synchronized frequency and various phase differences:

(a) phase difference = 0° , (b) phase difference = 45° , (c) phase difference = 90° , (d) phase difference = 135° , (e) phase difference = 180° , (f) phase difference = 315° .

Now, we will try to find to determine the phase difference between the wheel forces at the proving ground and customer usage by using the method (Cross Plots). To achieve this, all the wheel forces are normalized with its maximum amplitude (F_{\max}). Afterwards, the two signals are plotted one against another as explained above. The results for the proving ground can be seen at the following figures.

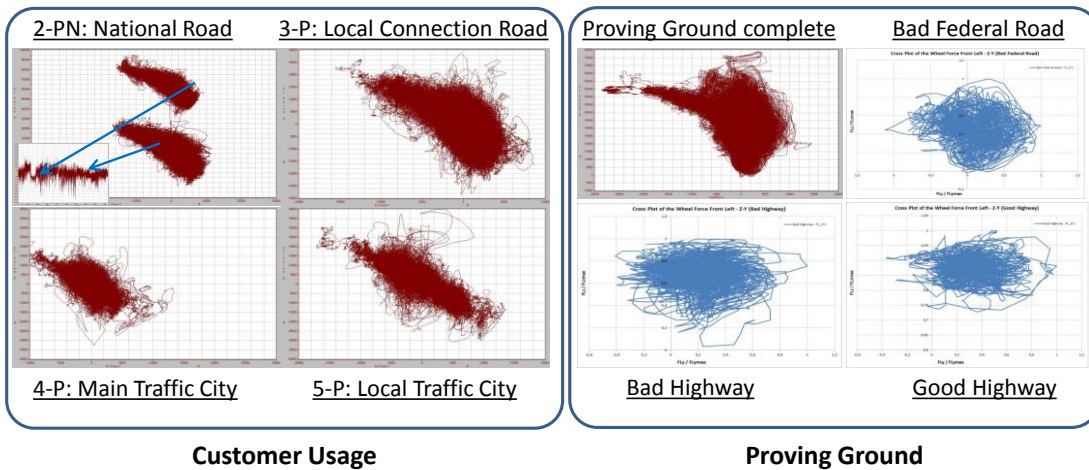
Cross Plot Wheel Force Front Left – ($F_{L,Z} - F_{L,X}$)



Legend
 Y- Axis: $F_{L,Z}$
 X- Axis: $F_{L,X}$

Legend
 Y- Axis: $F_{L,Z} / F_{Lmax}$
 X- Axis: $F_{L,X} / F_{Lmax}$

Cross Plot Wheel Force Front Left – ($F_{L,Z} - F_{L,Y}$)

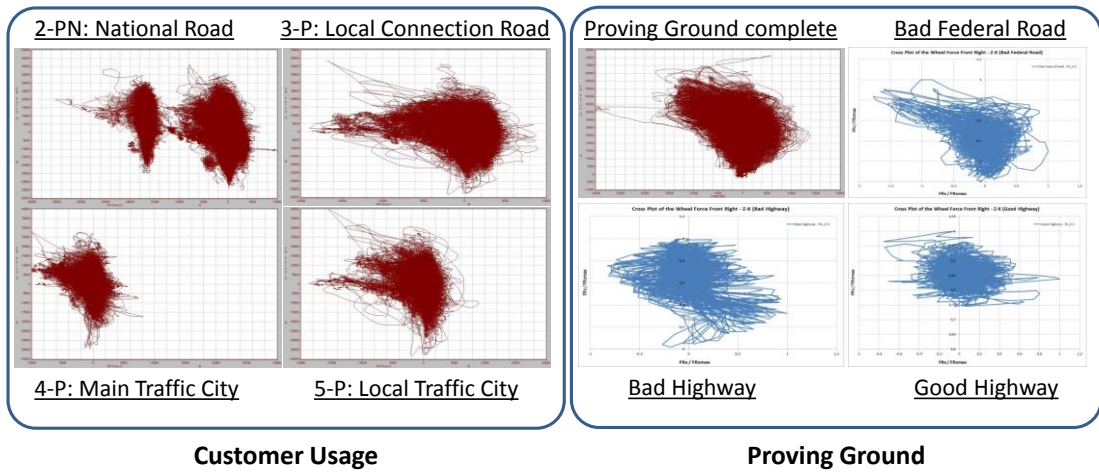


Legend
 Y- Axis: $F_{L,Z}$
 X- Axis: $F_{L,Y}$

Legend
 Y- Axis: $F_{L,Z} / F_{Lmax}$
 X- Axis: $F_{L,Y} / F_{Lmax}$

Figure 9.24 : Cross Plots of the normalized wheel forces at the PG and CU.

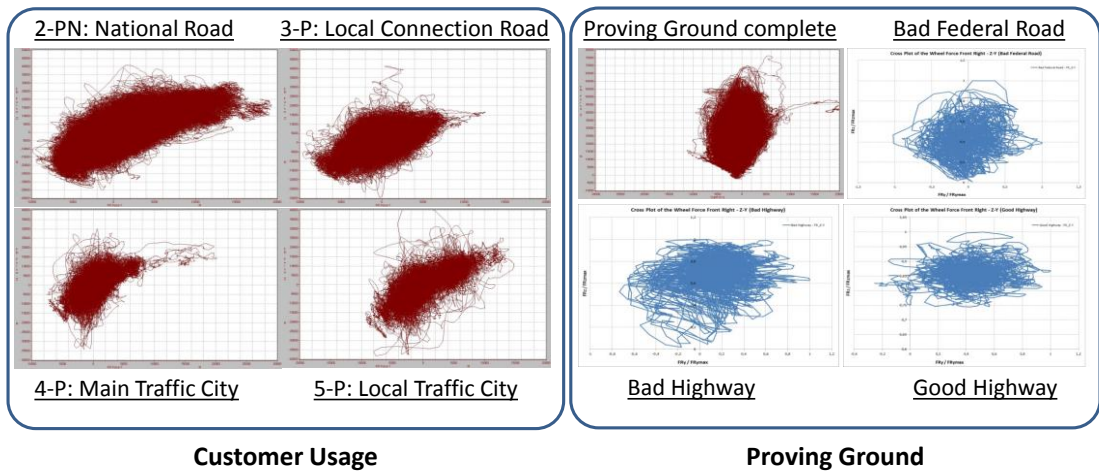
Cross Plot Wheel Force Front Right – ($F_{R,Z} - F_{R,X}$)



Legend
 Y- Axis: $F_{R,Z}$
 X- Axis: $F_{R,X}$

Legend
 Y- Axis: $F_{R,Z} / F_{Rmax}$
 X- Axis: $F_{R,X} / F_{Rmax}$

Cross Plot Wheel Force Front Right – ($F_{R,Z} - F_{R,Y}$)

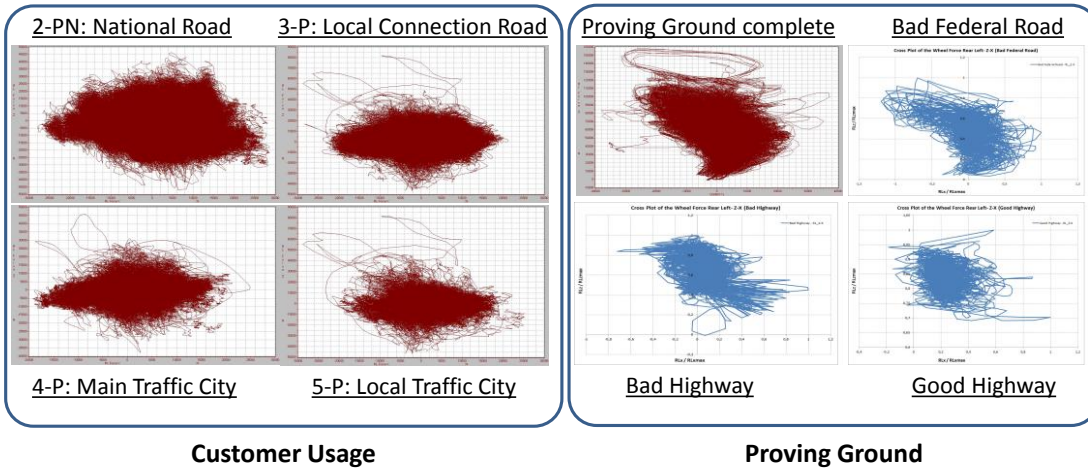


Legend
 Y- Axis: $F_{R,Z}$
 X- Axis: $F_{R,Y}$

Legend
 Y- Axis: $F_{R,Z} / F_{Rmax}$
 X- Axis: $F_{R,Y} / F_{Rmax}$

Figure 9.24 (continued): Cross Plots of normalized wheel forces at the PG and CU.

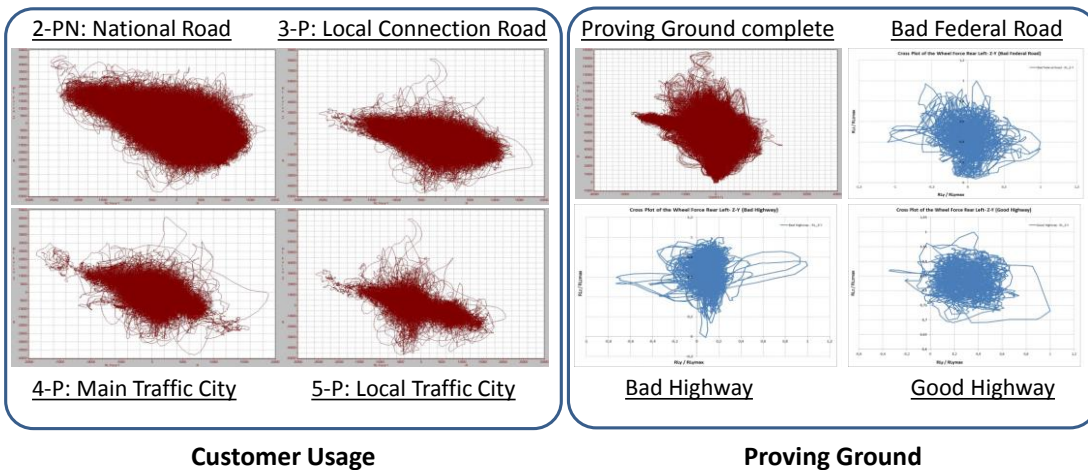
Cross Plot Wheel Force Rear Left – ($R_{L,Z} - R_{L,X}$)



Legend
 Y- Axis: $R_{L,Z}$
 X- Axis: $R_{L,X}$

Legend
 Y- Axis: $R_{L,Z} / R_{Lmax}$
 X- Axis: $R_{L,X} / R_{Lmax}$

Cross Plot Wheel Force Rear Left – ($R_{L,Z} - R_{L,Y}$)

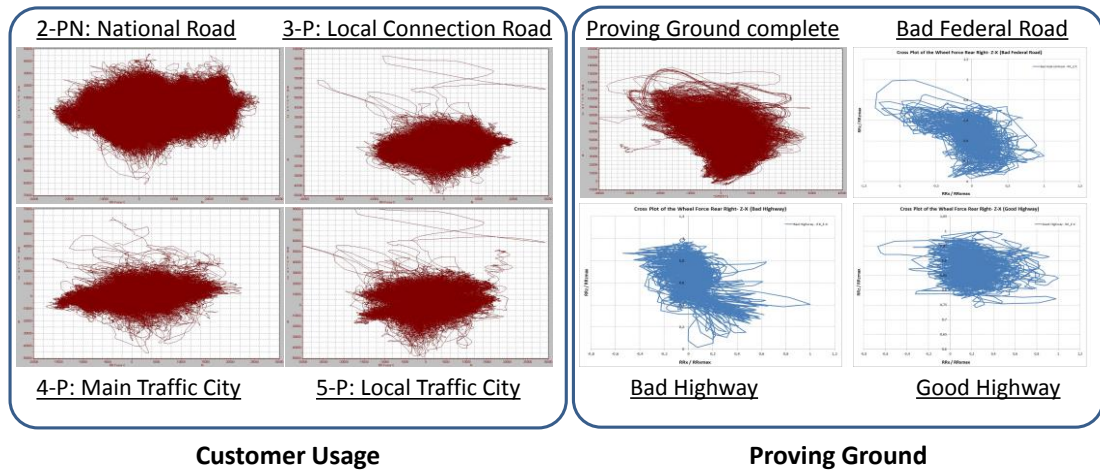


Legend
 Y- Axis: $R_{L,Z}$
 X- Axis: $R_{L,Y}$

Legend
 Y- Axis: $R_{L,Z} / R_{Lmax}$
 X- Axis: $R_{L,Y} / R_{Lmax}$

Figure 9.24 (continued): Cross Plots of normalized wheel forces at the PG and CU.

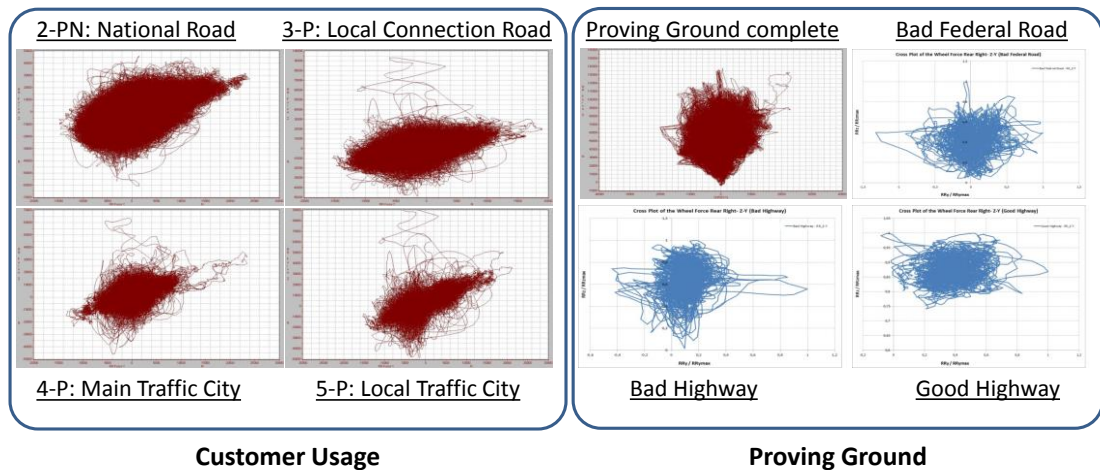
Cross Plot Wheel Force Rear Right – ($R_{R,Z} - R_{R,X}$)



Legend
 Y- Axis: $R_{R,Z}$
 X- Axis: $R_{R,X}$

Legend
 Y- Axis: $R_{R,Z} / R_{Rmax}$
 X- Axis: $R_{R,X} / R_{Rmax}$

Cross Plot Wheel Force Rear Right – ($R_{R,Z} - R_{R,Y}$)



Legend
 Y- Axis: $R_{R,Z}$
 X- Axis: $R_{R,Y}$

Legend
 Y- Axis: $R_{R,Z} / R_{Rmax}$
 X- Axis: $R_{R,Y} / R_{Rmax}$

Figure 9.24 (continued): Cross Plots of normalized wheel forces at the PG and CU.

In conclusion, when we consider all the methods explained in Section-9 in order to find the phase relation of the different wheel forces at the customer usage and at the proving ground, we can say that there is no representative and dominant phase relation between the measured wheel forces. On the other hand, there are some good correlation results between some investigated wheel forces; however, it is not valid for all the measurement intervals. At the following figure, these correlations are plotted schematically. Due to the road characteristics of the 4-P and 5-P, where the vehicle speed is relatively low, it is hard to generalize this relations for the all other

wheel force directions at the service life of the vehicle. In fact, all the wheel forces occur arbitrary due to the nature of road excitation at the customer usage.

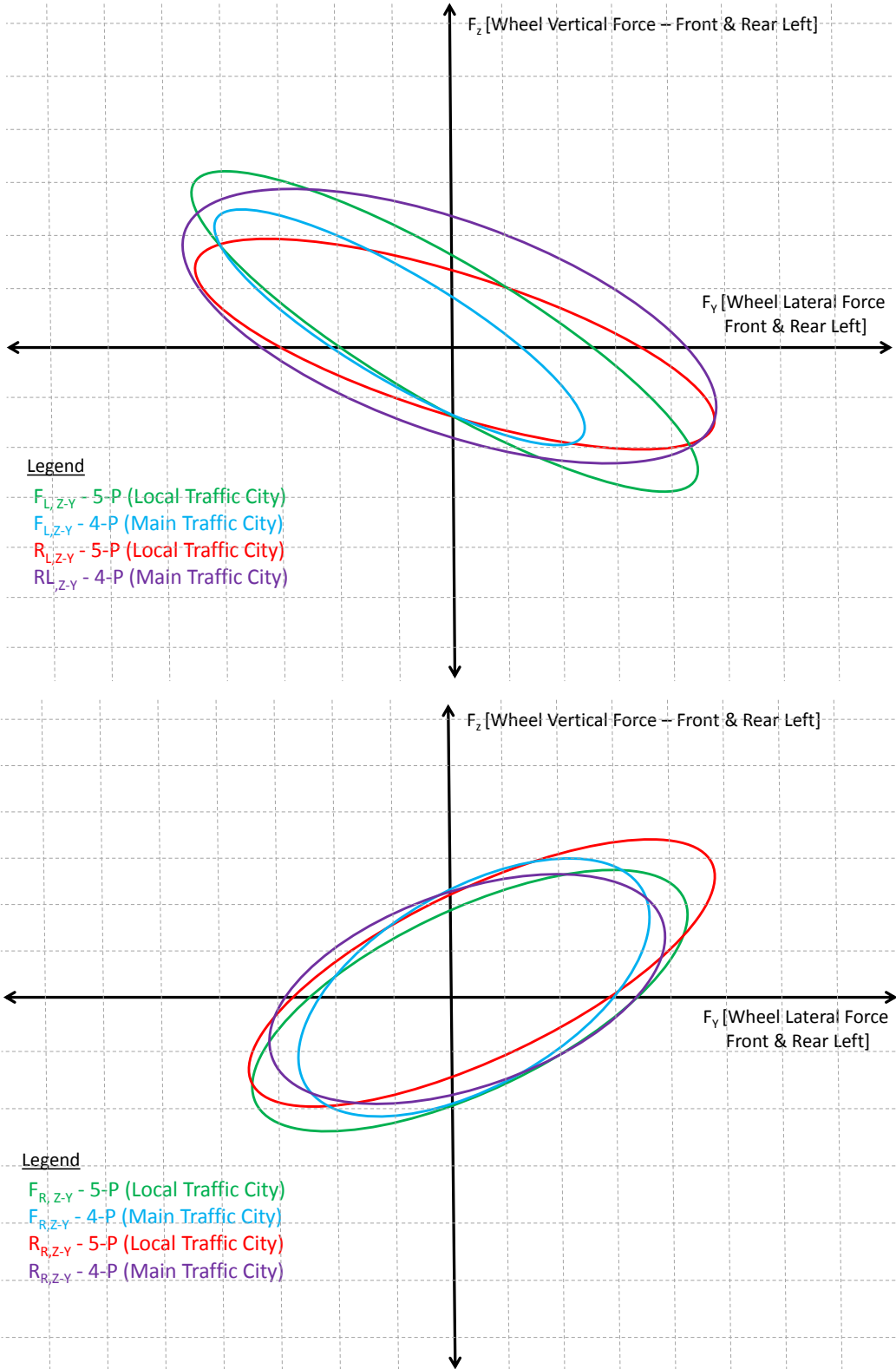


Figure 9.25 : Correlated wheel forces at the some intervals (schematically).

10. CALCULATION OF THE SHAPE PARAMETERS (v)

In order to characterize the shape of the spectrum of individual load-time histories by a single number, (9.47) specifies an additional number, the “spectrum shape parameter”. This idea is certainly not new. Shape parameters have traditionally been used in various formats, for example in fatigue standards, in order to characterize the combined effect of block size and cumulative frequency of load amplitudes – partly adopting Miner’s rule [26].

For an interpretation of the spectrum shape parameter, typified amplitude spectra as proposed by Gassner et al [27, 28] are considered, as in the figure below that may be described by

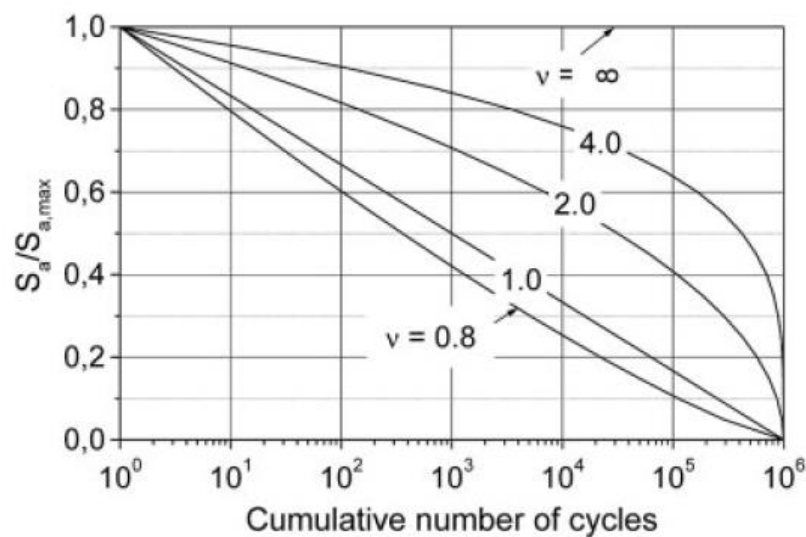


Figure 10.1 : Typified load amplitude spectra.

As in the following equation (9.47), we see the formula of the spectrum shape parameter.

$$\ln H_i = [1 - (S_{a,i}/S_{a,max})^v] \cdot \ln H_0 \quad (9.47)$$

where, H_i = cumulative frequency of load cycles for load level $S_{a,i}$, H_0 = block size (number of rainflow cycles) = shape exponent. With decreasing v values, the shapes of the amplitude spectra become more and more hollow. The following table details

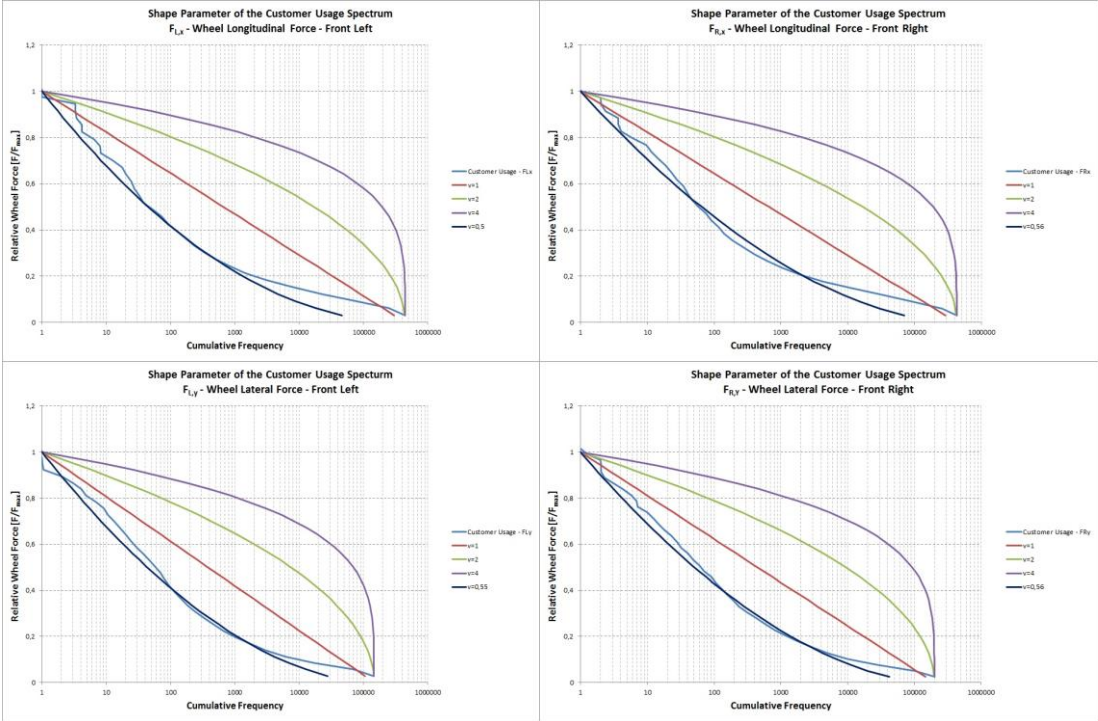
some numbers of ν for the spectra shown in the figure above for a block size $H_0 = 10^6$.

Table 10.1 : Spectrum shape parameters ν for typified amplitude spectra.

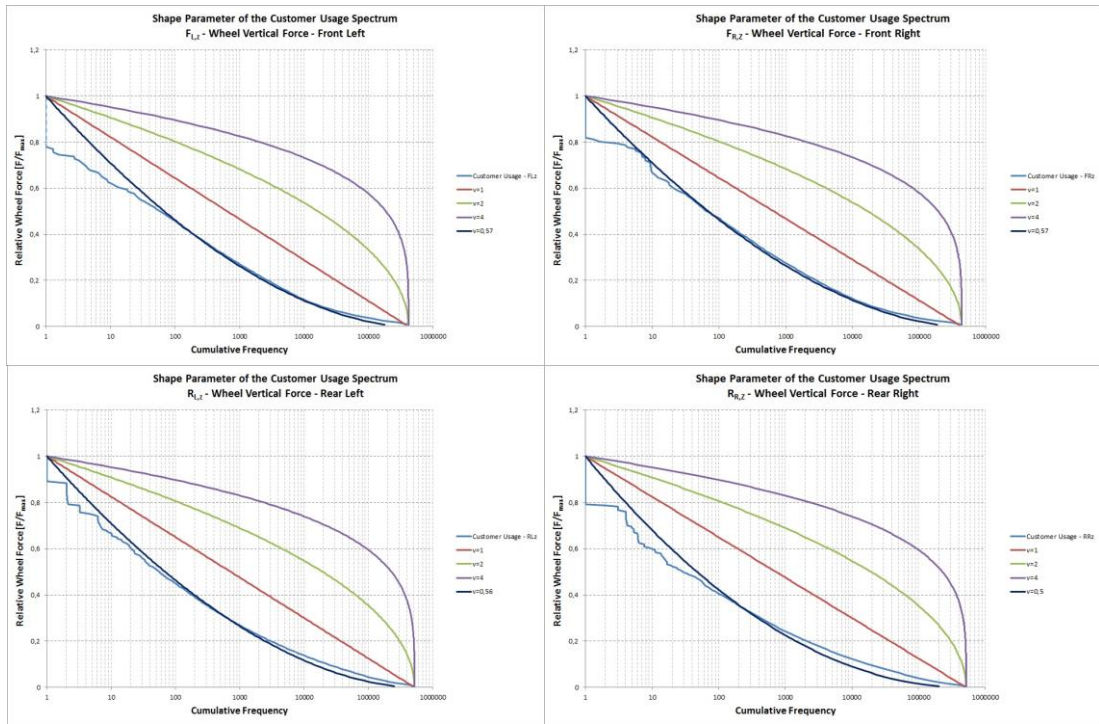
Spectrum	ν	Description
1	∞	constant amplitude loading
2	4	$\nu > 2$ typical for bridge and crane structures
3	2	stationary Gaussian random process
4	1	typical for road roughness induced loads
5	0,8	$\nu \leq 1$ typical for wind gusts, wave actions etc.

Spectrum Shape Parameters ν for typified Amplitude Spectra (block size $H_0 = 10^6$). According to the equation (9.47), the shape parameters of customer usage and proving ground spectrums are calculated. The results can be seen as the following figures.

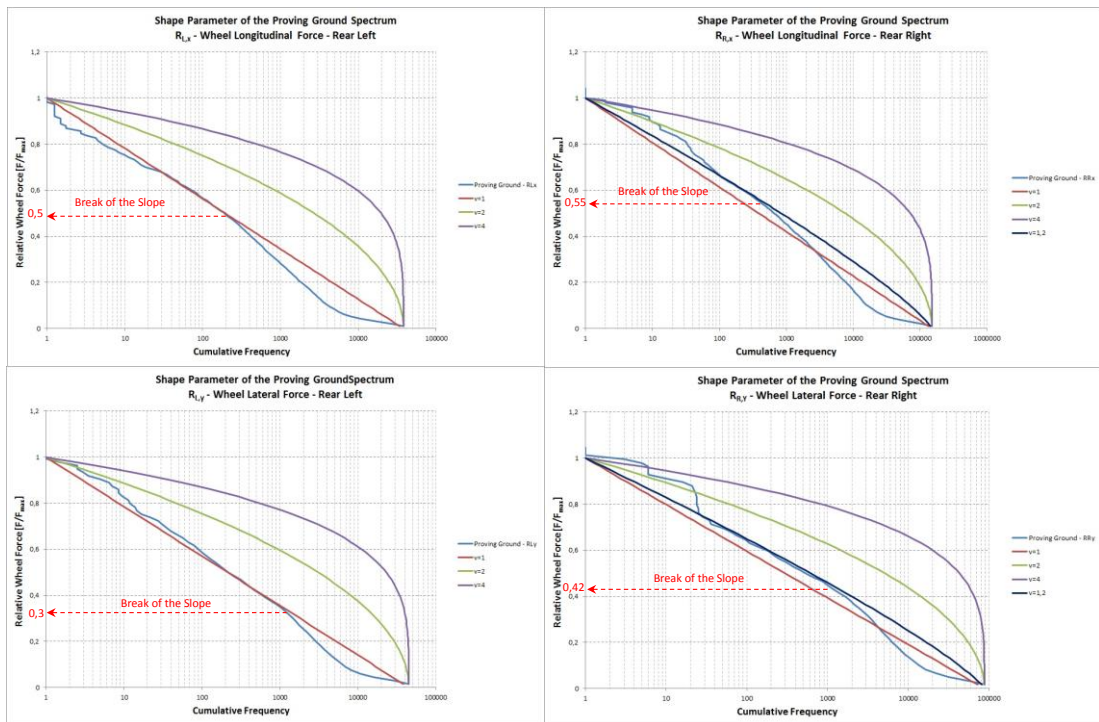
**Spectrum Shape Parameters of the Customer Usage
Front Wheel Longitudinal and Lateral Force**



Spectrum Shape Parameters of the Customer Usage Front and Rear Wheel Vertical Force



Spectrum Shape Parameters of the Proving Ground Rear Wheel Longitudinal and Lateral Force



Spectrum Shape Parameters of the Proving Ground Front and Rear Wheel Vertical Force

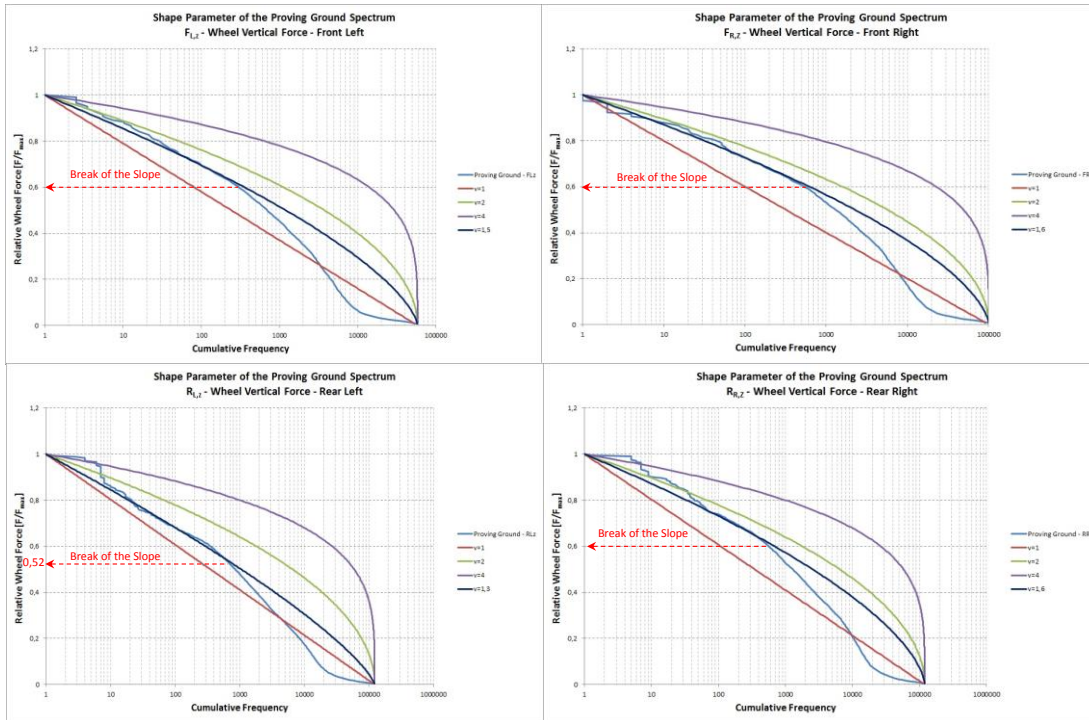


Figure 10.2 : Spectrum shape parameters and break of slope of CU and PG.

As you can see above, the spectrum shape parameters differ from customer usage and proving ground. In addition, this parameter depends on the coordinates of the forces acting on the wheel. Besides, the calculated parameters for the proving ground are valid until the break of the spectrum slope. After the break of the slope, the spectrums have other shape parameters. The second shape parameters, which define the parameters after the break of slope, are not analyzed in this study. In order to make a better view of the results, bar charts of the parameters are obtained as follows. At the following figures, we see the comparison of the shape parameters for the wheel forces on the customer usage and proving ground.

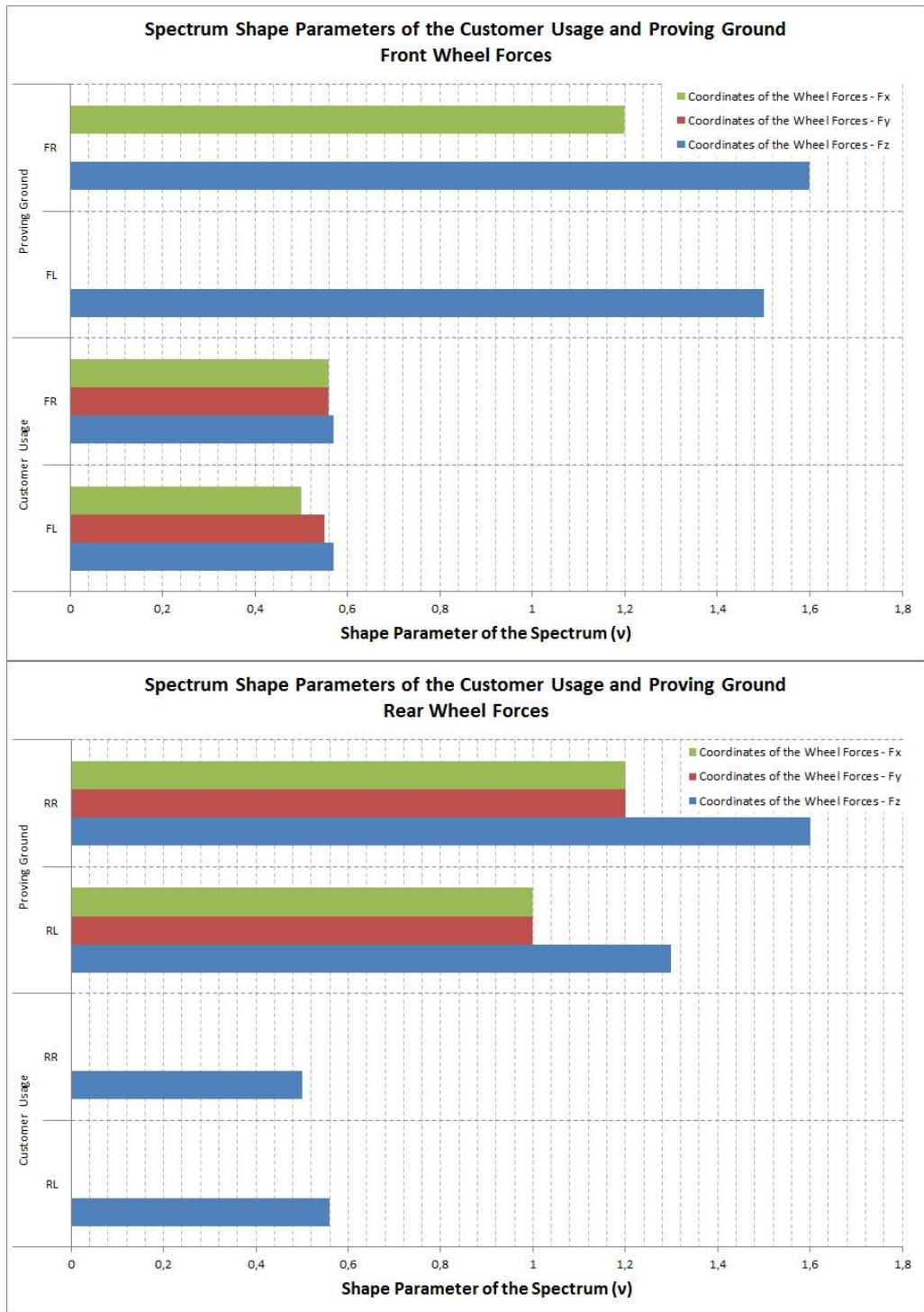


Figure 10.3 : Comparison of shape parameters on the CU and PG.

As mentioned above, the break of the spectrum slopes at the proving ground are also compared and shown at the following figure.

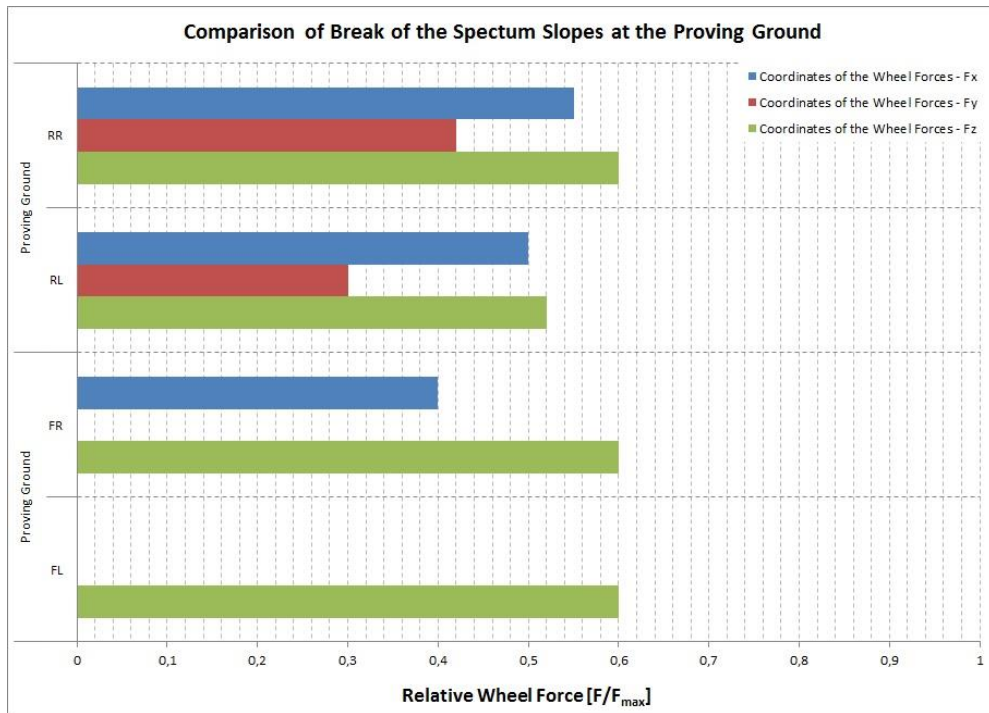


Figure 10.4 : Comparison of break of the spectrum slopes at the proving ground.

The shape parameters of the spectrum couldn't be calculated for some of the coordinates of the wheel forces on the customer usage because of the irregularities of the shape parameter. Here we can see spectrum, which we cannot define with our equation due to the anomaly of the shape parameter. At the following figure, we see two different distributions of a spectrum, which cause difficulties to calculate shape parameter.

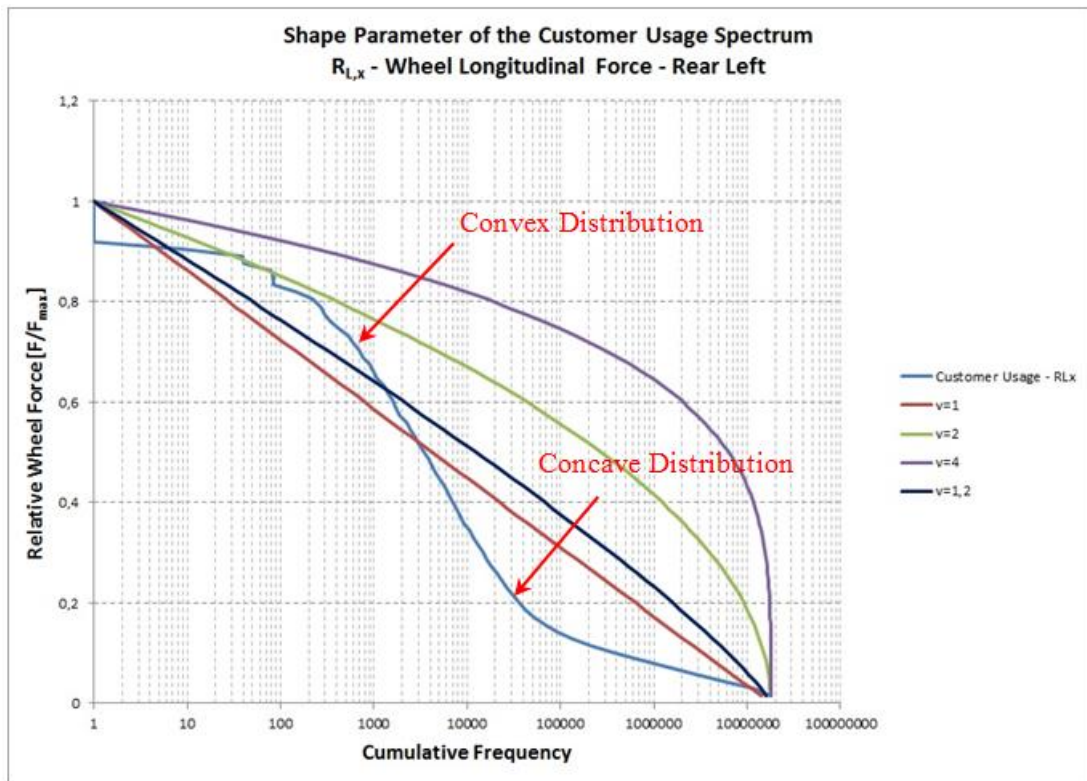


Figure 10.5 : Difficulty to calculate shape parameter of the CU for $R_{L,x}$

When we consider the following table, which summarizes all the results, we see that the spectrum shape parameter for the front wheels at the customer usage is around 0.55, which is a very hard concave distribution. In addition, at the rear wheel, a very similar value compared to front wheel, which is 0.55. We can say that the spectrums have a very hard concave distribution because the value of the shape parameter that is below 0.8. The shape parameter of the proving ground for the lateral and longitudinal coordinates of the wheel forces are almost same and around 1 which describes a straight line distribution, in other words typical for road roughness induced loads. However, the shape parameter for the vertical direction is around 1.50 that is 2.72 higher than customer usage. This means that the spectrum of proving ground in the vertical coordinates of the wheel forces is close to the normal distribution, in other words stationary Gaussian random process. As mentioned before, the spectrums at the proving ground have two regions. First region until the break of the slope, where we can define a shape parameter of the spectrum and the second region, after the break of the slope, where our shape parameters are not valid, are determined. The second region starts 0.58 of the relative wheel forces in vertical direction. Besides, for the longitudinal direction it starts from 0.46 of the relative wheel force. All the information above mentioned could be used to derive a

methodical and systematic approach for the testing of the commercial vehicle axles. At the following table, we see an overview of the spectrum shape parameters [v] and break of the slope related to relative wheel force [F/F_{max}] on customer usage and at the proving ground.

Table 10.2 : Overview of the spectrum shape parameters [v] and break of slope.

Coordinates of the Wheel Forces	Spectrum Shape Parameter [v]				Break of the Slope related to Relative Wheel Force [F/F _{max}]	
	Customer Usage		Proving Ground		Proving Ground	
	<i>Front</i>	<i>Rear</i>	<i>Front</i>	<i>Rear</i>	<i>Front</i>	<i>Rear</i>
F _x	0,53	-	1,2	1,1	0,4	0,53
F _y	0,55	-	-	1,1	-	0,36
F _z	0,57	0,53	1,55	1,45	0,6	0,56

11. CONCLUSIONS

The demands for cost and weight reduction in connection with an increase in payload are top priorities in lightweight construction of commercial vehicles, especially the safety components must not be failed under operational conditions. Axles and axle guiding components (suspension parts) are subjected to various external loads dependent of the field of application (long-distance or short-distance vehicles, off-road trucks, and busses), the stiffness of the vehicle structure, the nominal payload and the road conditions.

It is apparent that accurate knowledge of the failure critical load configurations as well as the frequency of their occurrence within a service life is fundamental to the development process of such safety components. Based on this knowledge, design load spectrum and correlations between wheel loads have to be derived taking into account the service loading conditions [29].

In order to derive of a load spectrum for structural durability approval of commercial vehicle axles, it is necessary to perform vehicle measurements as much as possible on the characteristic routes with the wheel force transducers (WFT). Thus, the loads acting on the axles will be measured and lately analyzed in terms of structural durability. For this purpose, a long-term vehicle measurement (Road Load Data Acquisition) is done on the characteristic routes in Turkey with a two-axle coach (an independent front axle and rigid rear axle) for the first measurement campaign. Afterwards, another measurement is also performed at the proving ground location (PG) of commercial vehicle manufacturer.

Based on the results of this study, a methodology to derive a standardized load spectrum to develop a test procedure for structural durability approval of commercial vehicle axles has been developed.

In this study, it has been observed that there are some main factors to be calculated in order to derive a load spectrum for structural durability approval of commercial vehicle axles. With respect to durability point of view, some main factors such as

scaling factors, phase relationship between wheel forces, extreme loads and shape parameters of the spectrums has been investigated by means of this methodology.

In order to make this study more understandable, the aim, the obtained methodology, the techniques that are used and the results are summarized as a flow chart or process as seen at the following figure.

1. Road Load Data Acquisitions and Analysis on the Customer Usage and at the Proving Ground

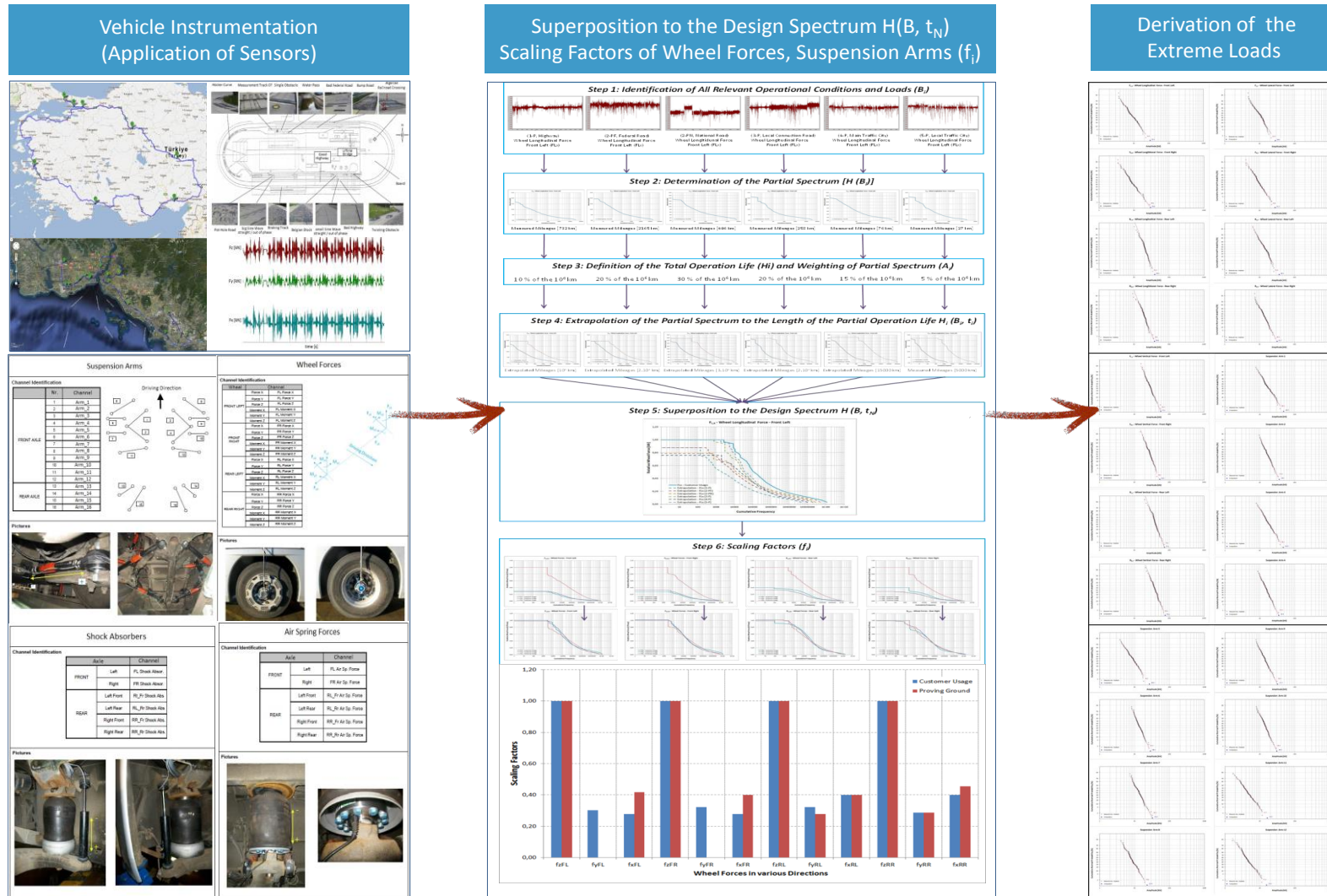
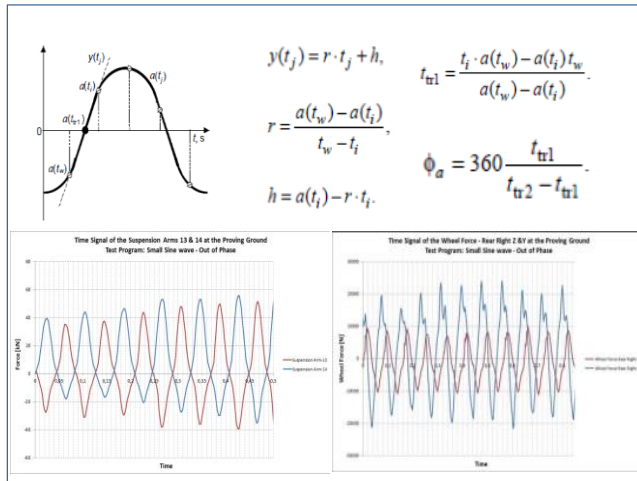


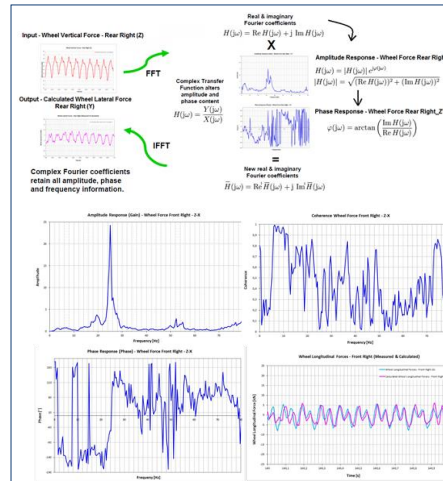
Figure 11.1 : Flow Chart of the methodical and systematic approach.

2. Determination of the Phase Relationship between Wheel Forces

Phase Angle of a Periodic Non-Sinusoidal Signal (Zero-Crossing Methods)



Phase Angle of a Non-Sinusoidal Signal (Frequency Response Analysis)



Phase Angle of a Non-Sinusoidal Signal (Correlation Analysis with Cross Plots)

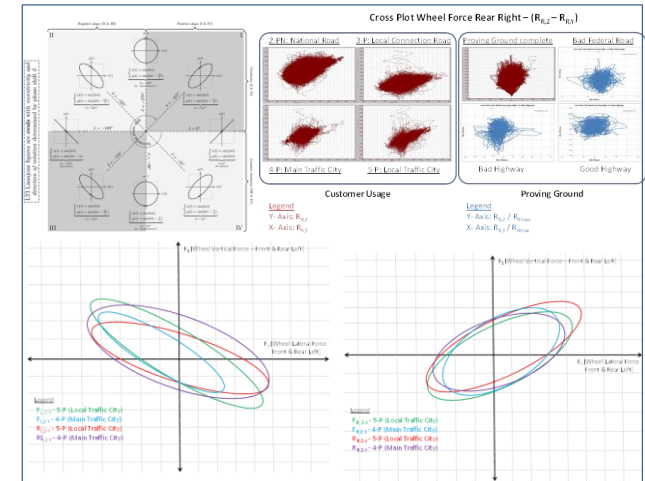
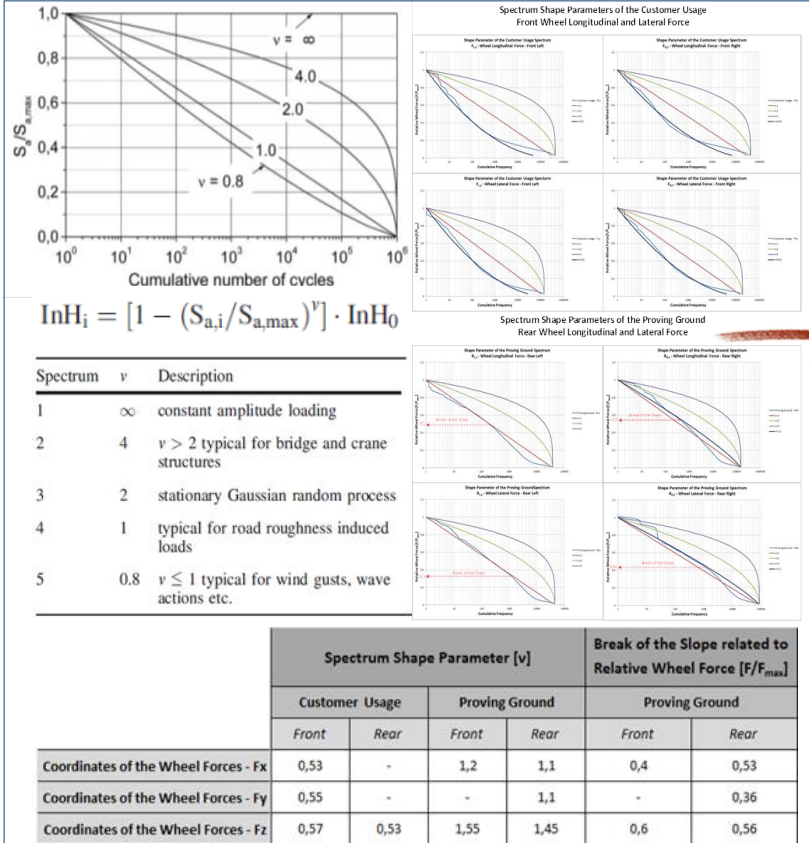
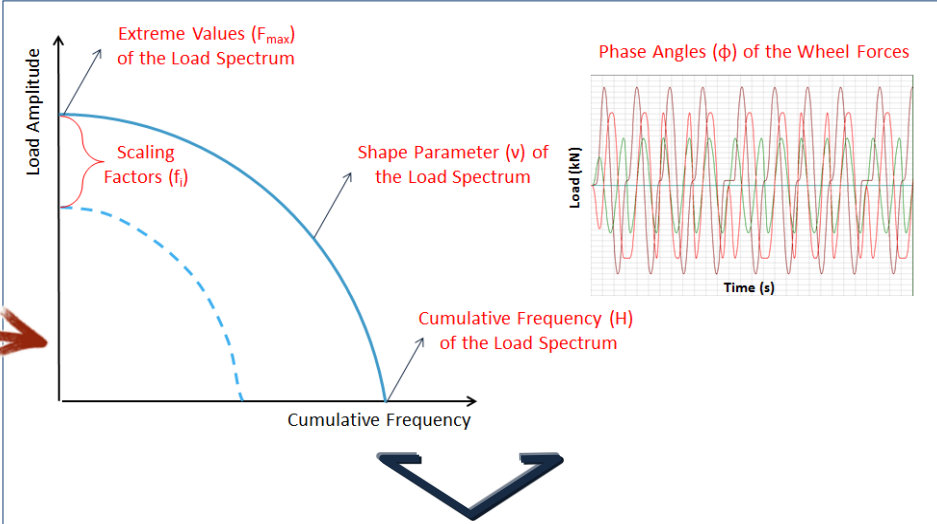


Figure 11.1 (continued): Flow Chart of the methodical and systematic approach.

3. Calculation of the Shape Parameters (ν) of the Customer Usage and Proving Ground Spectrums



4. Characterization of the Load Spectrum based on the Results of this Systematical Approach



Characterization of the Load Spectrum for the Axles of a two-axle Coach											
Axle Position	Coordinates of the Wheel Forces	Extreme Values (F_{max}) of the Load Spectrum		Cumulative Frequency (H) of the Load Spectrum		Shape Parameters (ν) of the Load Spectrum		Phase Angles (ϕ) of the Wheel Forces		Scaling Factors (f_i)	
		Customer Usage	Proving Ground	Customer Usage	Proving Ground	Customer Usage	Proving Ground	Customer Usage	Proving Ground	Customer Usage	Proving Ground
Front Axle	Vertical	1,20 · $F_{Fz,max}(PG)$	$F_{Fz,max}(PG)$	20 · $H_{PG,Fz}$	$H_{PG,Fz}$	0,57	1,55	All the wheel forces occur arbitrary due to the nature of road excitation at the customer usage.	-	1,00	1,00
	Longitudinal	0,86 · $F_{Fx,max}(PG)$	$F_{Fx,max}(PG)$	20 · $H_{PG,Fx}$	$H_{PG,Fx}$	0,53	1,20			0,28	0,41
	Lateral	1,11 · $F_{Fy,max}(PG)$	$F_{Fy,max}(PG)$	14 · $H_{PG,Fy}$	$H_{PG,Fy}$	0,55	-			0,31	-
Rear Axle	Vertical	0,83 · $F_{Rz,max}(PG)$	$F_{Rz,max}(PG)$	20 · $H_{PG,Rz}$	$H_{PG,Rz}$	0,53	1,45	There is no representative and dominant phase relation between the measured wheel forces.	-	1,00	1,00
	Longitudinal	0,98 · $F_{Rx,max}(PG)$	$F_{Rx,max}(PG)$	20 · $H_{PG,Rx}$	$H_{PG,Rx}$	-	1,10			0,40	0,43
	Lateral	1,35 · $F_{Ry,max}(PG)$	$F_{Ry,max}(PG)$	15 · $H_{PG,Ry}$	$H_{PG,Ry}$	-	1,10			0,30	0,28

Figure 11.1 (continued): Flow Chart of the methodical and systematical approach.

If we want to define a load or test spectrum, we need to know four main parameters, which are extreme value of the spectrum, the shape parameter of the spectrum, cumulative frequency of the spectrum and phase angle of the signal. In this study, based on the measurements on the customer usage and at the proving ground, it is aimed to determine these parameters which helps us lately to develop a test procedure for the structural durability approval of commercial vehicle axles. This developed methodology, which is necessary to derive a load spectrum to generate a test procedure for structural durability approval of commercial vehicle axles differentiate from other studies in the way of systematical analysis procedure. All the mentioned technique is available in literature; however, these techniques are used to create a systematical data analysis procedure for the commercial vehicle axles. This is the main difference of this study from others.

The main problem to derive a load spectrum for commercial vehicle axles is economic cost because the required long-time road load-data acquisitions with wheel force transducers are expensive. Apart from this, the analysis of the measured data is also significant time-consuming. On the other hand, the advantages of a standardized load spectrum are significant simplification of transfer the realistic load assumption from forerunner design to the new design and a time-optimized determination of test programs; as a result, the weak points will be rapidly identified.

As long as we do not have any idea of the loading acting to the axle, or if previous measurements are not available, then we have to perform some measurements, where we can define the loads acting to axle. This is a very important step of this study because of their costs. Certainly, it is also a point to discuss, which roads should be measured with which vehicle. The characteristic routes or so-called reference-customer usage profile is formed that contains all relevant loads of partially very different customer operations. During the customer-usage profile measurement, the vehicle was always full loaded. The choices of the roads have been done according to the traffic volume distributions with reference to the Turkey General Directorate of Highways and the information of the truck & bus services of the commercial vehicle manufacturer.

The aim of this phase is to record all the relevant load information on the vehicle through Turkish roads following the route defined. The results of this activity were the time histories of the signals coming from the sensors located in the vehicle during

the RLDA (Road Load Data Acquisition) performed over Turkish customer usage. In addition, another measurement is performed at the proving ground, where we can calibrate/rearrange our test track according to the measurement of the customer usage. Another main concern of this measurement is the make a comparison between the customer and test track, thus we can say how far our test track remain from the customer usage results. The output of this comparison is a relation or a function between test track and customer usage. Thus, it is possible to derive load spectrums without any expensive and time-consuming customer usage measurements.

Product validation tests are essential at later design stages of product development. In the automotive industry, durability testing in a laboratory is an accelerated test that is specifically designed to replicate fatigue damage and failure modes from proving grounds (PG) testing. Detailed damage analysis is needed to correlate the accelerated test to PG testing. Therefore, accurate representation of PG loading is essential for laboratory-durability test development. PG loading is measured by driving an instrumented vehicle over the PG. The vehicle is equipped with the same transducers for component loading histories and same sensors for other important vehicle parameters as mentioned. The proving ground (test track) measurement campaign is performed with three different vehicle loading conditions (empty, half-loaded and loaded).

In the next step, which is the load data analysis on the customer usage and the proving ground, is a significant step to determine and describe the service loads that in most cases display a random nature. In such cases, they can be illustrated through so-called design spectrum. In this point, we have determined the cumulative frequency of the spectrum. After obtained design spectrum, the scaling factors are calculated. The idea behind of this, it is a factor, which helps us to scale the wheel forces in one direction to another direction. As explained above, those factors give us enormous benefit to calculate or estimate the other wheel forces such as lateral and longitudinal when only vertical wheel forces are available.

Apart from these, the extreme values are derived from the short-term measurement on the customer usage in Turkey, which can be expected after 1 million km. Therefore, due to the low probability of obtaining extreme loads from short-term measurements, the derivation of reliable extreme load assumptions is necessary. These extreme loads are closely related to the dimensioning consideration of the

components. In this step, we have determined extreme value of the spectrum based on Gumbel's approximation.

In the second phase of this study is the determination of the phase angle, if it exists, between the wheel forces acting to directly to the commercial vehicle axles. In literature, there are some ways to determine the phase angles of stationary random signals in a rough estimate. It is intended to evaluate and determine the phase angles of non-sinusoidal signals of the wheel forces, which are measured on the customer usage and at the proving ground. This information enables us to evaluate and define whether the high loads occur simultaneously or chronologically in the each channel (each direction) of the wheel forces by the experimental durability tests of the axles.

In order to achieve this, three methods are used for the phase angle of a periodic non-sinusoidal signal and non-periodic non-sinusoidal signal. These methods are zero-crossing method, frequency response analysis (FRA) and correlation analysis with cross plots respectively. In conclusion, when we consider all the methods explained above in order to find the phase relation of the different wheel forces at the customer usage and at the proving ground, we can say that there is no representative and dominant phase relation between the measured wheel forces. On the other hand, there are some good correlation results between some investigated wheel forces; however, it is not valid for all the measurement intervals.

In fact, all the wheel forces occur arbitrary due to the nature of road excitation at the customer usage. The result of this analysis is the systematical analysis procedure to evaluate and determine the phase angle of wheel forces.

Finally, one of the most important parameter of a load or test spectrum is the shape parameter. In order to characterize the shape of the spectrum of individual load-time histories by a single number, the “spectrum shape parameter” is also calculated. Shape parameters have traditionally been used in various formats, for example in fatigue standards, in order to characterize the combined effect of block size and cumulative frequency of load amplitudes – partly adopting Miner’s rule.

The intention in the last phase of this study is to find/calculate these parameters, which helps us to characterize/define the spectrum of commercial vehicle axle on the customer usage and at the proving ground as seen the following table.

Table 11.1 : Characterization of load spectrum of a two-axle coach.

Characterization of the Load Spectrum for the Axles of a two-axle Coach											
Axle Position	Coordinates of the Wheel Forces	Extreme Values (F_{max}) of the Load Spectrum		Cumulative Frequency (H) of the Load Spectrum		Shape Parameters (v) of the Load Spectrum		Phase Angles (ϕ) of the Wheel Forces		Scaling Factors (f_i)	
		CU	PG	CU	PG	CU	PG	CU	PG	CU	PG
Front Axle	Z	$1,20 \cdot F_{Fz,max(PG)}$	$F_{Fz,max(PG)}$	$20 \cdot H_{PG,Fz}$	$H_{PG,Fz}$	0,57	1,55	no representative and dominant phase relation		1,00	1,00
	Y	$0,86 \cdot F_{Fy,max(PG)}$	$F_{Fy,max(PG)}$	$20 \cdot H_{PG,Fy}$	$H_{PG,Fy}$	0,53	1,20		0,28	0,41	
	X	$1,11 \cdot F_{Fx,max(PG)}$	$F_{Fx,max(PG)}$	$14 \cdot H_{PG,Fx}$	$H_{PG,Fx}$	0,55	-		0,31	-	
Rear Axle	Z	$0,83 \cdot F_{Rz,max(PG)}$	$F_{Rz,max(PG)}$	$20 \cdot H_{PG,Rz}$	$H_{PG,Rz}$	0,53	1,45		1,00	1,00	
	Y	$0,98 \cdot F_{Ry,max(PG)}$	$F_{Ry,max(PG)}$	$20 \cdot H_{PG,Ry}$	$H_{PG,Ry}$	-	1,10		0,40	0,43	
	X	$1,35 \cdot F_{Rx,max(PG)}$	$F_{Rx,max(PG)}$	$15 \cdot H_{PG,Rx}$	$H_{PG,Rx}$	-	1,10		0,30	0,28	

Based on the outcome of the studies conducted, the four main parameters for the definition of a load or test spectrum have been found/calculated for the experimental durability tests of the axle of a two-axle coach. At the last phase of this study, all the results/obtained parameters are summarized and documented. These calculated parameters define the load spectrum for the experimental durability tests of the axle of a two-axle coach. If the same methodical and systematic approach is considered and executed for the next long-term commercial vehicle measurements (for example, a truck measurement), then it is also possible to derive the standardized load sequence for the experimental durability tests of the commercial vehicle axles. Therefore, with the help of all these tests and improvements, this methodology can be beneficial reference/method for the generation and use of standardized load spectrum and load–time histories of the commercial vehicle axles that will be experimentally tested in the future. Another beneficial output of this study is the derivation the load spectrums without any expensive and time-consuming customer usage measurements because of the obtaining the parameters mentioned above.

REFERENCES

- [1] **Heuler, P., Bruder T., and Klätschke, H.** (2005). Standardized load-time histories – A contribution to durability issues under spectrum loading. *Mat.-wiss. u. Werkstofftech.* 36, No. 11.
- [2] **Alessandro D., and Andreas R.** (1998). Comparison of Procedures for Experimental and Theoretical Durability Approval of a Truck Axle. *SAE Technical Paper Series.* 982787.
- [3] **Neugebauer, J.R., Grubisic, V., and Fischer, G.** (1989). Procedure for design optimization and durability life approval of truck axles and axle assemblies. *SAE Technical Paper Series.* 892535.
- [4] **Schütz, W.** (1988). The significance of standardized load sequences. *Materialwiss Werkstofftechnik.* 19:282–9.
- [5] **Potter, J.M., Watanabe, R.T.** (1989). Development of fatigue loading spectra. *American Society for Testing and Materials*, p. 35–75.
- [6] **Schütz, W.** (1989). Standardized stress–time histories – an overview. *American Society for Testing and Materials*, p. 3–16.
- [7] **Schütz, W.** (2002). A review of standardised load–time histories for fatigue research and application. *International Journal of Fatigue.* 24(6):603–25.
- [8] **Dressler, K., Speckert, M., Weber, C.M., Müller, M., and Teutsch, R.** (2008). A new way to customer loads correlation and testing in truck engineering. *Congress Proceedings World Automotive Congress.*
- [9] **Kistler Instrumente AG,** (2000). *RoadDyn[®] Instruction Manual.* S6HT.
- [10] **Diefenbach, D.** (1994). Erfassung der mehraxialen Fahrbetriebsbelastungen mit dem Messrad – VELOS. Bericht aus dem Fraunhofer-Institut für Betriebsfestigkeit - *LBF Darmstadt, Sonderdruck aus ATZ Automobiltechnische Zeitschrift.* Nr.12, p.764-768.
- [11] **Sonsino, C.M.** (2007). Fatigue testing under variable amplitude loading. *International Journal of Fatigue,* Nr.29, p. 1080–1089.
- [12] **Zenner, H.** (2001). *Betriebsfestigkeit.* TU Clausthal.
- [13] **Yung-Li, L., Jwo, P., Hathaway, R., and Barkey, M.** (2005). *Fatigue testing and analysis. Theory and Practice.* Elsevier Inc.
- [14] **Buxbaum, O.** (1992). Betriebsfestigkeit, sichere und wirtschaftliche Bemessung schwingbruchgefährdeter Bauteile (Durability, safe and economic design of fatigue-loaded components). *Verlag Stahleisen mbH, Düsseldorf,* 2. Auflage.
- [15] **Gumbel, E.J.** (1958). *Statistics of extremes.* Columbia University Press.

- [16] **Richard, J., Marx, L.** (2000). *An introduction to mathematical statistics and its applications*. Prentice-Hall, Incorporated
- [17] **Haibach, E.** (2006). *Betriebsfestigkeit Verfahren und Daten zur Bauteilberechnung*. Springer-Verlag Berlin
- [18] **Harris, and Crede.** (1976). *Shock and vibration handbook*. McGraw Hill Professional
- [19] **Brüel & Kjør.** (n.d.). *Frequency analysis handbook*. Prentice-Hall, New Jersey
- [20] **O'Shea, P.** (2000). *Phase measurement*. Royal Melbourne Institute of Technology.
- [21] **Gol'dshtein, E. I., and Katz, I. M.** (2007) Determination of a phase shift between two non-sinusoidal signals represented by digital counts. *Russian Physics Journal*. Vol. 50, No. 10.
- [22] **Hammond, K.D.** (2008) *Frequency response analysis*. University of Massachusetts Amherst.
- [23] **nCode GlyphWorks.** (Version 7). [Computer software]. Glyph reference guide.
- [24] **Bendat, J.S., Piersol, A.G.** (1986). *Random data*. Wiley-Interscience.
- [25] **White, L.B., and Boashash, B.** (1990). Cross spectral analysis of non-stationary processes. *IEEE Transactions on Information Theory*. Vol. 36, No. 4, pp. 830-835.
- [26] **Hänel, B.** (1988) *IfL-Mitteilungen*. 27, Dresden.
- [27] **Gassner, E., Griese, F.W., and Haibach, E.** (1964). *Archiv Eisenhüttenwesen* 35, p.255.
- [28] **Hanke, M.** (1970). *ATZ Automobiltechnische Zeitschrift*. 72, p. 91.
- [29] **Decker, M., and Savaidis, G.** (2002). Measurement and analysis of wheel loads for design and fatigue evaluation of vehicle chassis components. *Blackwell Science Ltd. Fatigue & Fracture of Engineering Materials & Structures*. 25, pp. 1-17.

CURRICULUM VITAE



Name Surname: Metin Toprak

Place and Date of Birth: Istanbul / 04.06.1983

B.Sc.: Yıldız Technical University (2001-2006)

M.Sc.: Istanbul Technical University (2006-2008)

Professional Experience and Rewards:

- R&D Engineer, Responsible of Chassis Suspension for the Durability Approval, 2007-present
- Scientist Supporting Program Scholarship by The Scientific and Technological Research Council of Turkey (TUBITAK), 2008
- 3th rank in Yıldız Technical University at Mechanical Engineering Department, 2006

PUBLICATIONS/PRESENTATIONS ON THE THESIS

- **Toprak, M.**, Ereke, M. 2014. "Ticari Taşıt Akslarının Dayanım Testlerinde Kullanılacak Yüklerin Müşteri Çevrimindeki Taşıtların Ölçümlerinden Elde Edilmesi," *Mühendis ve Makina*, cilt 55, sayı 651, s. 26-42.

